AD NUMBER

AD822155

LIMITATION CHANGES

TO:

Approved for public release; distribution is unlimited.

FROM:

Distribution authorized to U.S. Gov't. agencies and their contractors; Critical Technology; JUN 1967. Other requests shall be referred to Air Force Institute of Technology, Attn: AFIT-SE, Wright-Patterson Air Force Base, OH 45433. This document contains export-controlled technical data.

AUTHORITY

AFIT ltr, 22Jul 1971

AIR FORCE INSTITUTE OF TECHNOLOGY

AIR UNIVERSITY
UNITED STATES AIR FORCE

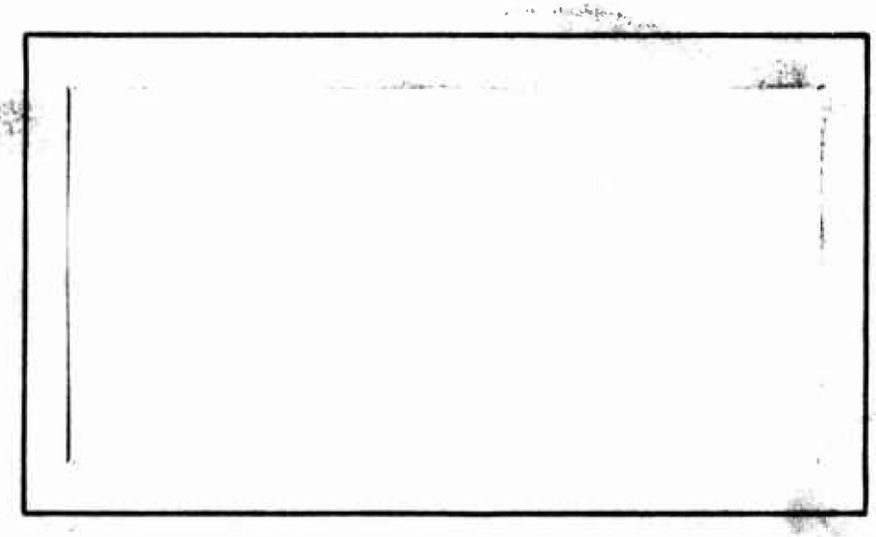

SCHOOL OF ENGINEERING

WRIGHT-PATTERSON AIR FORCE BASE, OHIO

OPTIMIZATION OF A GROUND EFFECT MACHINE

THESIS

GAM/AE/67-1

James C. McSherry
Capt USAF

AFLC-WPAFB-AUG 67 35

OPTIMIZATION OF A
GROUND EFFECT MACHINE

THESIS

Presented to the Faculty of the School of Engineering of
the Air Force Institute of Technology
Air University
in Partial Fulfillment of the
Requirements for the Degree of
Master of Science

By
James C. McSherry, B.S.A.E.
Capt USAF

Graduate Aerospace-Mechanical Engineering

June 1967

Preface

I became interested in Ground Effect Machines when reports on them began appearing in the technical periodicals, and the dream of a flying automobile has inspired every one who has ever been caught in a traffic jam. When Professor Bielkowicz told me of his idea of a ground effect machine that could be capable of flight, I was so fascinated with the concept that all other suggested thesis topics seemed hopelessly dull by comparison.

The thesis explores the concept, proves its practicality, through wind tunnel testing and analytical estimation. All assumptions were purposely made on the conservative side, because an idea of this magnitude will attract many critics. For this reason, it was hoped that no estimation would be required and that all data would be the result of wind tunnel testing. Only when the large AFIT tunnel was closed for repairs, did it become necessary to use any analytical prediction. I personally feel that if such a vehicle were built tomorrow, its performance would be significantly better than predicted by this analysis.

I would like to express my sincere gratitude to Professor Bielkowicz for his trust and his assistance, and special debts of thanks to Messrs. Barringer, Whitt and Lokai of the AFIT wind tunnel, and to Mr. Joseph Huff at the AFIT School Shops, who built the complicated models.

Contents

List of Figures

List of Figures

List of Figures

List of Tables

Symbol	Definitions	Units
A	Area	ft^2
a	Speed of Sound	ft/sec
AR	Aspect Ratio	
b	wing span	ft
c	wing chord	ft
C_l	non-linear lift coefficient	$1/degree^2$
C_D	coefficient of drag	
C_L	coefficient of lift	
C_{mac}	coefficient of moment about the aerodynamic center	
C_p	coefficient of pressure	
C_Q	coefficient of suction	
D	drag	lb
f	"a function of ..."	
h	height	ft
K_1	shape factor	
L	lift	lb
l	length	ft
M	moment	ft lb
M	Mach Number	
m	mass	slugs
$\dot{m}$	mass flow rate	slugs/sec
P	pressure	lb/ft^2
r	radius	ft
Re	Reynold's number	
S	surface area	ft^2

Symbol	Definitions	Units
S_F	flap deflection	degrees
U	local velocity	ft/sec
$\overline{U}$	mean velocity	ft/sec
U(x)	local free stream velocity	ft/sec
V	velocity	ft/sec
W	weight	lb
w	width	ft
X	horizontal distance	ft
α	angle of attack	degrees
γ	duct angle	degrees
Δ	"a change in...."	
δ	boundary layer thickness	ft
δ_F	flap deflection angle	
e	wing efficiency factor	
ϵ_{sb}	solid blocking factor	
ν	dynamic viscosity	ft^2/sec
ρ	density	$slugs/ft^3$

Subscripts

B_L	boundary layer
Blow	blowing slot
EP	end plate
F	flap
n	nacelle
f	forward wing

Subscripts

o	stagnation(or initial conditions)
Q	suction
s	stabilizer and slot
T	"As tested"
∞	free stream conditions

Abstract

Professor Peter Bielkowicz conceived the idea of a ground effect machine that could also fly. This thesis tests the concept and improves on the original design. Two wind tunnel models were built to determine the aerodynamic characteristics of the vehicle. When the wind tunnel was closed because of safety problems after the test program had just begun, a third, sub-scale, model was built and tested in a smaller tunnel to test improvements dictated by first tests.

The results from these tests were combined with some analytical techniques to predict the performance of the full scale vehicle.

The final vehicle will carry one pilot and two passengers (if necessary). When armed with two 7.62 mm machine guns, carrying a full fuel load and a 200-lb. pilot, the gross weight of the vehicle is 2400 pounds. Its dimensions are 7.2 feet wide, 17.9 feet long and 13.0 feet high, including the end plates necessary for such a low aspect ratio wing. This small size will allow the vehicle tc travel over back trails or unimproved roads. Despite the severe limitations imposed by the dimensions, the vehicle will become airborne at 99 feet per second, and clear a 50-foot obstacle 545 feet from the take off point, when powered by the 300-horsepower Curtiss-Wright RC-2-90-y rotating cylinder engine.

OPTIMIZATION OF A GROUND EFFECT MACHINE

I. Introduction

A need for ground effects machines exists in the military services. The advantages of a vehicle which can go anywhere has been effectively demonstrated by the performance of helicopters in Korea and Vietnam.

The ground effect machine has thus far in its development not approached the versatility of a helicopter. This is primarily because the ground effect machine was limited to very low ground clearance. Obstacles, such as ditches, walls, and fences forced the early experimental models to look for routes around these obstacles. Therefore, the successful ground effect machines have been those that operate primarily over water. The British series of "hovercraft" are excellent examples (Ref 2).

Professor Peter Bielkowicz of the Air Force Institute of Technology conceived the idea of a ground effect machine with an air foil-shaped structure that would produce aero-dynamic lift whenever required. A wall could be negotiated simply by flying over it, a ditch would be jumped, a low bridge could be hopped and rough terrain could be negotiated by increasing the ground clearance with the aerodynamic lift.

Professor Bielkowicz performed a preliminary design

analysis of such a vehicle. This thesis is concerned with the optimization of this original design. Its objectives are: To determine through wind tunnel tests, the feasibility of the concept by determining the maximum weight and minimum velocity at which the vehicle could become airborne: to perform a preliminary design, including duct performance, weight and balance estimates. To improve on the original design to improve performance, increase simplicity and reduce costs.

Specifically not included as part of this thesis is a detailed stress analysis and a stability and control study.

II. Mission

The mission envisioned for this vehicle is primarily reconnaissance, but the versatility of the craft would also allow for general transportation and evacuation of wounded. This mission, together with considerations for flexibility, imposed certain design restrictions, which are as follows.

1. The vehicle should be relatively small, carrying one pilot, with a capability for two passengers.

2. The vehicle should be as simple and uncomplicated as possible for ease of maintenance and high reliability under combat conditions.

3. The vehicle must be able to operate continually over unimproved roads, water, and open fields for six hours, at speeds up to 85 feet per second. It must also be able to fly over an obstacle, jump a ditch and negotiate uneven terrain for shorter periods of time.

4. The vehicle must be less than 8 feet wide, to follow narrow roads, and less than 14 feet high to pass under bridges and overpasses.

5. The design of the vehicle should be such that it is not vulnerable to small arms fire.

6. The vehicle should be capable of carrying light armament, such as machine guns.

If all these restrictions can be successfully met, the resulting vehicle would have the performance of a light aircraft and the versatility of a helicopter with the maintenance record of a station wagon.

III. Basic Design and Test Philosophy

The basic design scheme is to utilize a peripheral jet ground effect machine, the upper surface of which is an airfoil. This airfoil would then be a wing with a very low aspect ratio. To increase the effectiveness of the wing, the aspect ratio must be artificially increased by the use of large end plates. Because the wing must operate near its maximum coefficient of lift, i.e., at high angles of attack, separation and stall is likely. This suggests that a boundary layer control system is required.

For protection from small arms fire, the engine should be internally mounted. For small overall size and high power to weight ratio, the Wankel rotating cylinder engine was selected. Similarly, but also for the reason of greater efficiency, a ducted fan was chosen for propulsive power, rather than a conventional exposed propeller.

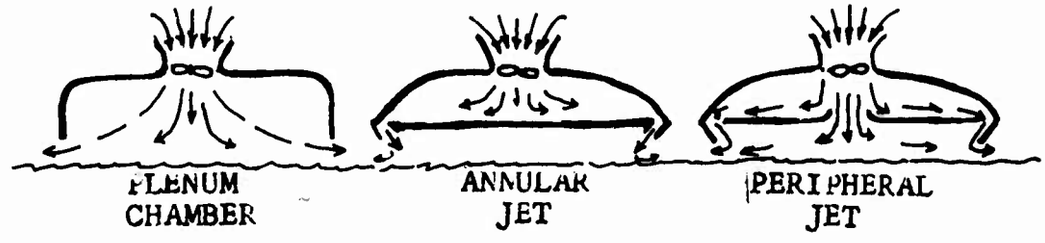

FIG. 1 : GROUND EFFECT SCHEMES

The air for the ground cushion is to be provided by two fans, also duct mounted and powered by the same engine which powers the propulsion fan. The ground effect scheme is to be of the peripheral jet principle, in order to in-

crease the efficiency of the lift fans. The normal procedure in ground effect machines is to draw the lift air through an inlet in the upper surface of the vehicle. As this would ruin the aerodynamic lift in this design, the inlets must be placed in the front of the vehicle. This will require a duct system with a 90-degree turn.

With this philosophy, and with the constraints imposed by the mission, it is now possible to visualize how such a vehicle would look. It would be about the size of a light panel truck, with the side panels extended to serve as end plates, and the roof shaped as an airfoil. Rudders and a stabilizer might be added at the rear. The front of the vehicle would be rounded to reduce drag, as would the rear, and the "grill" would consist of two or three large inlets.

The testing philosophy is equally straight forward and logical. It was decided to build two models for wind tunnel testing. The first model would consist of an airfoil with end plates and control surfaces. The fuselage would contain no ducting.

The second model would have all ducts in the fuselage and incorporate any changes found necessary from the testing on the first. If the tests were successful, then a detailed preliminary design could proceed immediately.

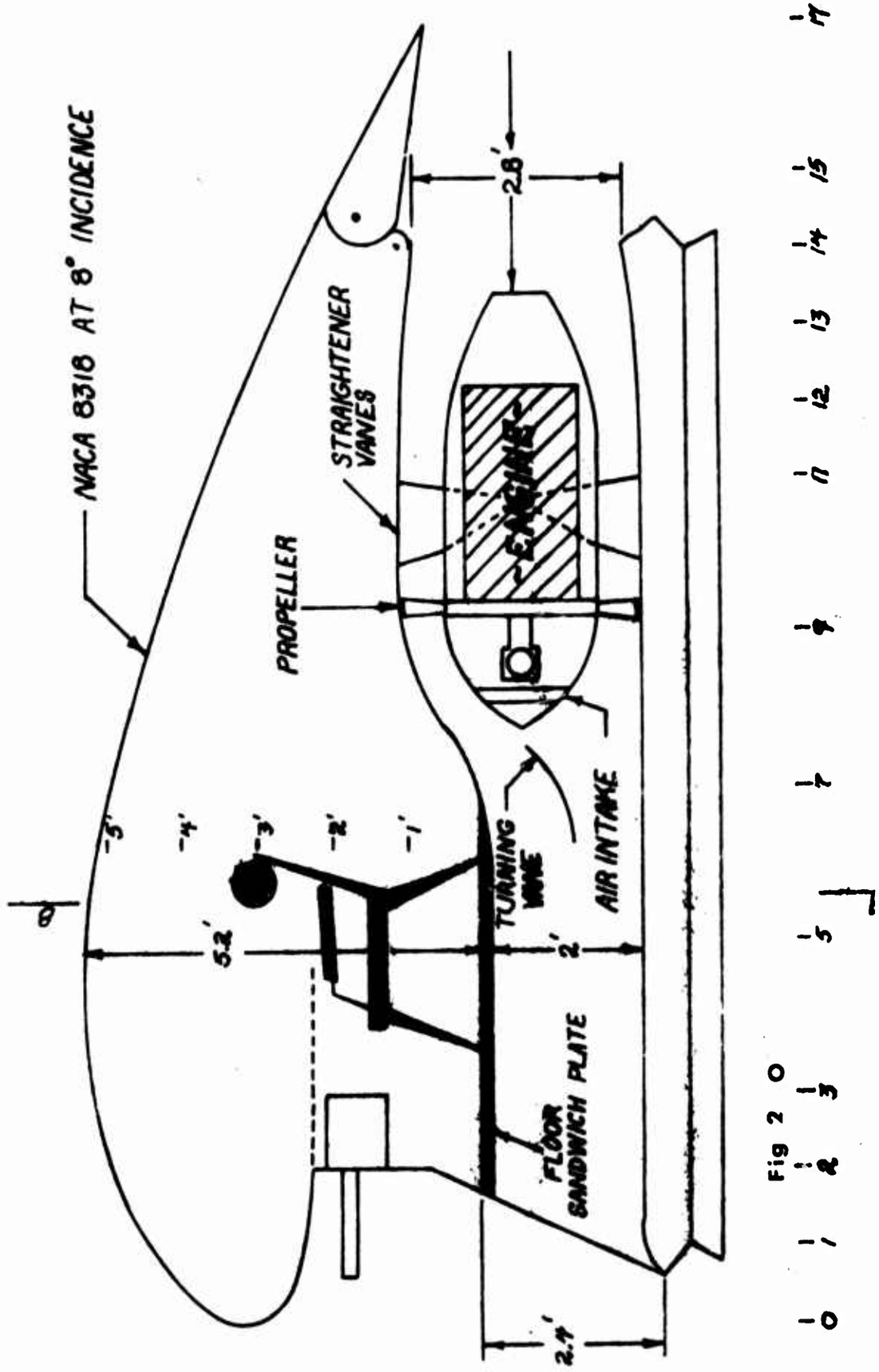
NACA 8318 AT 8° INCIDENCE
STRAIGHTENER VANES
PROPELLER
ENGINE
2.8'
TURNING VANE
AIR INTAKE
FLOOR SANDWICH PLATE
5.2'
2'
2.4'
-5'
-4'
-3'
-2'
-1'
0
1
2
3
5
7
9
11
12
13
14
15
17

Fig 2 0

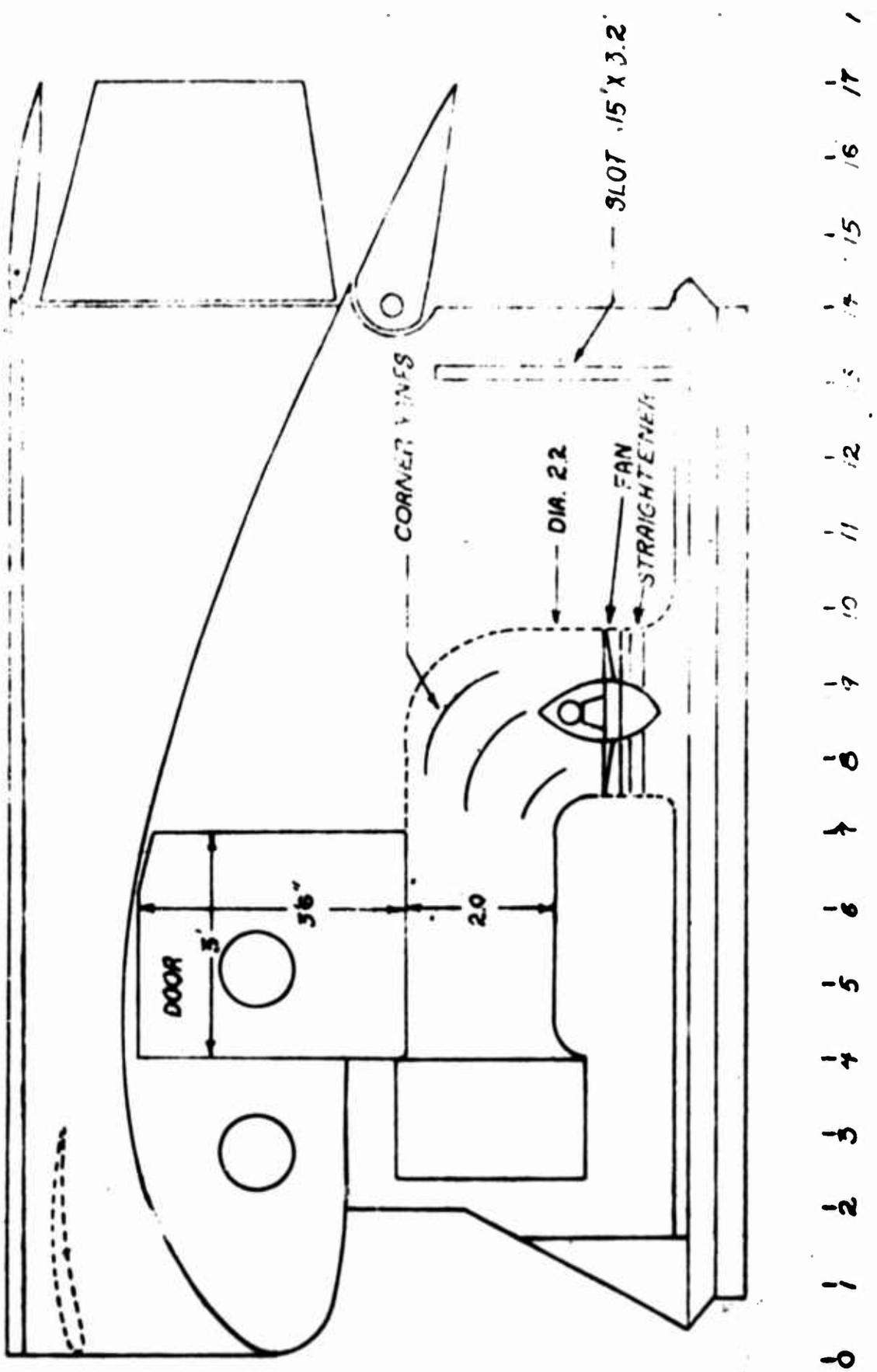
SLOT .15'X 3.2'
CORNER VANES
DIA. 22
FAN
STRAIGHTENER
DOOR
3'
5'6"
2.0

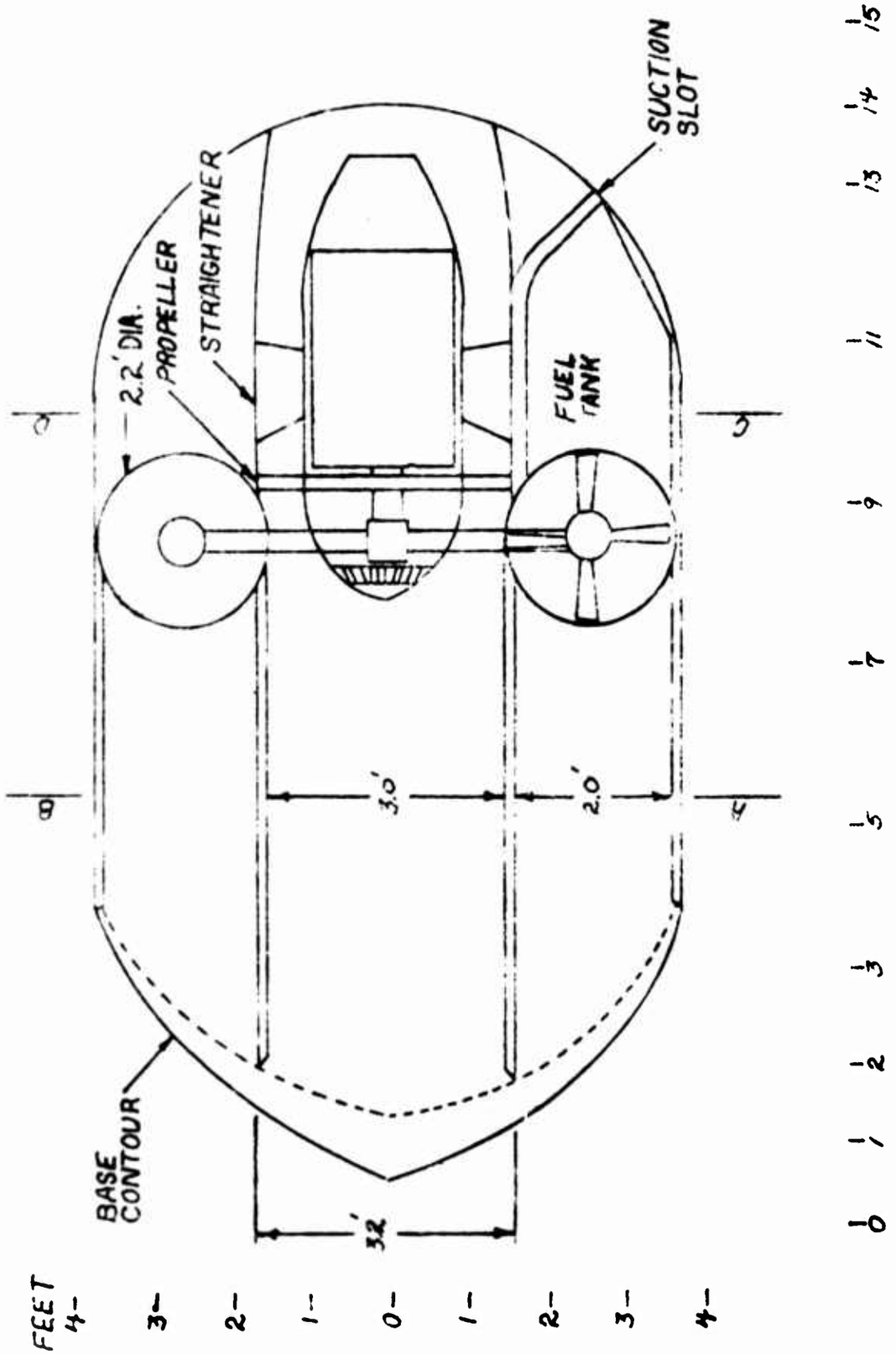
SUCTION SLOT
STRAIGHTENER
2.2' DIA. PROPELLER
FUEL TANK
3.0'
2.0'
1.32'
BASE CONTOUR
FEET
4
3
2
1
0
1
2
3
4
1/15
1/14
1/13
1/11
1/9
1/7
1/5
1/3
1/2
1/1
0

IV. Design of Wind Tunnel Models

Original Design

The starting point was the original design of Professor Bielkowicz. During the initial portion of this study; several changes were made to the original design, which make it somewhat difficult to establish exactly what was the original design.

For the purpose of this thesis, the "original design" will be taken as shown in Figures 2, 3 and 4. Among the changes included in this version are the introduction of the forward wing, and a rear suction slot. The propeller is positioned near the forward end of the engine nacelle, rather than the rear end of the nacelle where it had been placed in earlier versions. Although the wing suction slot is not shown in these drawings, suction boundary layer control was a part of the concept from the beginning.

A turning vane is present in the propeller duct and the angle of duct divergence behind the pilot's chair is quite high. The center of the propeller and the center of the fans are at the same longitudinal station.

The overall length of the vehicle is 17 feet, the width is 7.2 feet and the height is 10.2 feet. The incidence angle of the airfoil is 8 degrees.

Selection of Scale

The first step in the design of the model was the

selection of the scale. This is determined by the size of the tunnel and the parameters to be duplicated. In this case, the parameters are Reynolds numbers and Mach number.

The selection of a scale is, at best, a compromise. The model should be as small as possible in order to reduce blockage in the tunnel. Conversely, the model should be as large as possible to duplicate Reynolds number without encountering compressibility effects of high Mach number.

The diameter of the AFIT subsonic wind tunnel is five feet, thus the absolute maximum cross sectional dimension for the model is five feet. This, of course is impractical. In addition to blockage, another consideration is that the model must travel through a range of angle of attack. Additionally, an arbitrary value of two inches was determined to be the minimum clearance, to allow for any fittings and attachments that might be needed.

The proportions of this model are:

$$l = 1.75h$$

$$w = 0.76h$$

and the pivot point, when placed at the quarter chord of the wing is 0.68h above the bottom of the model. Then, referring to Fig. 5, the maximum dimension h, in inches, can be calculated from Eq (1).

$$900-.1296h^2 = .68h \cos 10^{\circ}+.75(1.75)h \sin 10^{\circ}+2 \qquad (1)$$

simplifying yields the quadratic:

$$1.1246h^2+3.992h-896=0$$

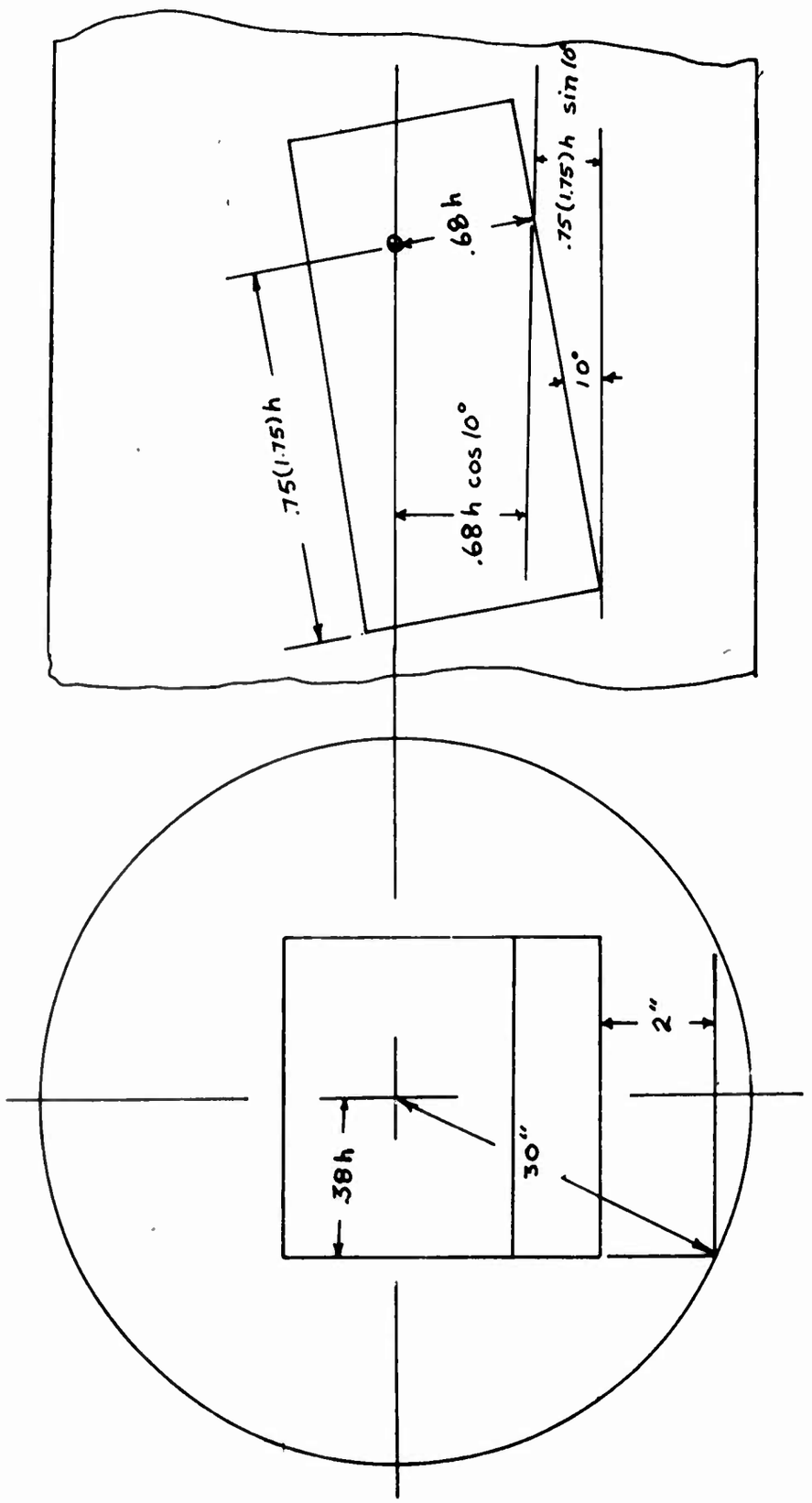

FIG. 5 DETERMINATION OF MODEL SCALE

and solving for h, h=26.51 inches. Which would result in a scale factor of 0.224, smaller than one-fourth scale but larger than one-fifth. If this scale would not create too much blockage in the tunnel, then one-fifth scale would be selected. Pope, gives the blockage factor as

$$\epsilon_{sb} = \frac{K_1 \text{ (model volume)}}{C^{3/2}} \tag{2}$$

where ϵ_{sb} is the ratio of the velocity increment due to blocking to the tunnel velocity, C is the cross-sectional area of the tunnel and K is a shape factor ranging from 0.5 to 0.75 when the dimension used are feet (Ref 15). Taking the highest value of K, gives a value for ϵ_{sb} of .0378. This means that the true velocity of the air passing the model would be 103.78 feet per second when the tunnel instruments indicate 100 feet per second. This is an acceptable blockage factor.

The only remaining question is now the simulation of Reynolds number and Mach number. Reynolds number is given by $R_e = \frac{Vc}{v}$ (3)

where V is the velocity, c is the chord length and v is the dynamic viscosity. The actual Reynolds number of the vehicle at a take-off speed of 100 feet per second under standard conditions is

$$R_e = \frac{100\ (17.2}{1.551 \times 10^{-4}} = 10.98 \times 10^6 \tag{4}$$

where the chord is measured in feet, the velocity in feet per second and the dynamic viscosity in ft^2 per second. To duplicate this number with a one-fifth scale model would require a test velocity of 500 ft per second. The dynamic pressure at this velocity is 297.2 pounds force per square foot. If the lift coefficient were 1.0, then the model would generate a lift of 1486 pounds, which exceeds the measuring capability of the tunnel. Additionally, at this speed compressibility effects would be encountered.

Therefore, exact duplication of the Reynolds number is not possible. However, experience has shown that aerodynamic characteristic do not vary significantly at high Reynolds numbers (Ref 5). That is, if the test number is greater than a million, the test is generally valid for all higher Reynolds numbers until Mach number becomes significant. The test Reynolds number is (1/5) (10.98×10^6) = 2.196×10^6 at 100 feet per second. The one-fifth scale, then, can simulate the Reynolds number acceptably well.

The scale for the model was then chosen as one-fifth. This scale fits the tunnel, does not cause excessive blockage, simulates the Reynolds number and exactly matches the Mach number of the full size vehicle.

Wing and Flap Design

Selection of Airfoil. The airfoil NACA 8318 was part of the original design by Professor Bielkowicz. It was picked for its high lift coefficient, its thickness which

facilitates interior design, its smooth stalling characteristic and its flat bottom surface (Ref 8). The importance of the flat bottom is that little lift is generated by the bottom surface. In this design the bottom of the airfoil is displaced downward by several feet. An undercambered airfoil would be impractical in that the installation of a peripheral jet in the lower surface would greatly increase the difficulty of fabrication and correspondingly the cost.

The NACA 8318 airfoil shows a remarkable similarity to the vintange Clark-Y-20 (Ref 20). The coordinates of the Clark-Y-20 at one degree angle of attack and the NACA-8318 agree to within 1/2% at all stations. The aerodynamic characteristic are practically identical, when displaced one degree. It appears that the NACA-8318 is a "modernized" Clark-Y-20. Considering the tolerances necessary in making a wooden model, the airfoils are, for all intents and purposes, the same.

Boundary Layer Control. The suction slot is positioned at 55% of the chord, as part of the original design. The slot is inclined at 55 degrees to the horizontal. A model allowing for experimental change in the position of the slot would be necessarily complex. Therefore it was decided to proceed with a fixed slot on the first model. If the suction did not increase the performance of the airfoil, the slot could be redesigned on the second model.

The width of the slot, however, will not necessarily be one-fifth of the full-scale slot, due to the differences in boundary layer thickness, Reynolds number etc. The optimum width of the slot was to be determined by the tests.

The principle of boundary layer control by suction is simply that the lower energy levels near the surface are removed, leaving a more energetic boundary layer, less likely to separate. Therefore, the maximum suction would be the removal of the entire boundary layer. Any suction beyond this would create no change in performance. The slot, then, should be sized to carry this maximum flow rate. The mass flow rate in the boundary layer can be calculated by

$$\dot{m} = \rho A \bar{U} \tag{5}$$

where ρ is the density of the air, A is the area of flow, equal to the wing span times the thickness of the boundary layer, and $\bar{U}$ is a mean velocity throughout the boundary layer. Schlicting gives this mean velocity as

$$\bar{U} = \int_0^{\delta} \frac{u \, dy}{\delta} \tag{6}$$

which for turbulent flow becomes

$$\bar{U} = 0.8167 \, U_{(x)} \tag{7}$$

where $U_{(x)}$ is the local free-stream velocity. The boundary layer thickness for turbulent flow is

$$\delta = \frac{0.37x}{\sqrt[5]{R_{ex}}} = \frac{0.37x}{\sqrt[5]{\frac{U(x)}{\nu}}} \tag{8}$$

where x is this distance from the leading edge. Although this formula was developed for turbulent flow over a flat plate, its application to an airfoil gives a reasonable estimation of the thickness, and is certainly accurate enough for this application (Ref 4).

The remaining unknown is the local free-stream velocity at 55% chord. This can be determined by the equation

$$C_p = 1 - \left(\frac{U(x)}{V}\right)^2 \tag{9}$$

where C_p is the coefficient of pressure, which is available from the literature and presented in Fig. 6 (Ref 20). At a C_L of 1.0, C_p is equal to -0.99 at the 55% chord.

In this specific application, the local velocity, at 100 feet per second tunnel velocity, is 141 feet per second, from Eq (6). The local Reynolds number is 1.56x 10^5, which gives the boundary layer thickness as 0.0398 feet. The boundary layer mass flow rate is then

$$\dot{m}_{BL} = \rho b \delta (.8167) U(x) \tag{10}$$
$$= 0.1972 \text{ slugs/sec}$$

The mass flow rate through the slot must match this

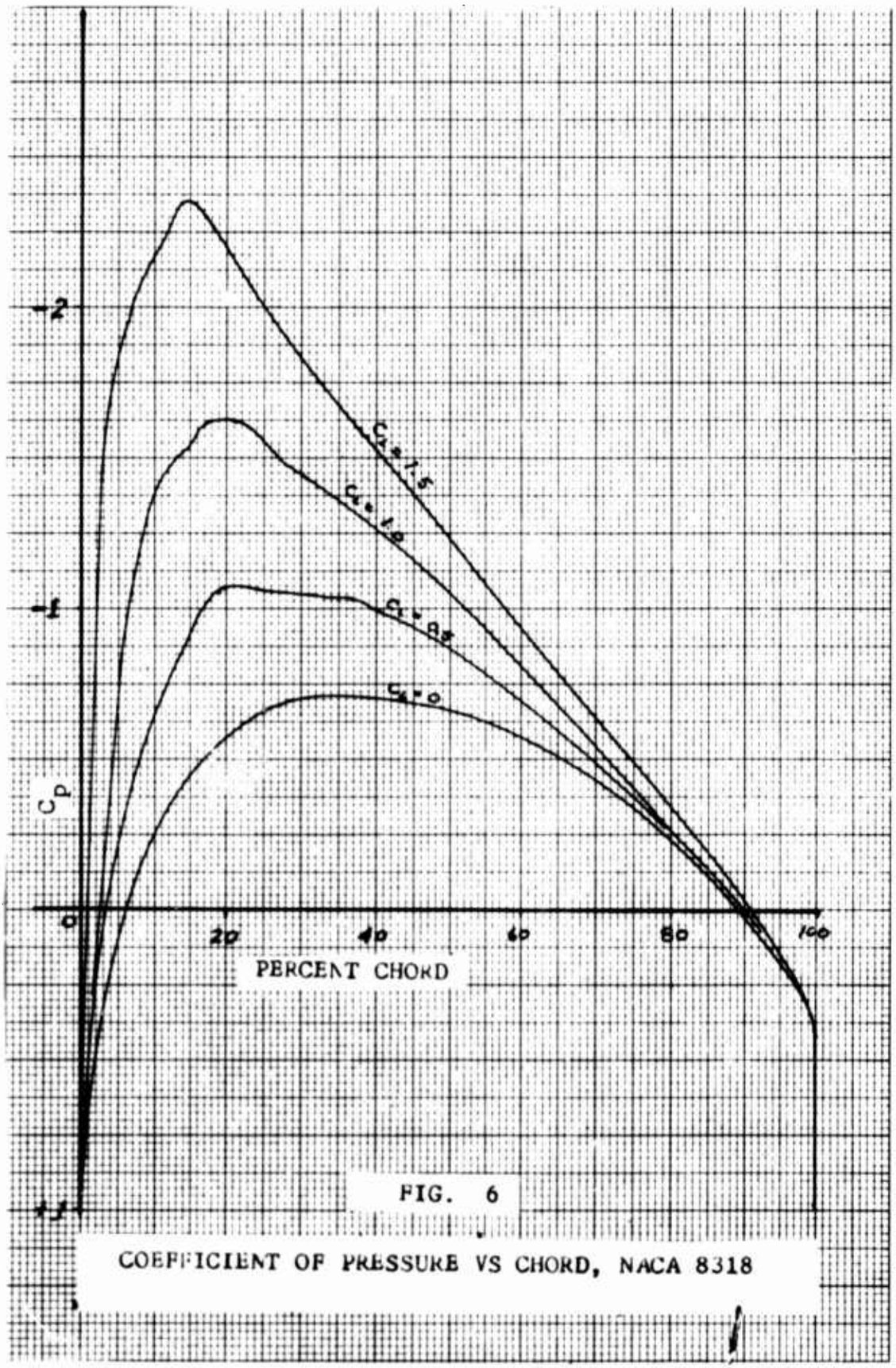

FIG. 6

COEFFICIENT OF PRESSURE VS CHORD, NACA 8318

value. The mass flow rate can be determined by $\dot{m} = A_Q U_Q = \rho b w U_Q$ where w is the width of the slot, b the wing span and U_Q the velocity in the slot. U_Q can be expressed by Bernoulli's incompressible equation as

$$U_Q = \sqrt{\frac{2}{\rho}(P_x - P_Q)} \tag{11}$$

where P_x is the pressure on the wing at the 55% chord and P_Q is the pressure in the slot. The wing pressure can be found from the C_p, so

$$U_Q = \sqrt{\frac{2}{\rho}\left(\frac{Cp\ \rho V_\infty^{\ 2}}{2} + P - P_Q\right)} \tag{12}$$

Since the AFIT wind tunnel extracts air from the atmosphere

$$P = Pa - \tfrac{1}{2}\rho V_\infty^{\ 2} \tag{13}$$

then

$$U_Q = \sqrt{\frac{2}{\rho}\left(\frac{Cp}{2}\rho V_\infty^{\ 2} + Pa - \tfrac{1}{2}\rho V_\infty^{\ 2} - P_Q\right)} \tag{14}$$

or,

$$U_Q = \sqrt{\frac{2}{\rho}\left[(1-C_p)\frac{\rho V_\infty^{\ 2}}{2} + (Pa - P_Q)\right]} \tag{15}$$

The mass flow rate can be written:

$$\dot{m} = \rho b w \sqrt{\frac{2}{\rho}\left[(1-Cp)\frac{\rho V_\infty^{\ 2}}{2} + (Pa - P_Q)\right]} \tag{16}$$

Where all values are known except the width of the slot, w, and the suction required, $(P_a - P_Q)$. It was assumed that a standard vacuum cleaner could achieve a suction of ten inches of water, and that two inches of

water would be lost to duct friction. Then a value of eight inches of water (41.405 pounds per square foot) could be substituted for $(P_a - P_Q)$.

The above equation now contains only one unknown, the required slot width. The equation was solved for w, with the result w = 0.0456 feet = 0.548 inches at V = 100 feet per second. With this width slot, and a vacuum cleaner capable of providing a suction of eight inches of water after duct losses, the entire mass flow rate in the boundary layer could be removed. It was anticipated of course, that not all the boundary layer need be removed. During the tests the suction would be varied, and the mass flow rate measured. The optimum mass flow could then be determined and the full scale slot could be sized by a similar analysis.

Flap Design

The design of the model flap merely involved devising a mechanical system which allowed movement of the flap and a system to measure the deflection angle. The design used on the model is shown in Fig. 7. The flap is deflected manually by loosening the bolts. A 1/4-inch-pin is inserted through the end plate into the desired key holes located at 0,15,30,45 and 60 degrees of deflection. The bolts are then secured. This allows for movement of the flap through 60 degrees, with positive stops at 15-degree-intervals.

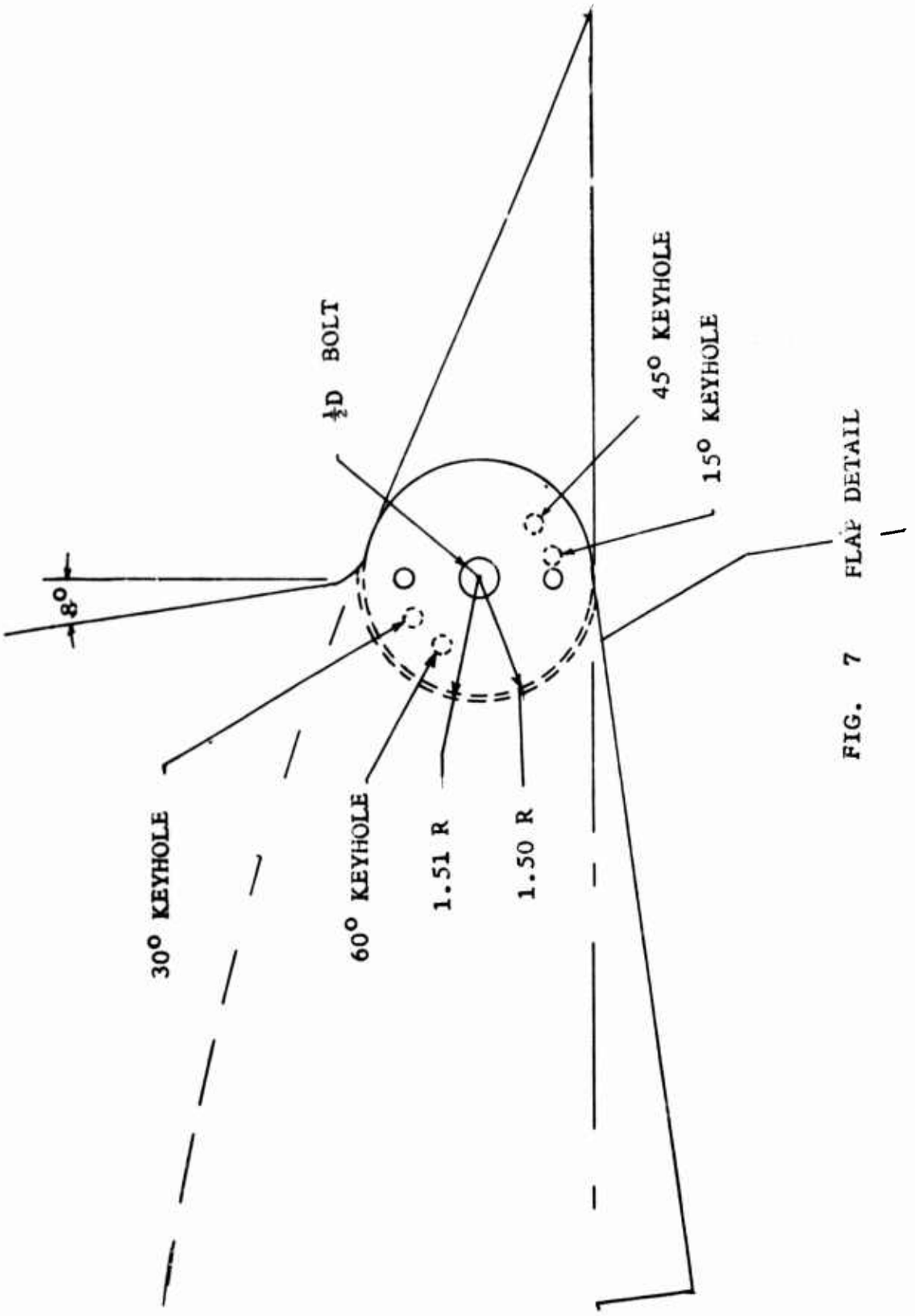

FIG. 7 FLAP DETAIL

Construction

The wing was constructed by laminating 22 sections cut to NACA 8318 coordinates. The slot intake was ducted to a position near the quarter-chord where the external vacuum line is attached (see design of test equipment). The quarter-chord point was chosen to minimize problems of fitting the vacuum line through the tunnel walls. To provide more rigidity for the upper surface a dowel was installed in each third lamination.

To accommodate the eight degree angle of incidence, the lower surface of the wing sections were extended and inclined eight degrees so the resulting surface would be horizontal when mated to the lower body section.

The end plates were cut from 1/4-inch mahogany plywood. Because no movement of the rudders was planned during testing, these surfaces were built as simply extensions to the end plates.

Control Surface Design

Stabilizer. The purpose of the stablizer is to provide longitudinal stability and control during the "hop" maneuver. This is accomplished by using an airfoil mounted behind the center of pressure of the wing. Because this airfoil must produce both positive and negative lift, a symetrical airfoil was selected. Of the symmetrical airfoils listed in the NACA literature, NACA 0012 gave the best lift to drag ratio, and was therefore

selected (Ref 9).

The location of the stabilizer was determined to be at the rear of the end plates and mounted as high as possible. In the original design, the complete tail assembly was to be moveable. In ground cruise mode the assembly would be retracted to the rear of the end plates, but extended rearward on rails for flight. To keep the model simple, it was decided to test in the retracted position. The aerodynamic characteristics of the stabilizer would be determined and the required extension could then be calculated analytically.

Forward Wing

The forward wing is a means of control in angle of attack which contributed positive lift rather than negative. This control surface not only aids in the control, but also generates an increase in overall lift.

A high lift airfoil was selected. A search of the NACA literature revealed that NACA 6512 was an excellent airfoil for this purpose (Ref 9). Its high lift, high lift-to-drag ratio, smooth stalling characteristics, and reasonable thickness (a help in structural design) represented one of the best sections for this use.

The location of this surface is not a simple problem, because the effect on the characteristics of the forward wing caused by the presence of the main wing is an unknown quantity. Likewise, the presence of the forward wing will

FIG. 8
FORWARD WING CROSS SECTION

FIG 9
STABILIZER CROSS SECTION

affect the main wing by acting as a leading edge slot. It was obvious that, for control purposes, the wing should be mounted as far forward as possible. The question of height and angle of attack was solved by constructing the model so that these parameters could be varied. A series of mounting holes were placed in the end plates. The forward wing could be placed in any of these holes and the angle of attack varied. In this manner the optimum position and angle of attack could be determined during the testing program.

Construction. Both surfaces made of laminated hardwood. The mounting point on both surfaces was at the quarter-chord. This is the zero moment point on the stabilizer, and the aerodynamic center on the forward wing. Using this point, a simple friction fitting, held in place by a machine screw is adequate to prevent changing of the angle-of-attack during the test. These fittings are visible in Figs. 10 through 12.

Body of First Model

The body of the first model was simply a shell designed to the outlines of Professor Bielkowicz' original design. It was constructed over a white pine lower frame (simulating the outline of the periperal jet), by using 1/4-inch bending plywood. Simple 2-by-4-inch bracing was added where the wind tunnel attachment fixtures were installed.

Figures 10, 11, and 12 show the completed model prior to installation of the wind tunnel attachments. These photographs show the relative locations of the control surfaces, the suction slot, and the outlet where the external vacuum system will be installed.

Internal Ducting in the Second Model

Purpose. The ducting in the second model was designed to simulate as closely as possible the lift and drag of the full scale vehicle. There are three ducts: two for the ground cushion effect and one for the forward propulsion.

The ducts present some unusual design problems. All three ducts begin with rectangular cross-sections and terminate with circular cross-sections. The propulsion duct contains the engine, and the ducted propeller. The lift fan ducts must turn downward 90 degrees, and contain the lift fans and a gear housing.

It was decided to not simulate an engine, or the ground cushion effect. These problems have been investigated and can be handled analytically after the wind tunnel testing has been completed. The problem which is of primary interest is the airborne performance of the machine, with no assist from the ground effect.

To avoid confusion, the term "fan ducts" will be used to denote the ducts which supply air for the ground cushion and the term "propeller duct" will be used to denote the

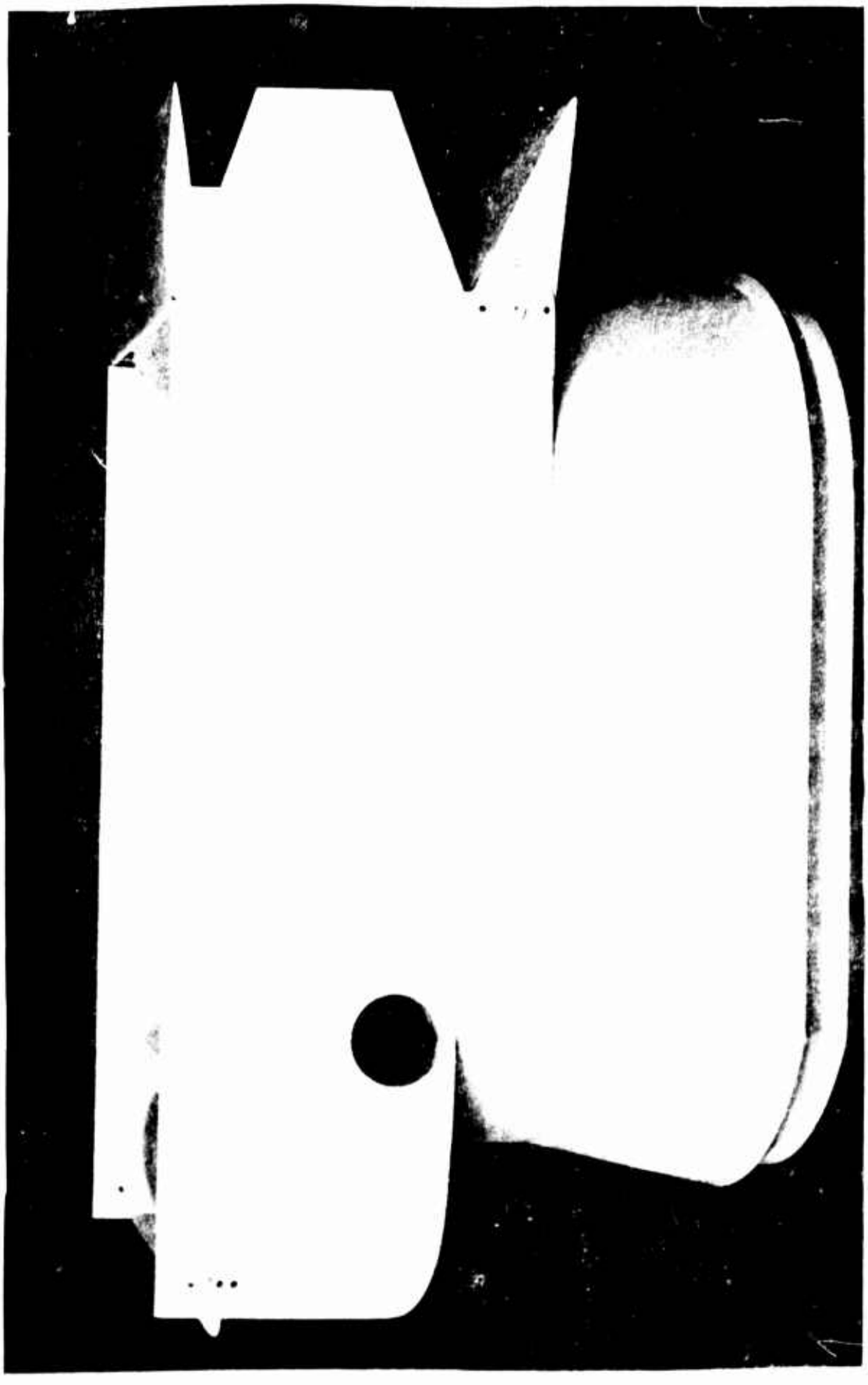

FIG. 10. FIRST MODEL:SIDE VIEW

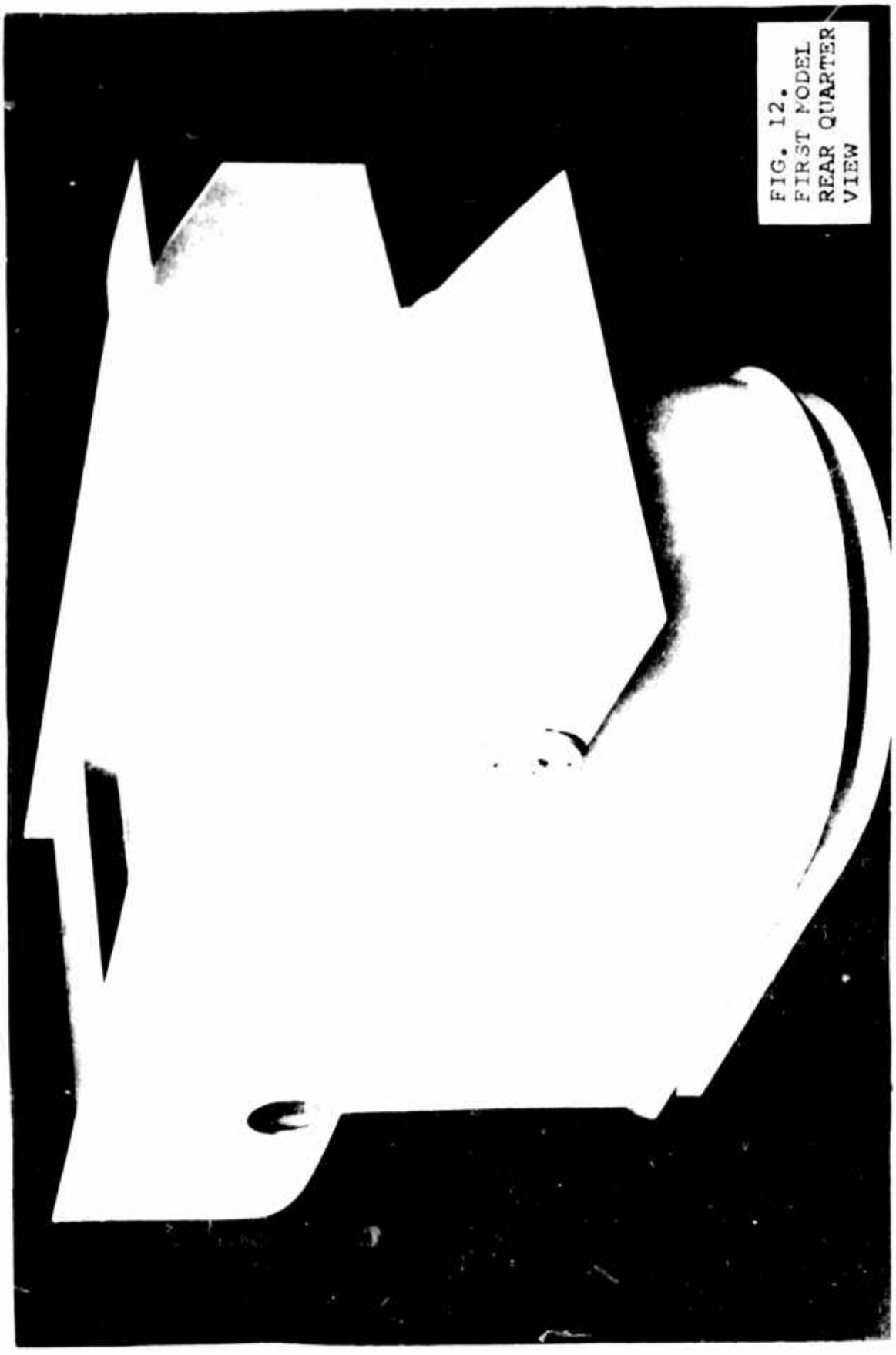

FIG. 12.
FIRST MODEL
REAR QUARTER
VIEW

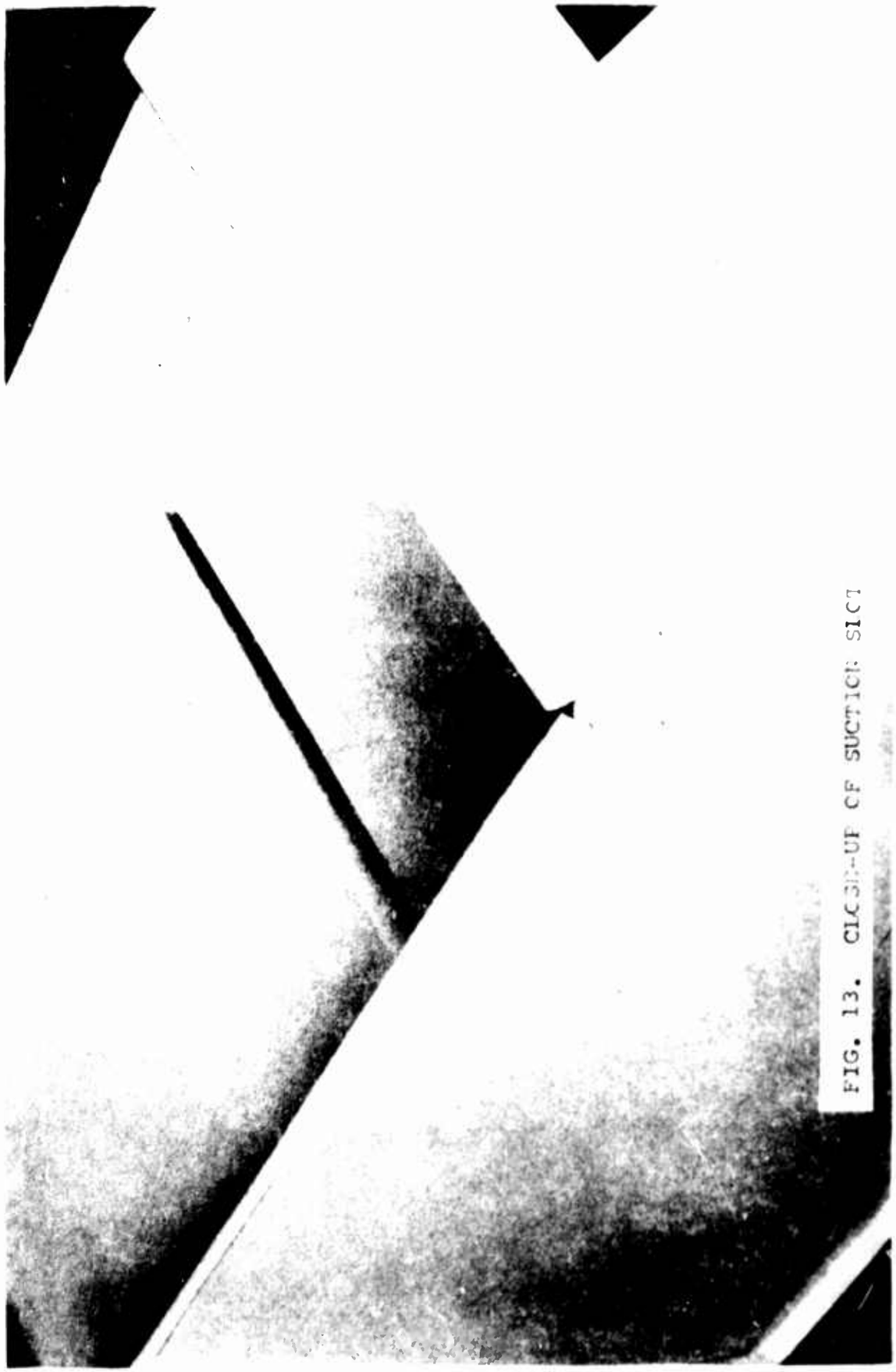

FIG. 13. CLOSE-UP OF SUCTION SLOT

duct containing the engine.

Fan Ducts. The fan ducts were designed with three objectives: to obtain an economical duct, low loss in total pressure, and, to deliver symmetrical flow to the lifting fans.

The basic approach was to continue the rectangular portion of the duct until the turn was completed. Turning vanes would be necessary to avoid asymmetric loading of the fan. After the turn the transition to a circular cross-section would be rather than direct the flow directly downward it was decided to turn the flow through an angle of only 82 degrees. If the flow were turned 90 degrees, then when the vehicle was in a take off position, 8 degrees, the momentum of the lift air and the

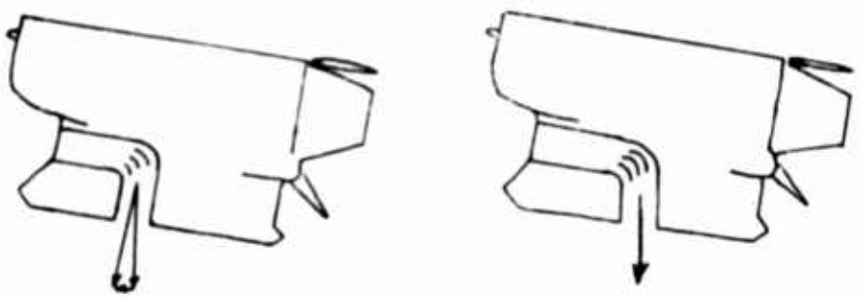

90° TURNING ANGLE

82° TURNING ANGLE

FIG. 14 FAN DUCT TURNING ANGLES

lift of the fans would contribute a drag force equal to the lift times the sine of 8 degrees, and decrease the net lift by 1.3 per cent. By turning the flow 8 degrees less, the entire momentum lift would be directed downwards and there would be no drag increase. The three turning vanes were positioned to divide the mass flow rate into fourths in the horizontal portion of the duct and to direct the flow into equal areas of the lower circular portion. This scheme will achieve a constant mass flow rate per area across the lift fans.

The mass flow rate per area in the horizontal portion was assumed to a constant across the duct, except in the boundary layer. The thickness of the boundary layer and the mass flow rate in the boundary layer were calculated using the same technique previously mentioned in the design of the suction slot.

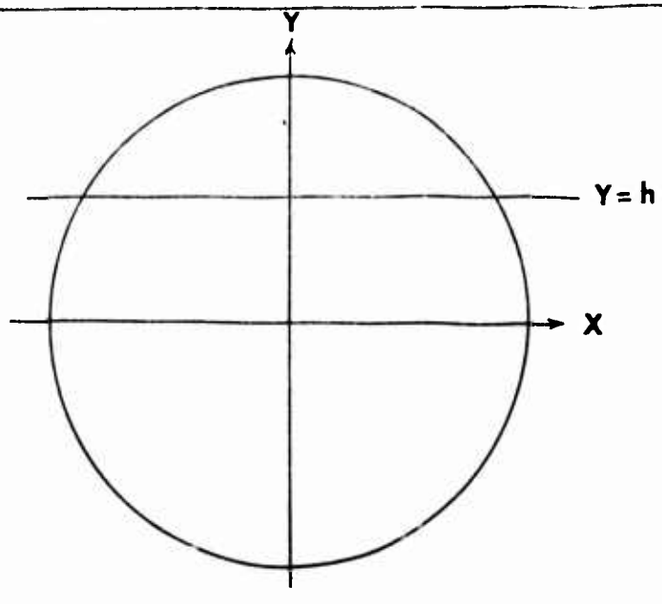

FIG. 15 COORDINATE SYSTEM

The area of circular portion was simply divided into fourths by direct integration, using the coordinates of Fig. 15. The area between y = h and the x-axis was found to be

$$A = h\, r^2 + r^2 \text{ arc sin } h/r \qquad (17)$$

The area was set equal to one-fourth the total area and h was found to be 0.402r. This dimension was used to fix the position of the trailing edges of the turning vanes. The vanes were made circular for ease of fabrication. The best fitting radius was determined by graphical layout, and the cross section was NACA 0006 coordinates laid out radially about this mean radius.

The transition section was designed by graphical layout. The thickness of the transition section was arbitrarily set at 3/4 inches, because this is the standard thickness of the wood sections used in the AFIT shops.

Propeller Duct. The first layout revealed that if the dimensions of the original design were unchanged, the propeller would not be symmetrically loaded. This was corrected by two decisions.

The location of the lift fans were moved forward 1.5 inches on the model (7.5 inches full scale) to smooth the duct contours near the propeller. The minimum width of the propeller duct must occur at the maximum width of the fan ducts. By moving the fans forward, the minimum width of the propeller duct was moved further away from the maximum

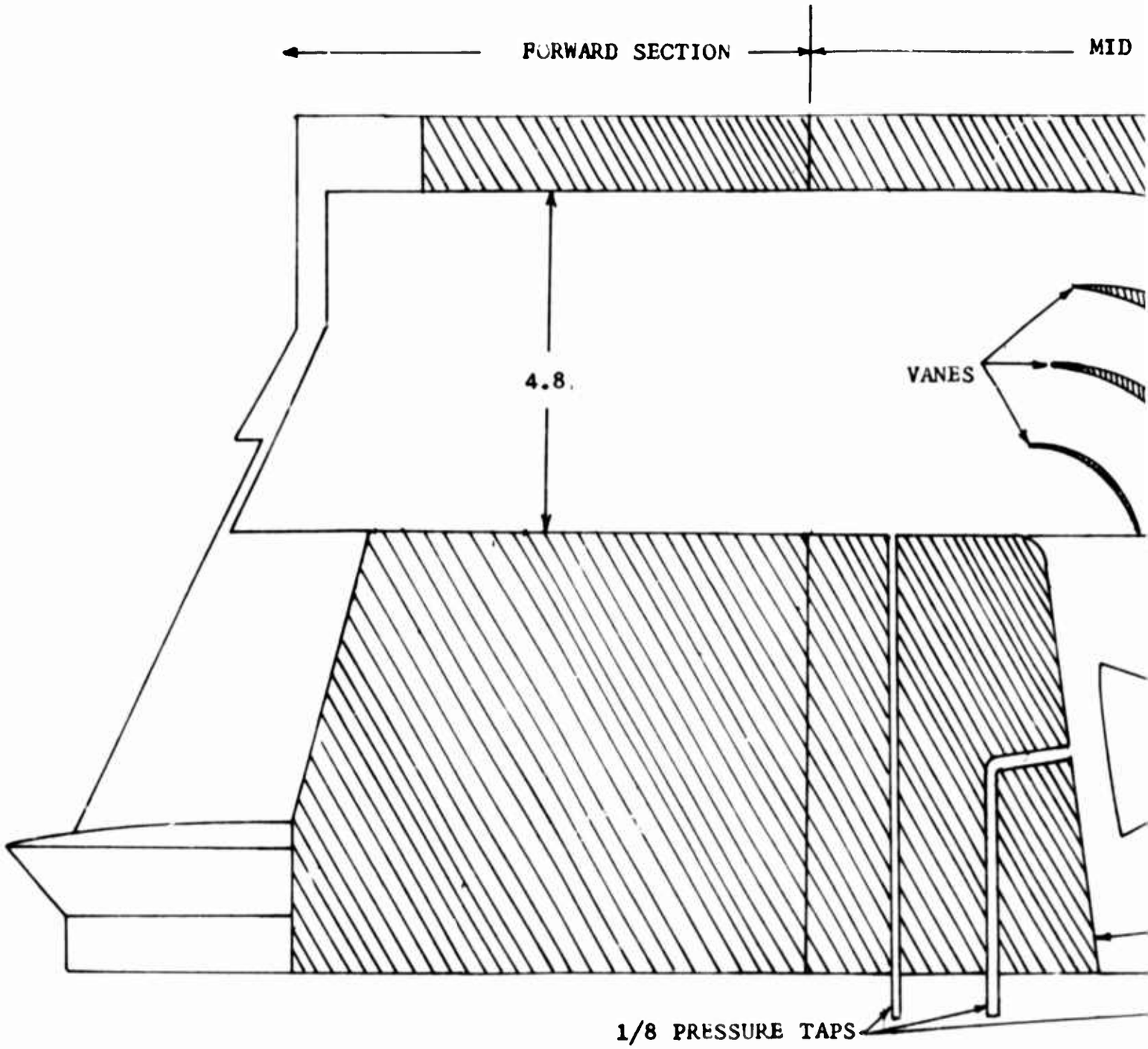

FIG. 16 SECTIONAL VIEW

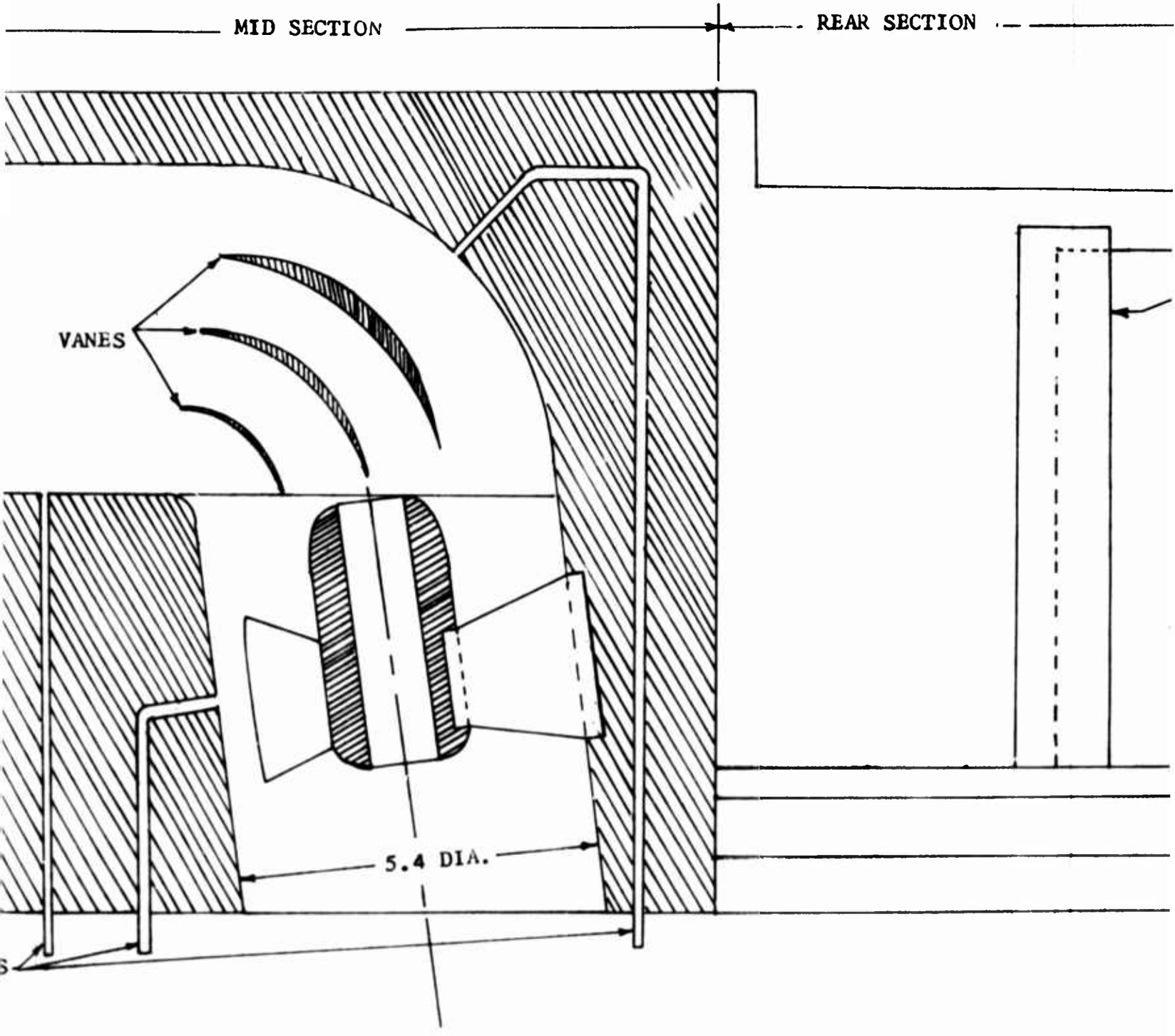

6 SECTIONAL VIEW OF FAN DUCT IN SECOND MODEL

SCAL

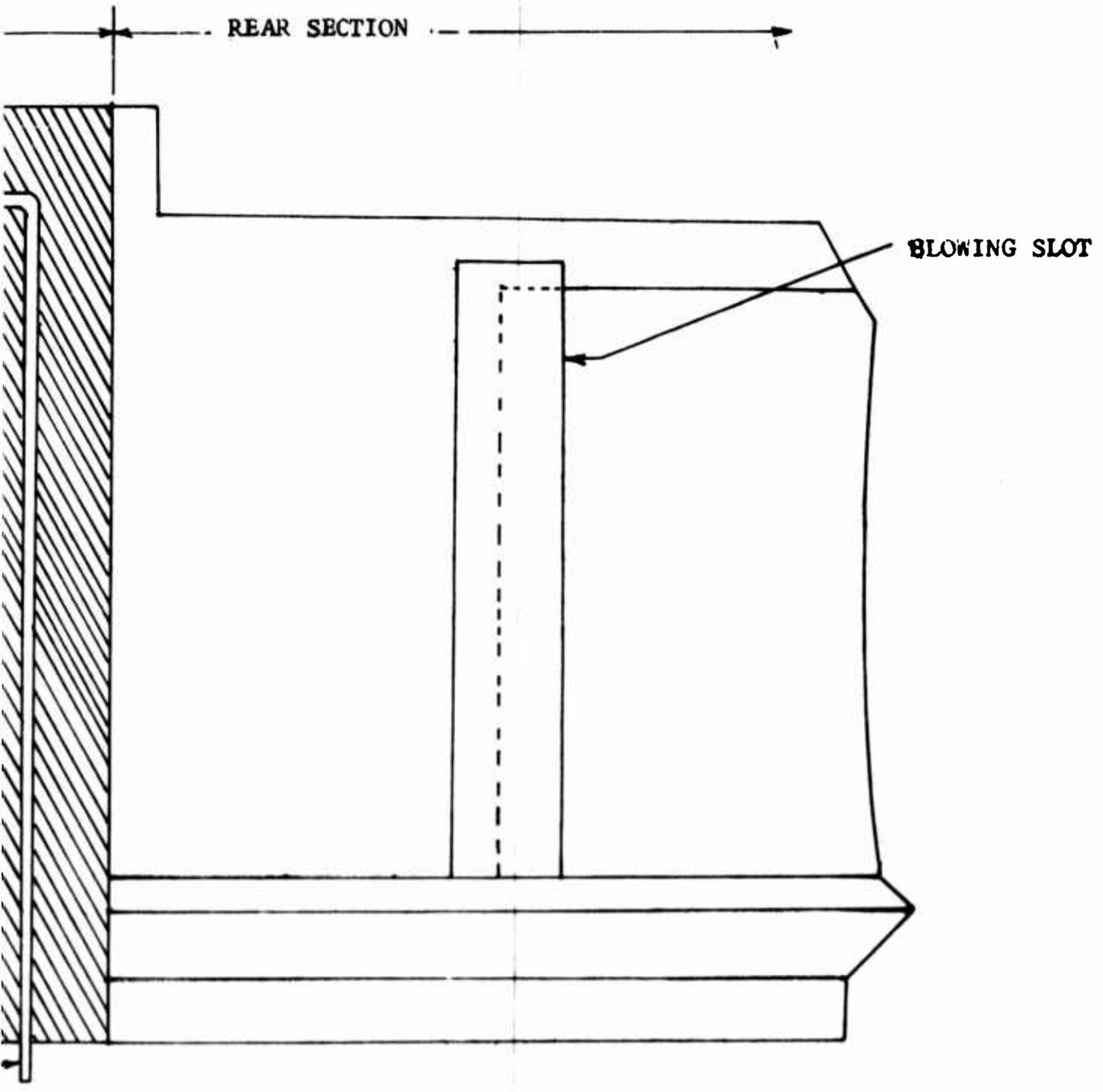

DEL

SCALE: ½ ALL DIMENSIONS IN INCHES

width of the propeller duct. The move allowed better contours in the sections immediately preceding the propeller.

The second decision was to move forward the point where the constant area portion of the duct ends. In the original design, this point was only two feet in front of the propeller. A turning vane was required in the duct. By moving the "break point" forward to the front leg of pilot's seat, the contours could be made so gradual that a turning vane was unnecessary.

The contours of the duct were determined by a graphical method. Forward of the propeller, three dimensions were known: the propeller diameter, the minimum width, and the inlet size. The cross section at the break point is identical to the inlet. The top of the duct was established by drawing a straight line from the break point to the section in front of the propeller. The duct was divided into three section (see construction below) and a rectangular cross section was maintained until the end of the forward section. The mid section was divided in 3/4-inch-sections. The propeller was at section 12 and the fans at section eight. These sections were superimposed on each other and the area between the sections equally divided to obtain the smoothest contours possible. For example, the construction of section eight is shown in Fig. 17. Section zero was overlaid on section twelve, the maximum diameter. The width of section eight was laid out on the drawing. The lower contour of section was a curve

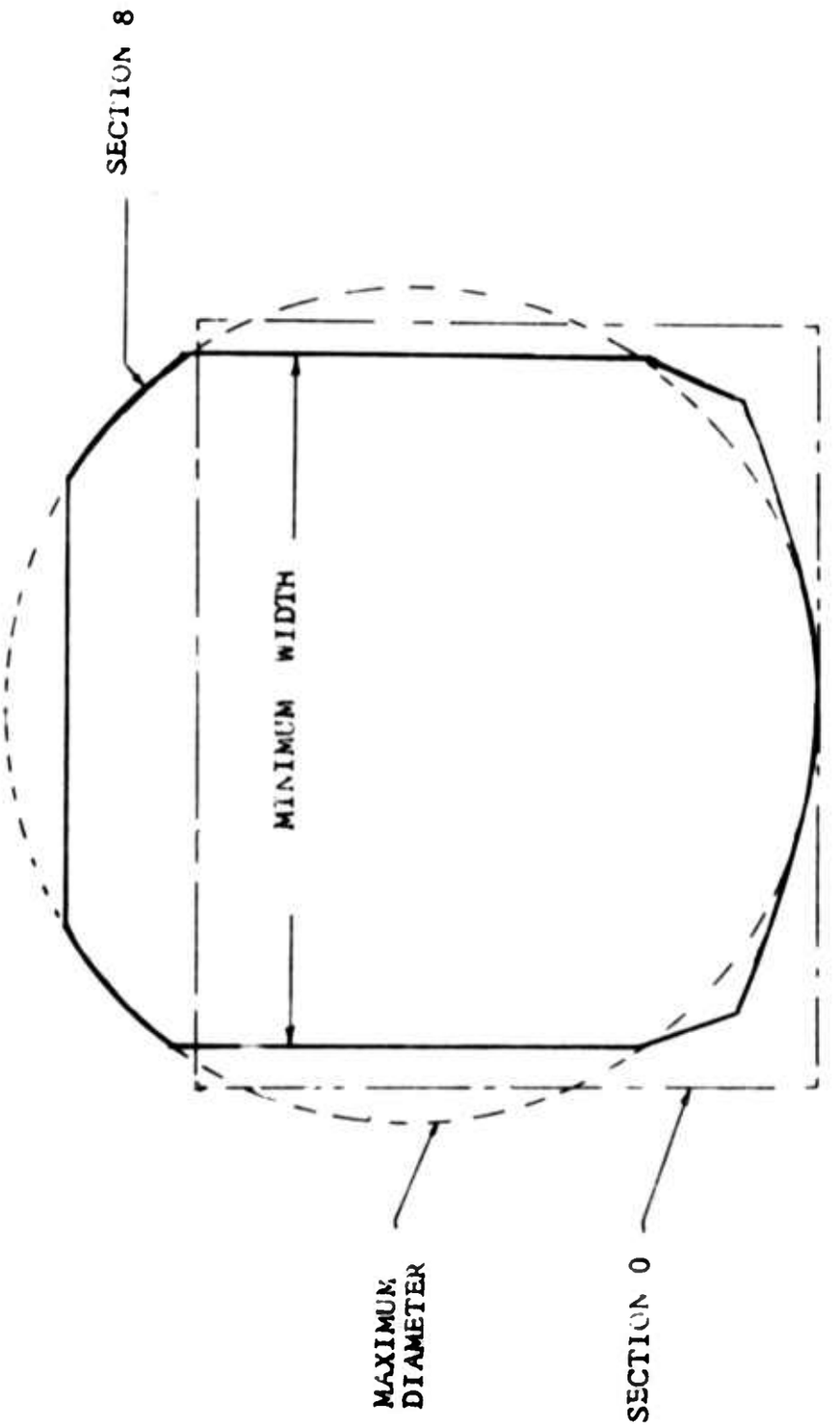

FIG. 17 CONSTRUCTION OF CONTOUR OF SECTION 8

fitted through points 2/3 of the way between the contours of sections zero and twelve. The upper contour was established by a straight line through a point 2/3 of the distance between the height of sections zero and twelve.

The other sections were constructed in a similar manner. The result was a duct of gradual changes which will give symmetrical loading on the propeller.

An engine nacelle is included in the propeller duct to simulate the drag characteristic. The nacelle was sized by the practical requirements of the Wankel engine, and the lenght of a transmission necessary to power the lifting fans.

A duct is cut through the nacelle to simulate the air flow requirements of the engine. Five straightener vanes are required to cancel the rotational velocity induced by the propeller. These vanes also serve as engine supports.

Rear Blowing Slot. The original design used a suction slot at the rear of the vehicle to maintain attached flow for increased flap efficiency and reduction of wake drag.

This was changed to a blowing slot. The blowing will accomplish the same objective, but much simpler ducting is possible for blowing than for suction. The high pressure air behind the straighteners could easily be tapped for this purpose. Suction would, at best, require a long duct to a point forward of the propeller. If the pressure differential required for suction is too great, a separate vacuum pump would be required.

The design of the rear slot in the model was begun by assuming that the rear of the model acted as the rear half of a cylinder. Studies have shown that cylinders in high Reynolds number flow tend to have a separation point at 110° (Ref. 3). In this case, the flow would remain attached for 20 degrees beyond the joint between the flat sided portion and the cylindrical portion of the fuselage. It is therefore reasonable to assume that if new air were introduced at this point with a velocity equal to or greater than the initial velocity of the separating flow, then the flow would remain attached for another 20 degrees. If this assumption is correct, then the flow will remain attached until intersecting the exit of the propeller duct.

To design this slot, an arbitrary slot thickness of 1/4 inch was selected. The height of the slot was 7.8 inches. The velocity required was selected as 1.25 times the velocity at the beginning of the curved portion. The C_p of the cylinder at the 90 degree point is -2.36. Therefore the velocity is (at a vehicle of 100 feet per second) $V = 100(-2.36+1)^2 = 185$ feet per second and the required velocity at the slot is $V_s = 125 \times 185 = 232$ feet per second. The velocity in the propeller duct between the straighteners is 146.2 feet per second (see V, Duct Performance). Therefore, the capture area required in the duct is

$$A_{cap} = \frac{A_s V_s}{V_{duct}} = 6.2 \text{ in.}^2 \qquad (18)$$

Rear section, nacelle and fan housings

Mid-section joined to rear section

FIG. 18. SECOND MODEL UNDER CONSTRUCTION

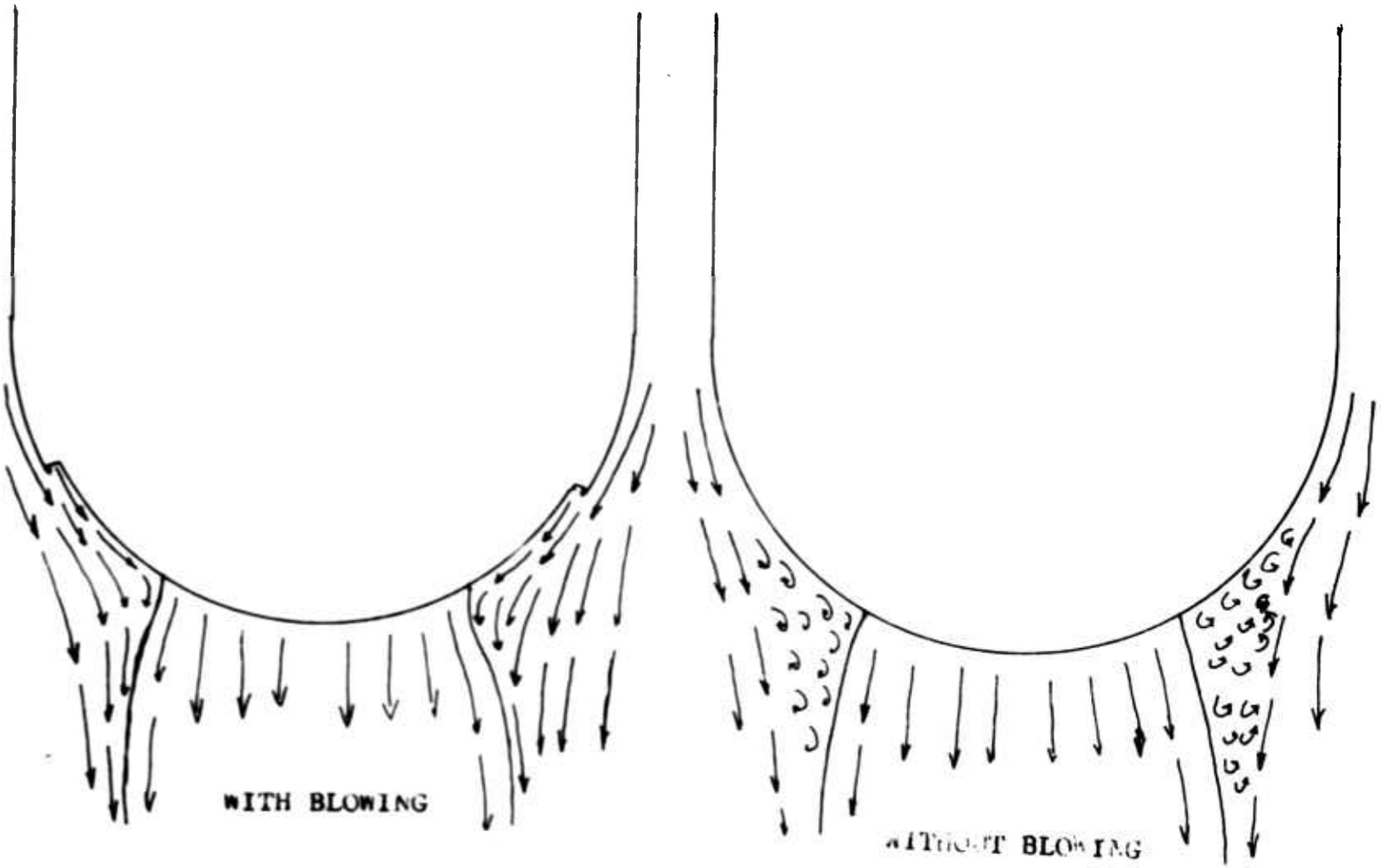

FIG. 19 FLOW PATTERNS WITH AND WITHOUT BLOWING

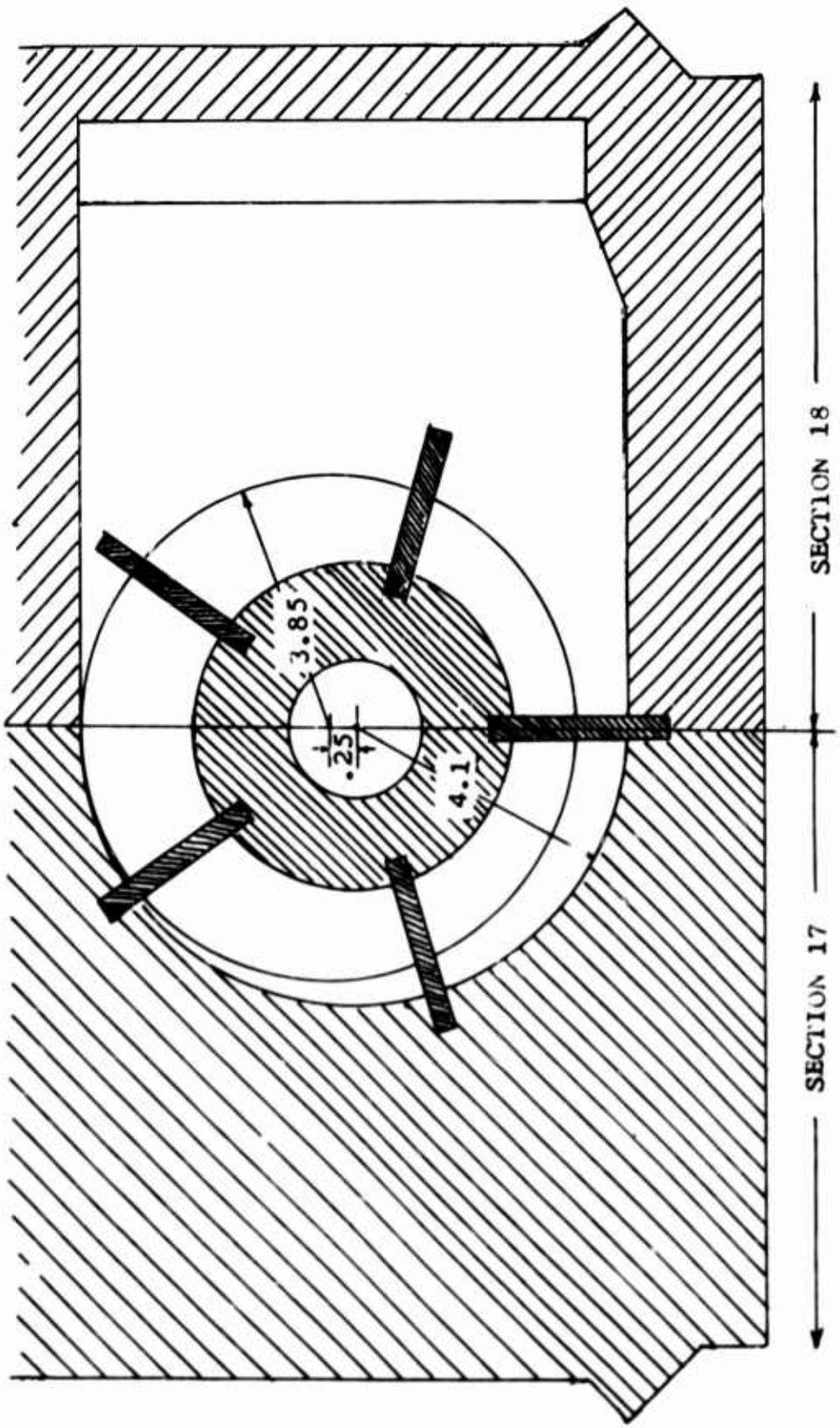

FIG. 20 PICK UP FOR BLOWING SLOT

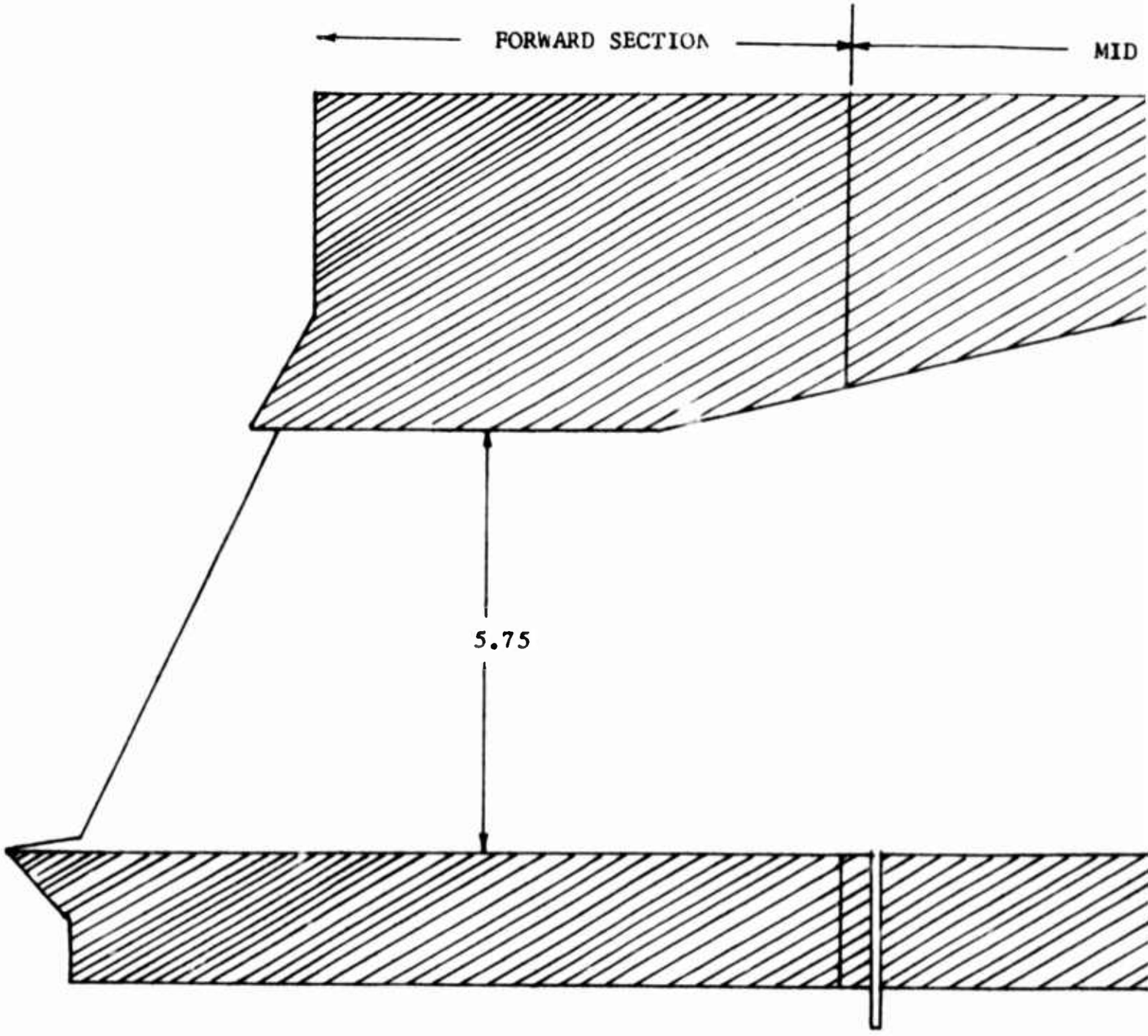

FIG. 21 SECT

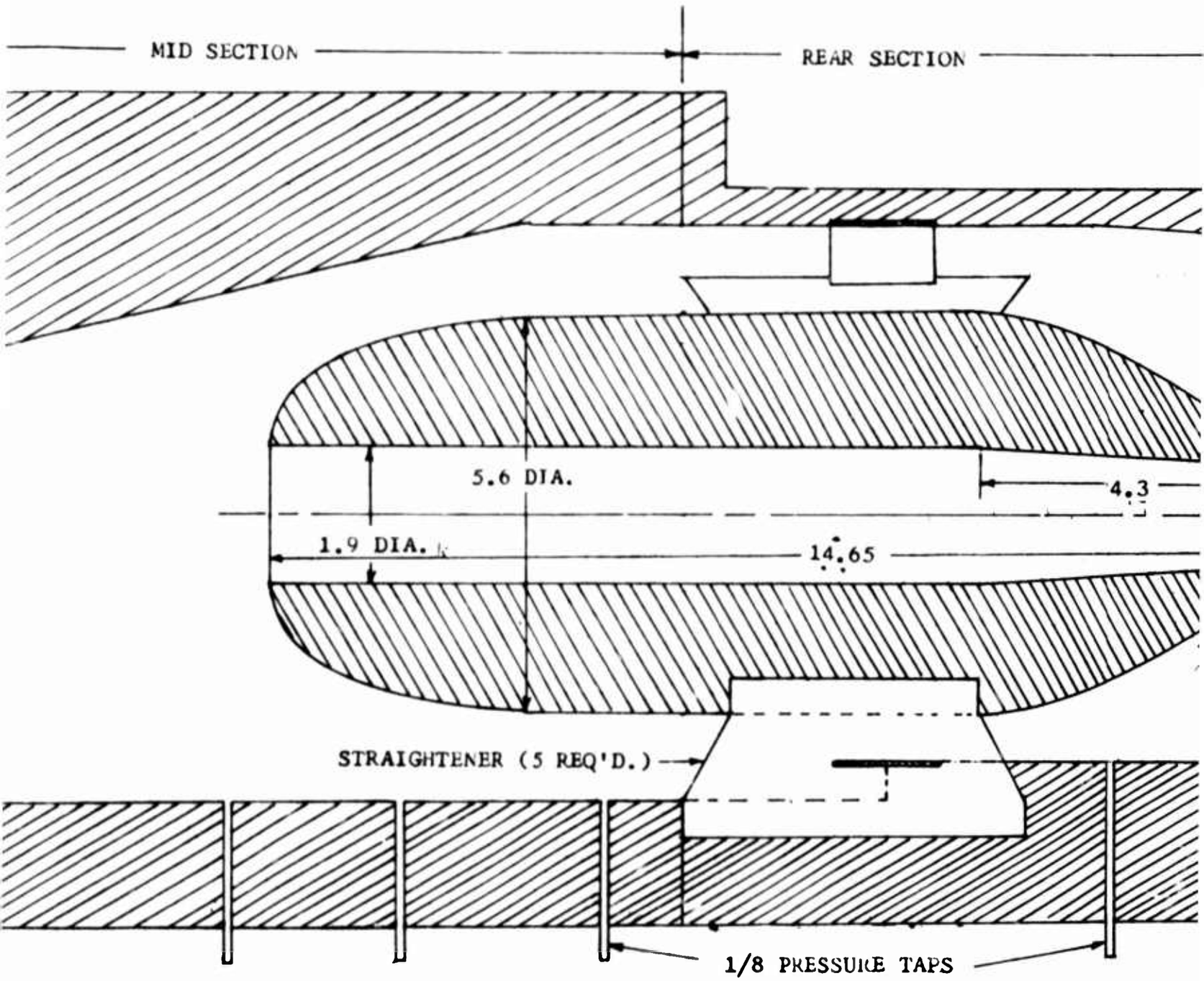

FIG. 21 SECTIONAL VIEW OF PROPELLER DUCT IN SECOND MODEL SCALE: $\frac{1}{2}$ A

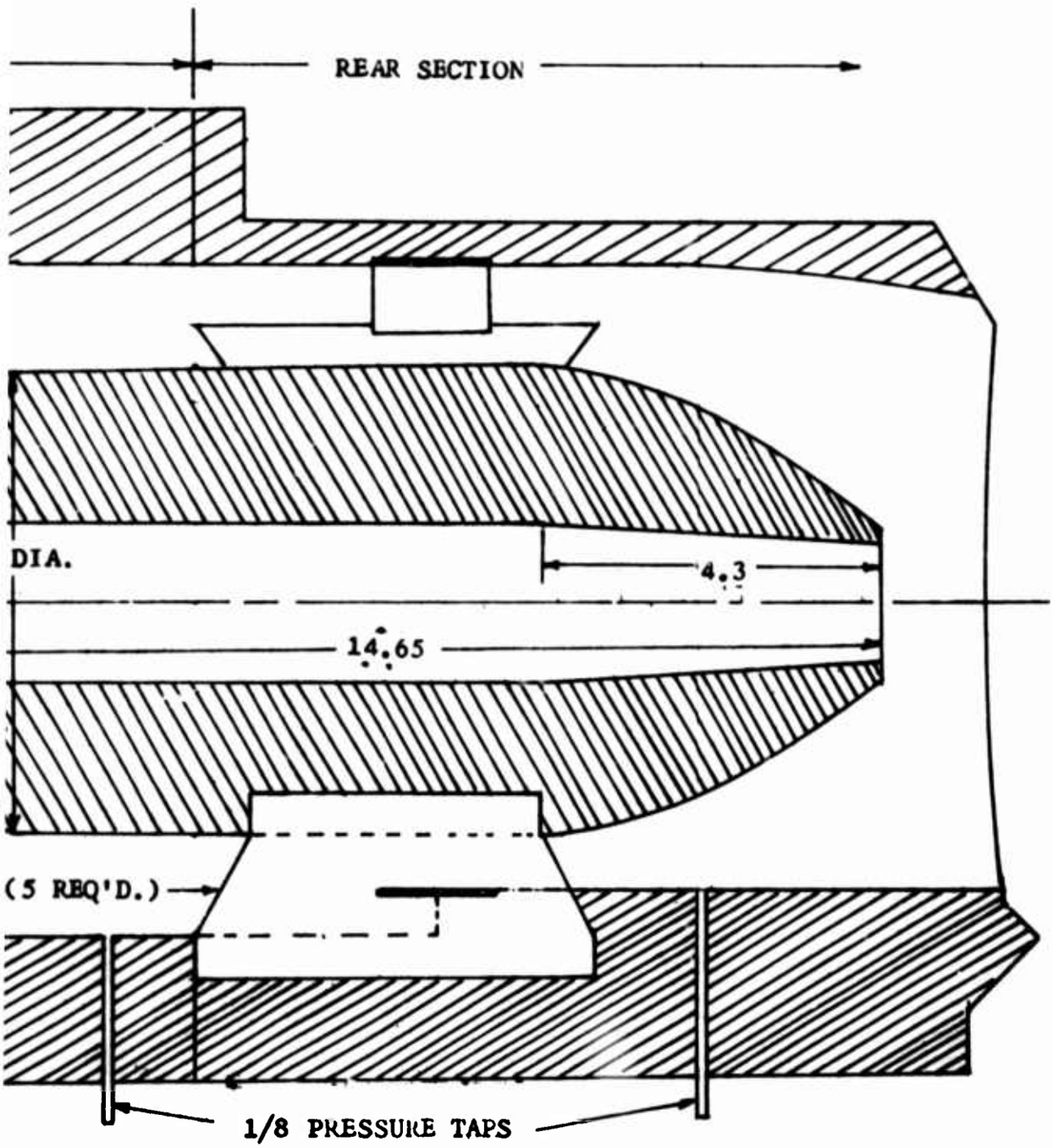

R DUCT IN SECOND MODEL

SCALE: ½ ALL DIMENSIONS IN INCHES

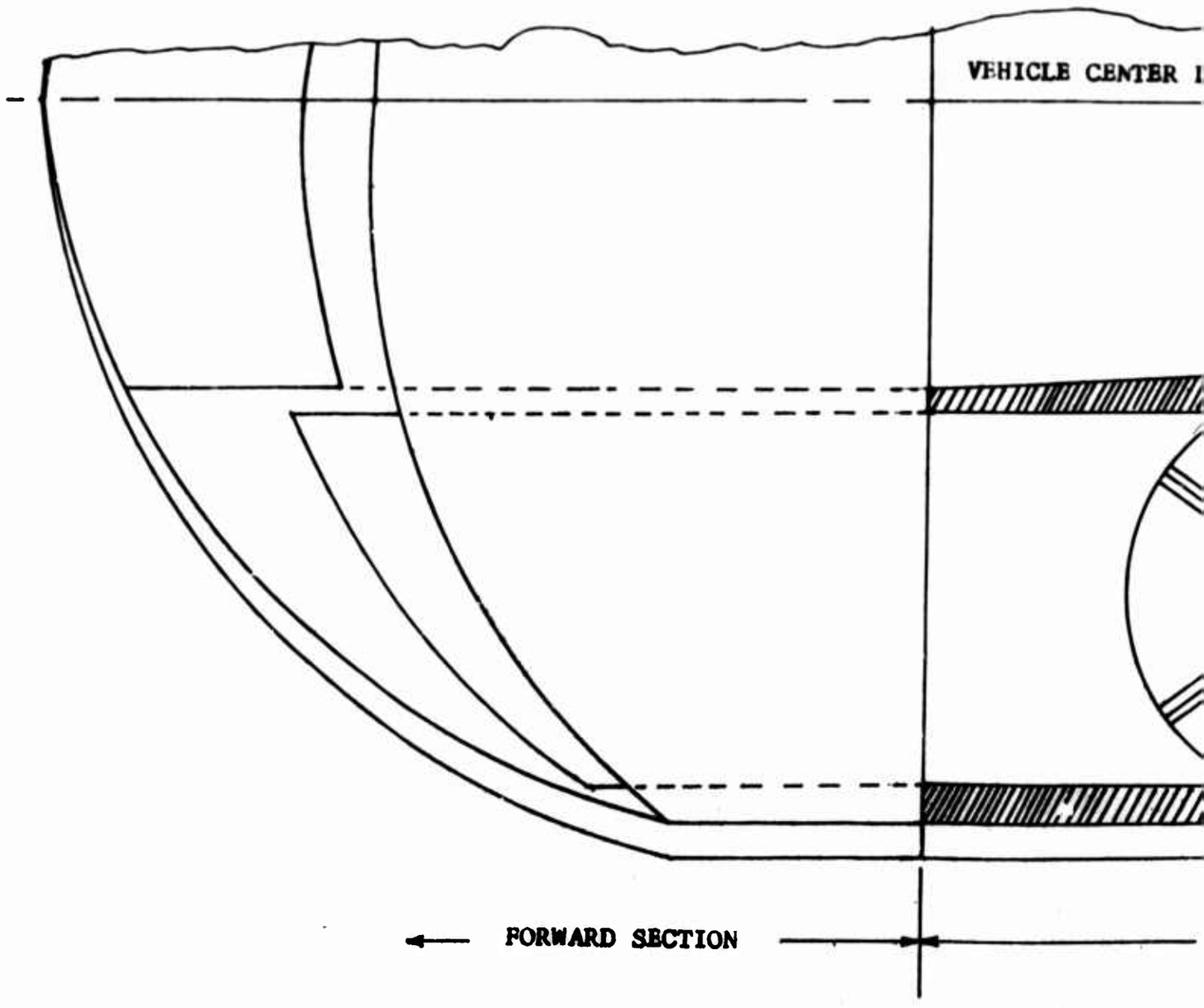

FIG. 22. TOP

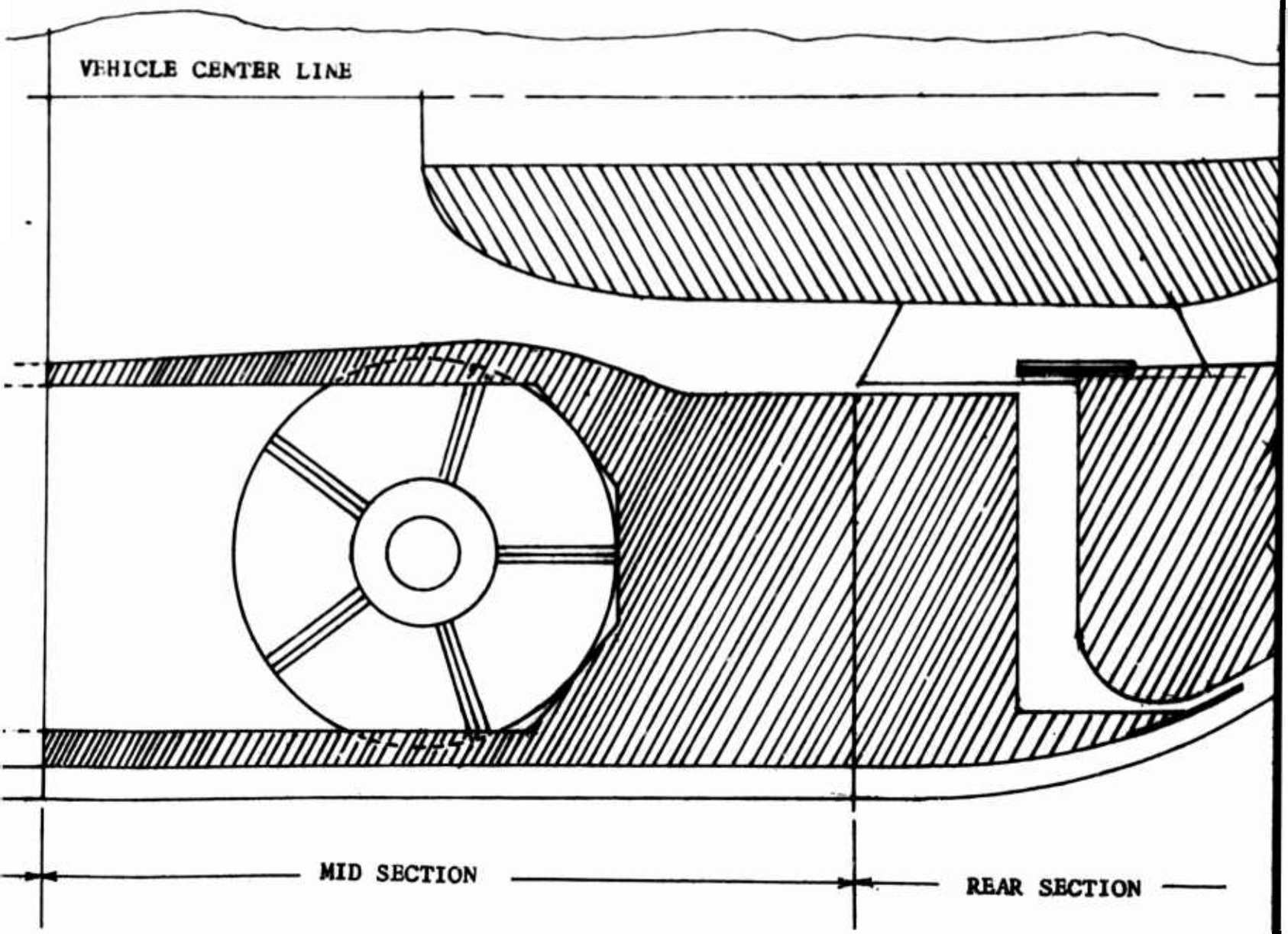

FIG. 22. TOP VIEW OF DUCTING IN SECOND MODEL

SCA

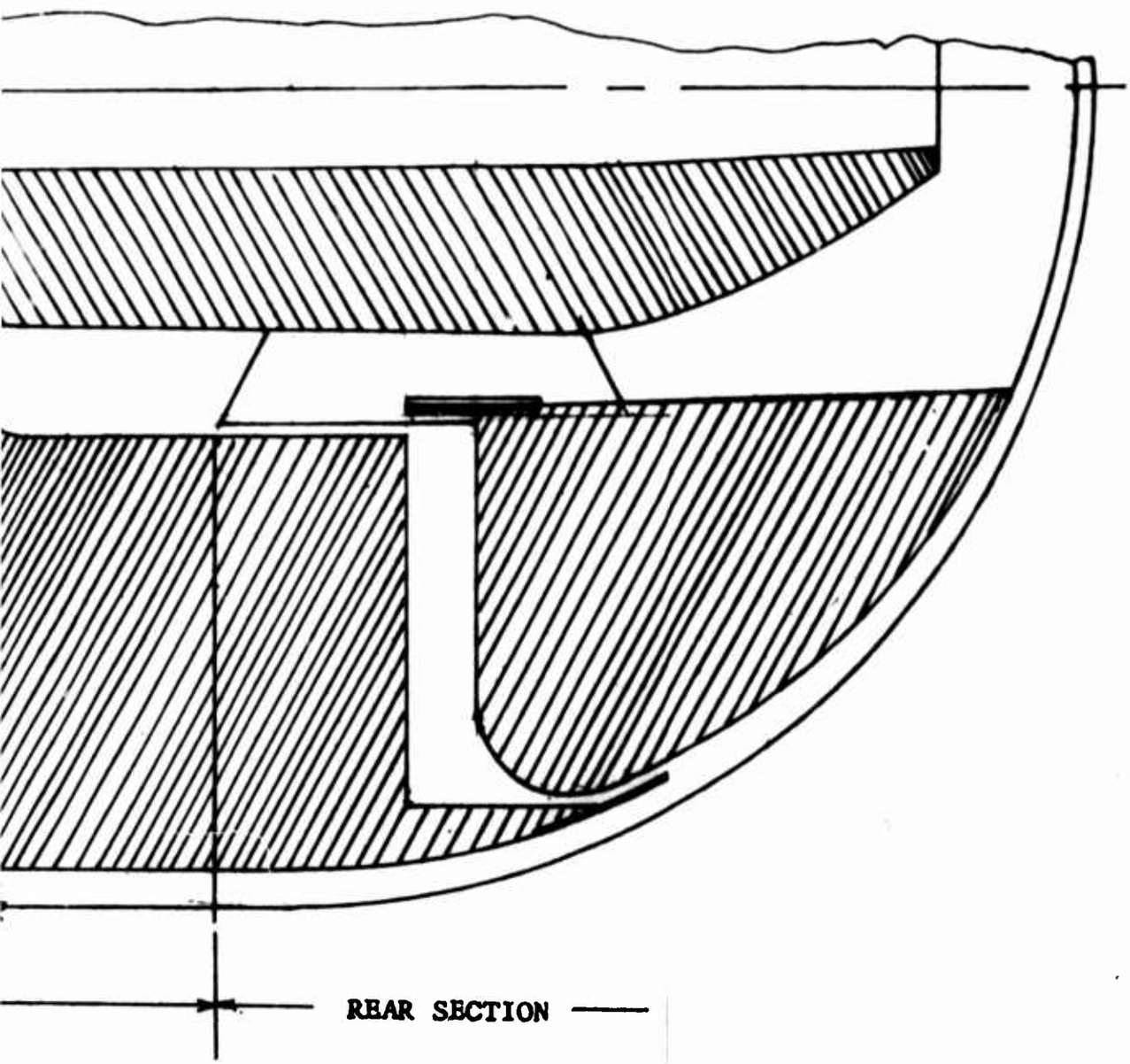

D MODEL

SCALE: $\frac{1}{2}$

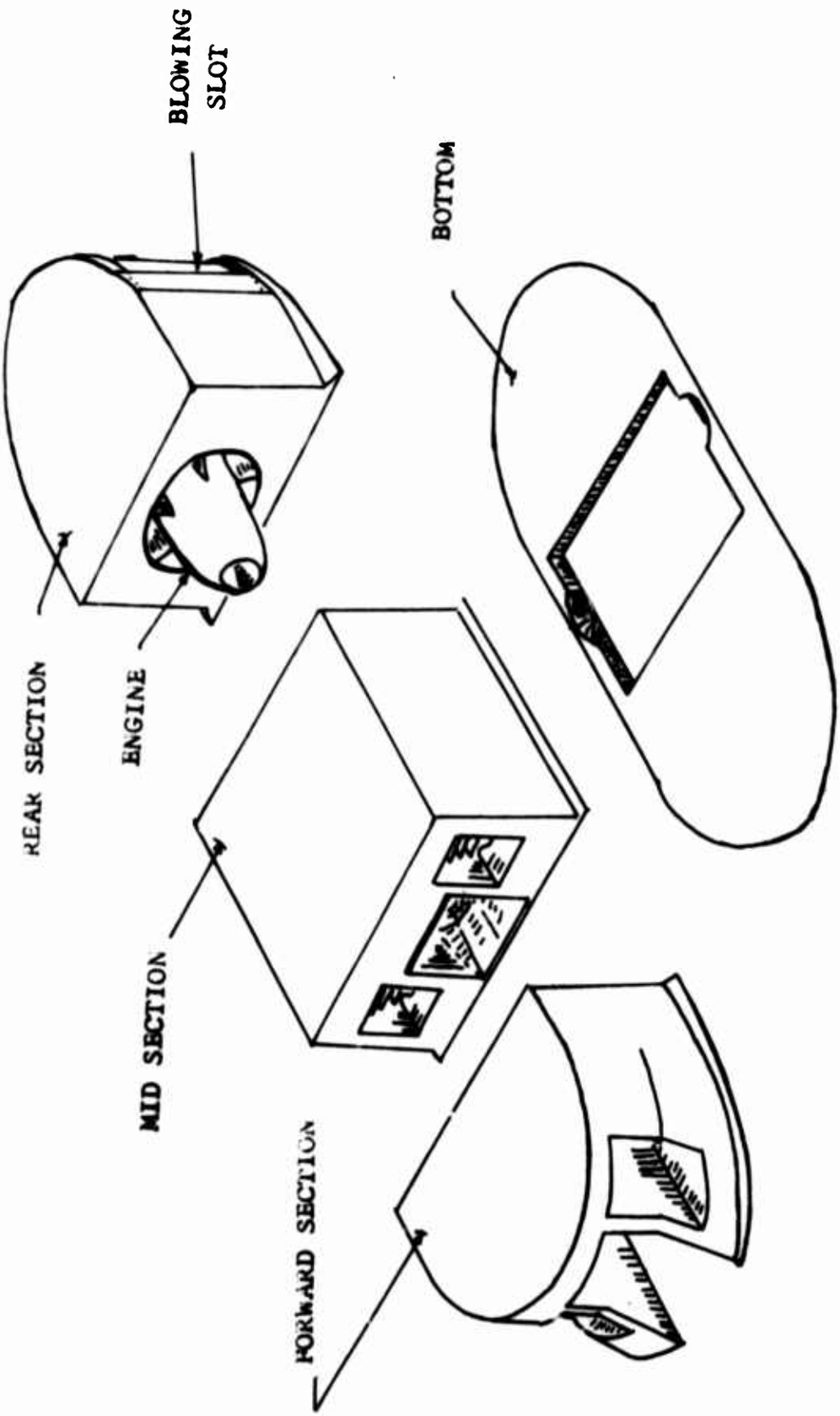

FIG. 23 SECOND MODEL CONSTRUCTION TECHNIQUES

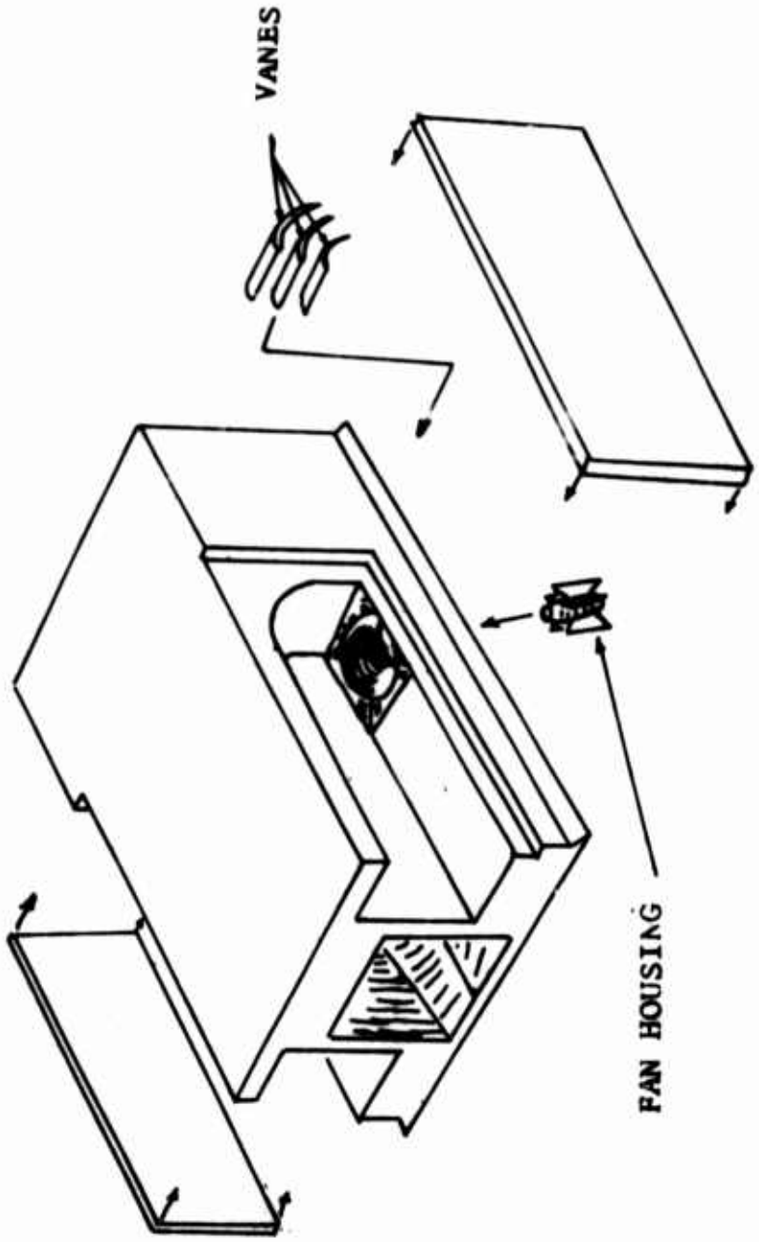

FIG. 24 MID-SECTION CONSTRUCTION

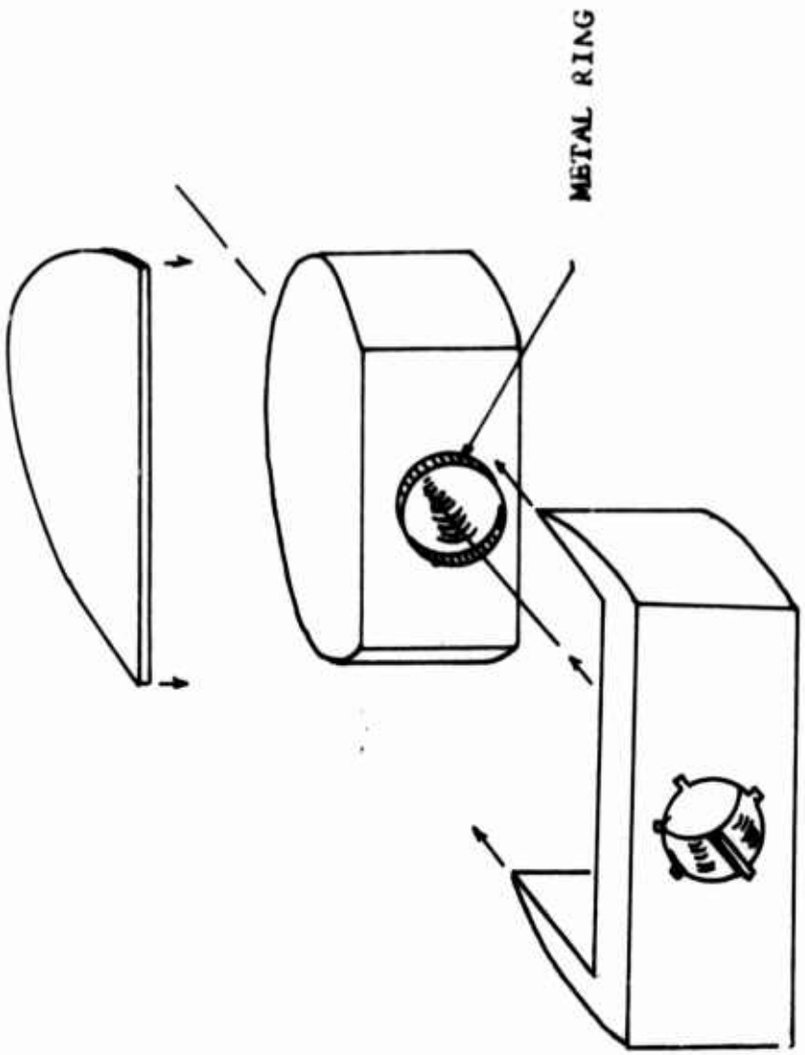

FIG. 25 REAR SECTION CONSTRUCTION

This capture area is shown in Fig. 20. The final configuration of the propeller duct is shown in Fig. 21, and Fig. 22 shows the relative positions of all the ducts in the second model.

Construction. The model was fabricated by dividing the model into sections. The center and rear sections were constructed by laminating 3/4-inch-thick pieces of white pine. The propeller duct contours were cut in each lamination, then after joining the laminations together the duct was hand-sanded until smooth. The front section was built-up of plywood and white pine. The transition sections in the fan ducts were hand carved, and the rest of the model constructed by conventional techniques, such as boring, turning, and shaping.

Design of Test Equipment

Installation. The AFIT five foot wind tunnel uses a wire balance system to measure aerodynamic forces. A schematic of the system is shown in Fig. 26. The model is suspended from the wires and the counterweights are added to place all wires under tension. Prior to each data run, a series of static scale readings were taken at each angle of attack. The differences between the static readings and the readings taken during the data run give the aerodynamic forces.

The attachment fittings were made from standard hardware. Some problems were encountered in installing the

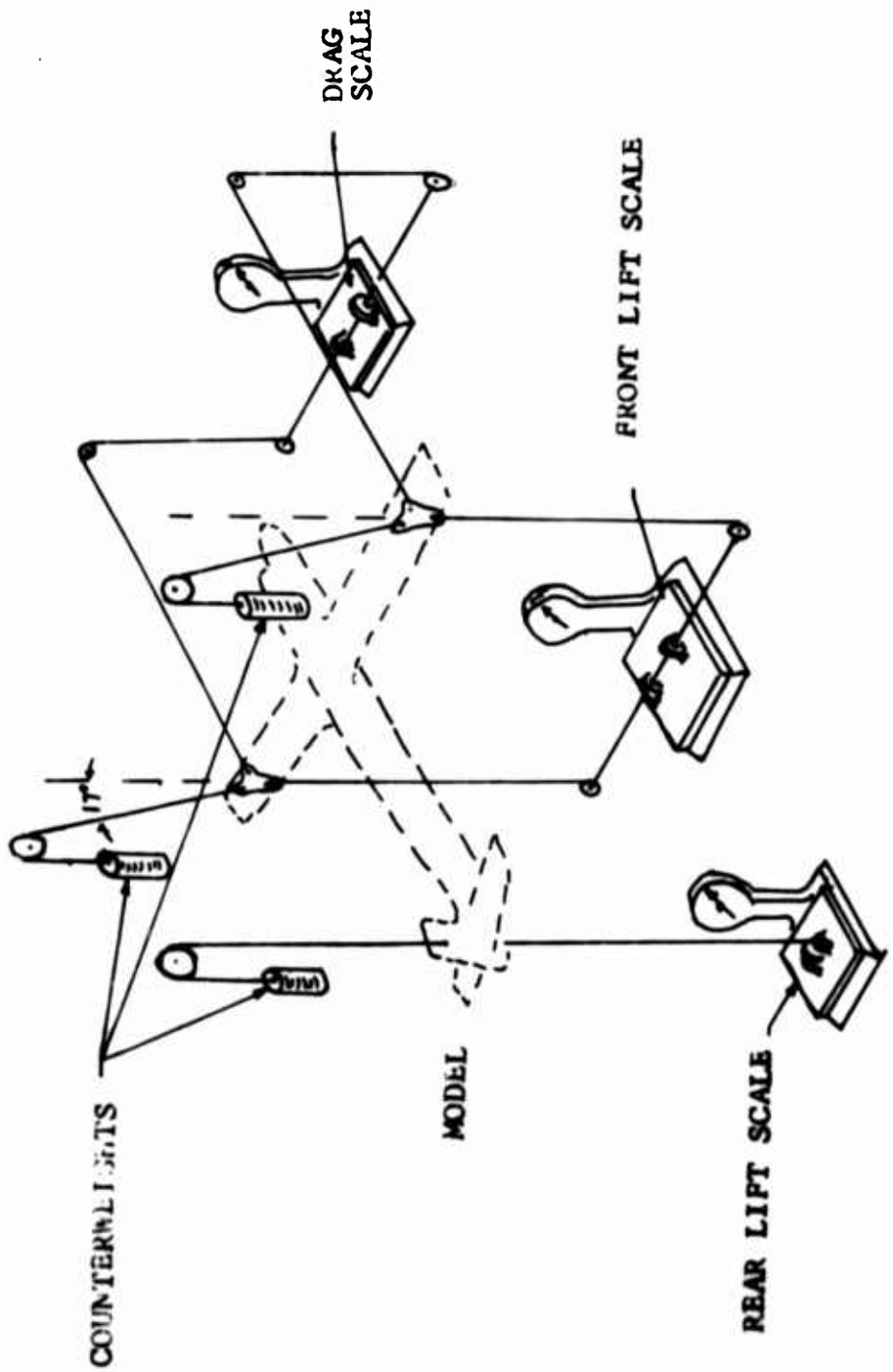

FIG. 26 SCHEMATIC OF WIND TUNNEL WIRE BALANCE SYSTEM

model, particularly with the rear lift scale which must move in order to keep the rear wire always vertical. The problems, though time-consuming and frustrating were minor.

The vacuum system consists of a shop vacuum cleaner, a three inch diameter flexible air hose, and an orifice to measure mass flow rate. The hose diameter was determined from analysis of the mass flow rate required. In order to maintain the assumption of constant density, the Mach number in the hose must be 0.3 or less.

The orifice was designed as specified in the ASME Report on Fluid Flow Meters (Ref. 1). The particular orifice selected was a concentric sharp-edged orifice with a radius ratio of 0.6, and vena-contracta taps were used to measure the pressure differential across the orifice plate. A plot is shown in Fig. 27, which gives the suction coefficient (C_Q) as a function of the pressure differential. The suction coefficient is defined as

$$C_Q = \frac{\dot{m}_{suction}}{\rho} \cdot \frac{1}{S\ V_\infty} \tag{19}$$

assuming constant density this expression can be written as

$$C_Q = \frac{\dot{m}_{suction}}{constant} = f(\Delta p) \tag{20}$$

for the given test velocity of 100 feet per second.

Control of the vacuum system consists of venting the hose behind the orifice. This was accomplished with a

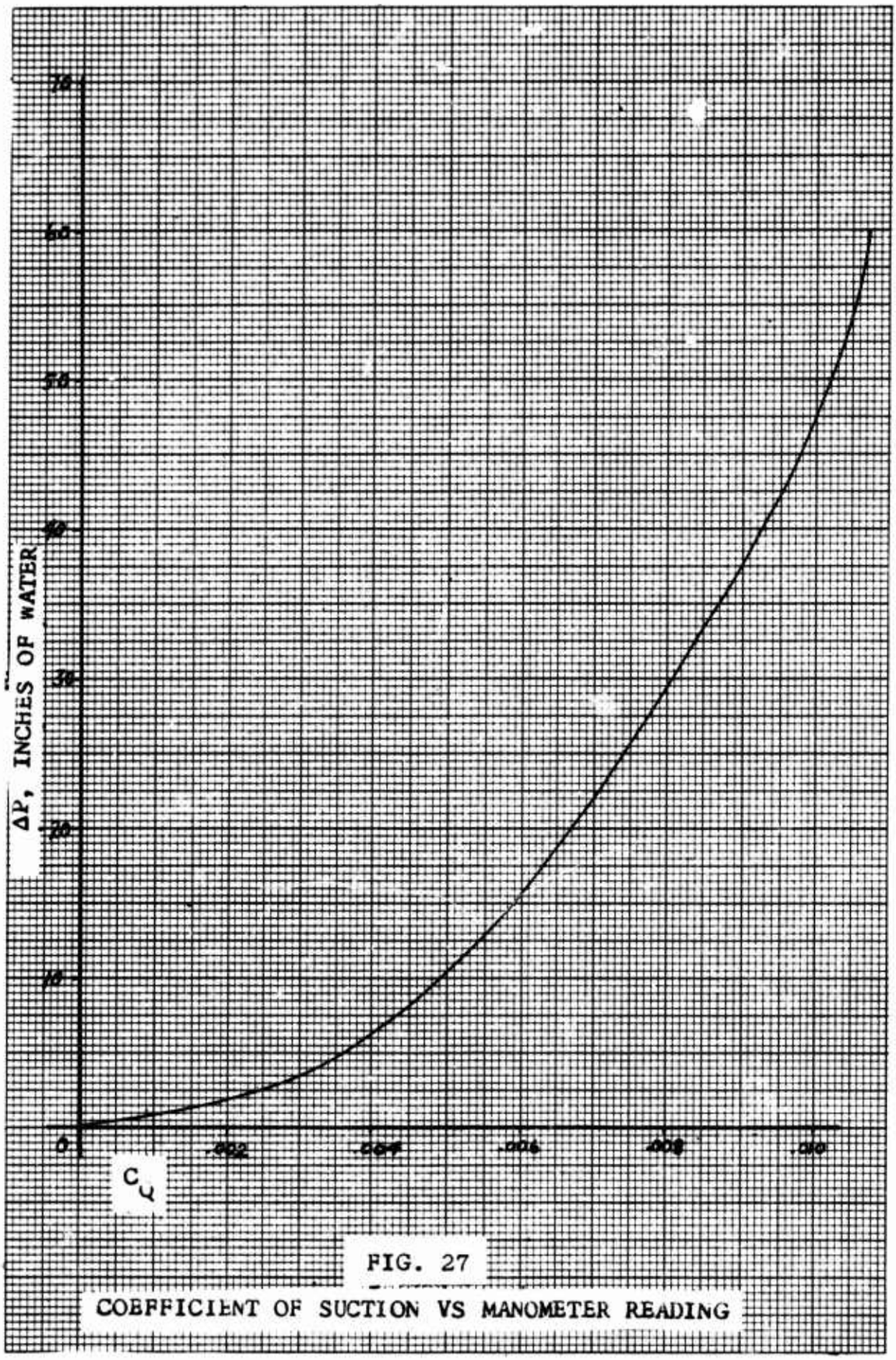

FIG. 27

COEFFICIENT OF SUCTION VS MANOMETER READING

series of holes drilled into the pipe holding the orifice plates. The hose connecting the pipe to the vacuum cleaner can be moved to cover as many holes as necessary to vary the mass flow rate being extracted from boundary layer of the model (see Fig. 28).

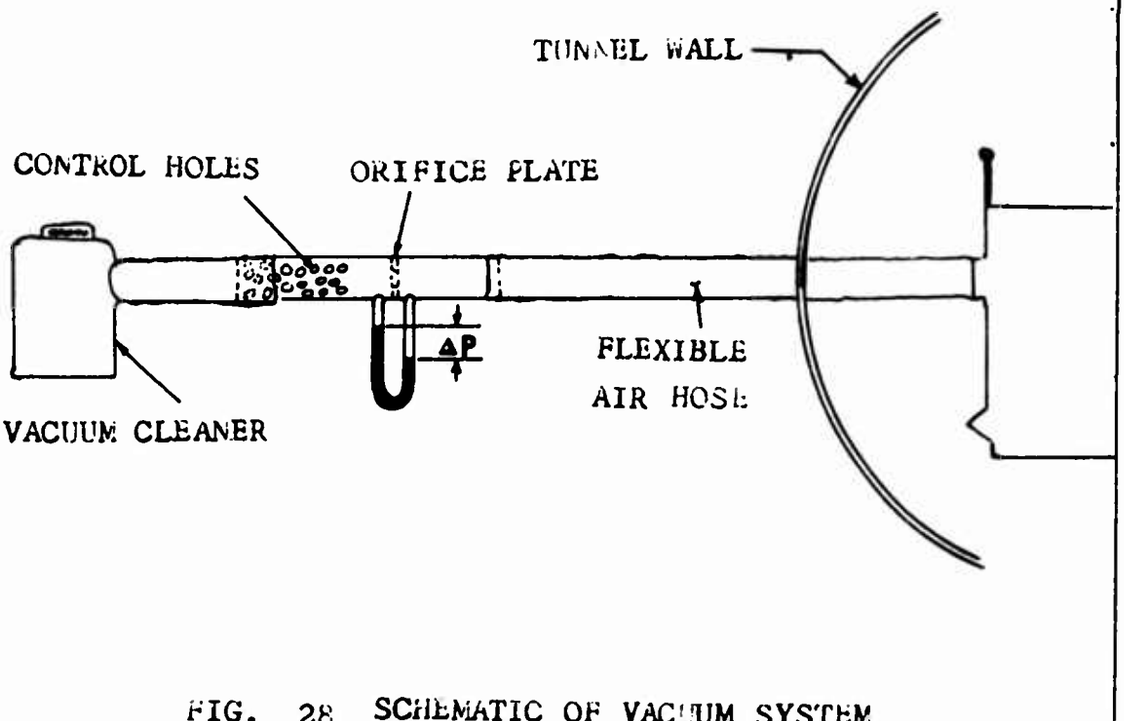

FIG. 28 SCHEMATIC OF VACUUM SYSTEM

The regular door in the tunnel wall was removed during runs with the vacuum system, and replaced with a special door to allow the hose to extend out of the tunnel. The interference of the hose was evaluated by comparing the runs with no hose present, with those on which the hose was present but with zero mass flow rate in the vacuum system. The forces obtained from subsequent runs with suction were then corrected for this interference.

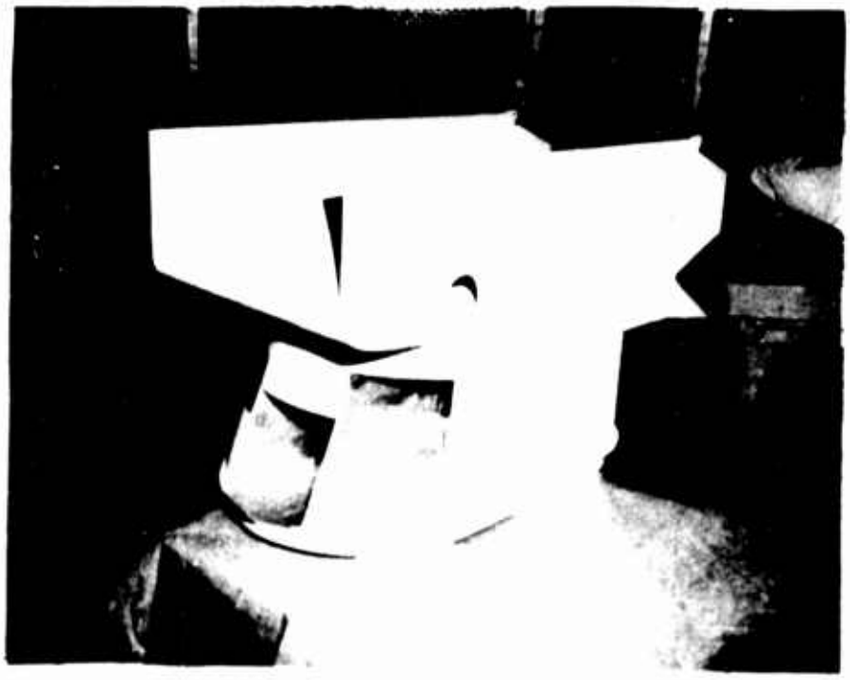

Completed Model, Front Quarter View

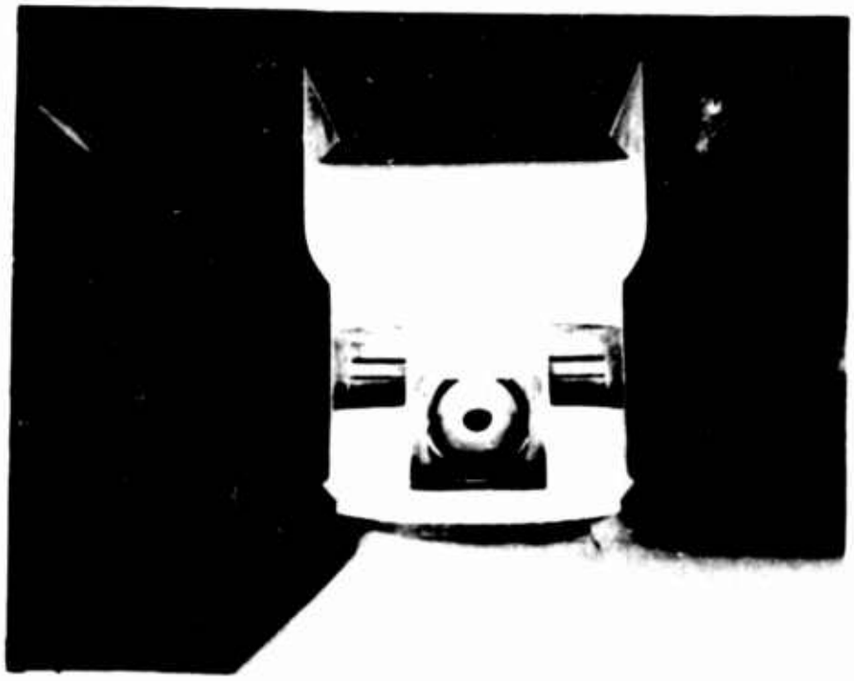

Close-up of Propeller Duct and Fan Ducts

FIG. 29 SECOND MODEL, FORWARD VIEW

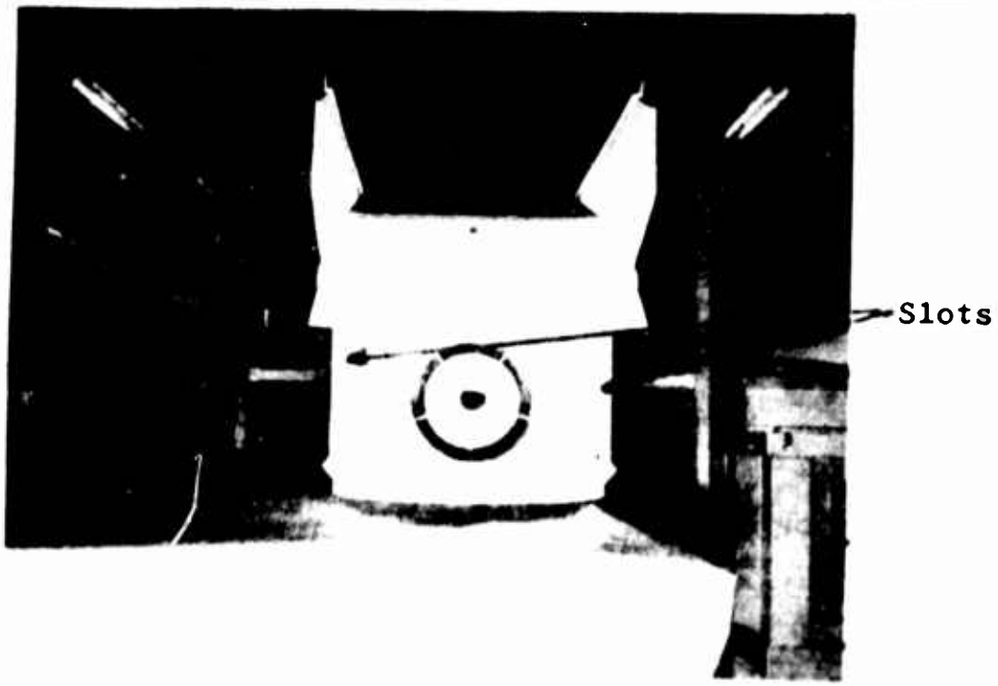

Blowing Slots and Nacelle, Rear View

Bottom View with Fan Duct Exits

FIG. 30 SECOND MODEL, REAR VIEW

V. Results of Wind Tunnel Investigation

Tests in the AFIT 5-foot Wind Tunnel

The test plan was to test the first model to determine the aerodynamic coefficients. Initially the model without the control surfaces would be tested. The next step would have been to deflect the flap through 60 degrees. Each control surface would then be added and its effect on the performance determined. Finally, the suction would be added and its effect measured.

The results of testing on the first model would be evaluated and the second model could be changed as necessary. The second model would be tested on one run to measure any differences. On this run all the ducts would be plugged with clay. On subsequent runs each duct would be opened until the final configuration would be tested. The detail test plan is shown in Table one.

Unfortunately, the unforeseen happened after test number two. A report of the maintenance inspection on the wind tunnel revealed a safety problem in the electrical system of the tunnel. The decision was made to close the tunnel until funds could be obtained for repair and the repairs accomplished. The time required to do this task was such that no further testing could be conducted in the time allowed for this study. Therefore only two data runs were conducted, and the results of these runs are shown in Figures 31 and 32.

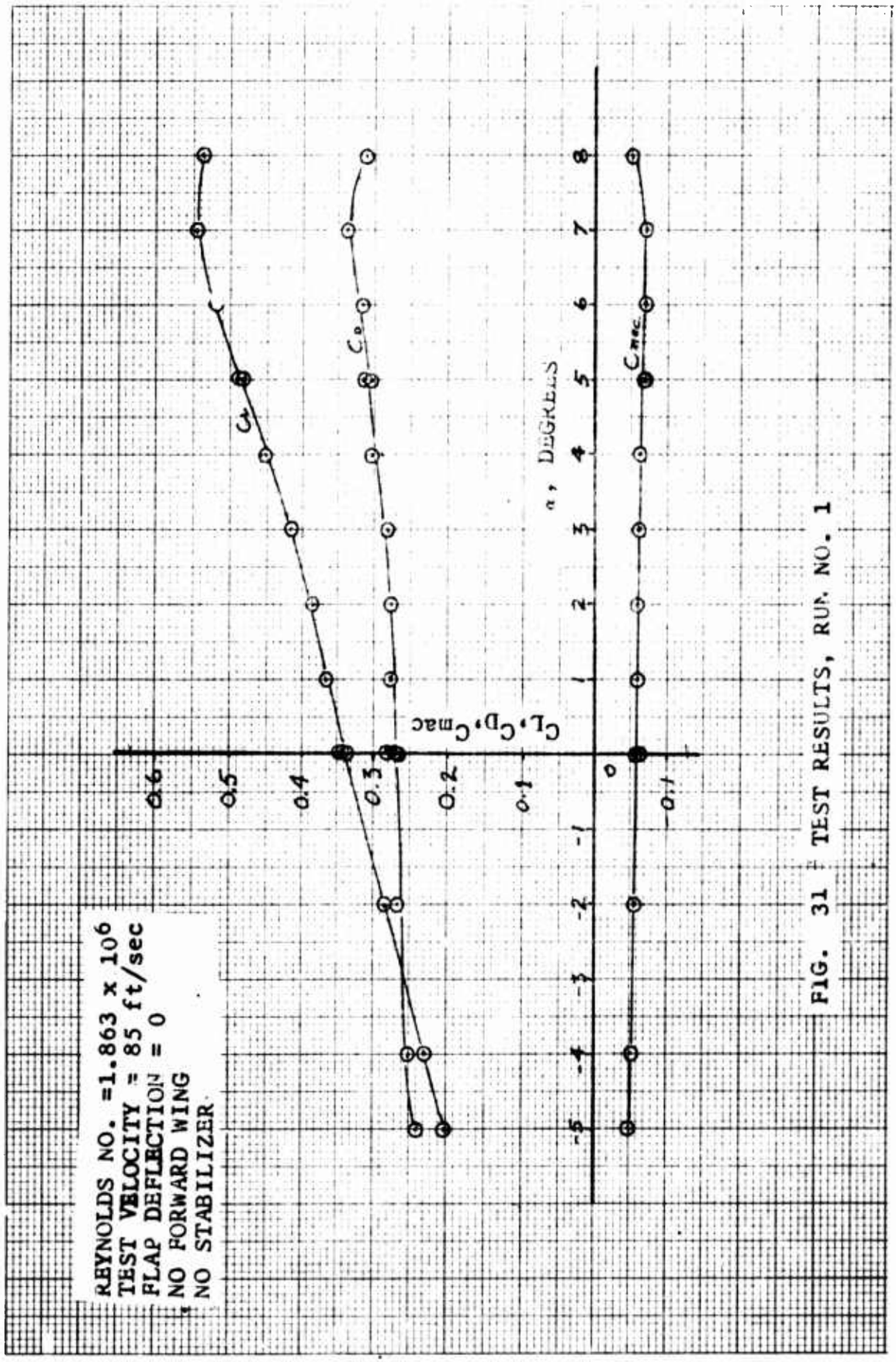

FIG. 31 TEST RESULTS, RUN NO. 1

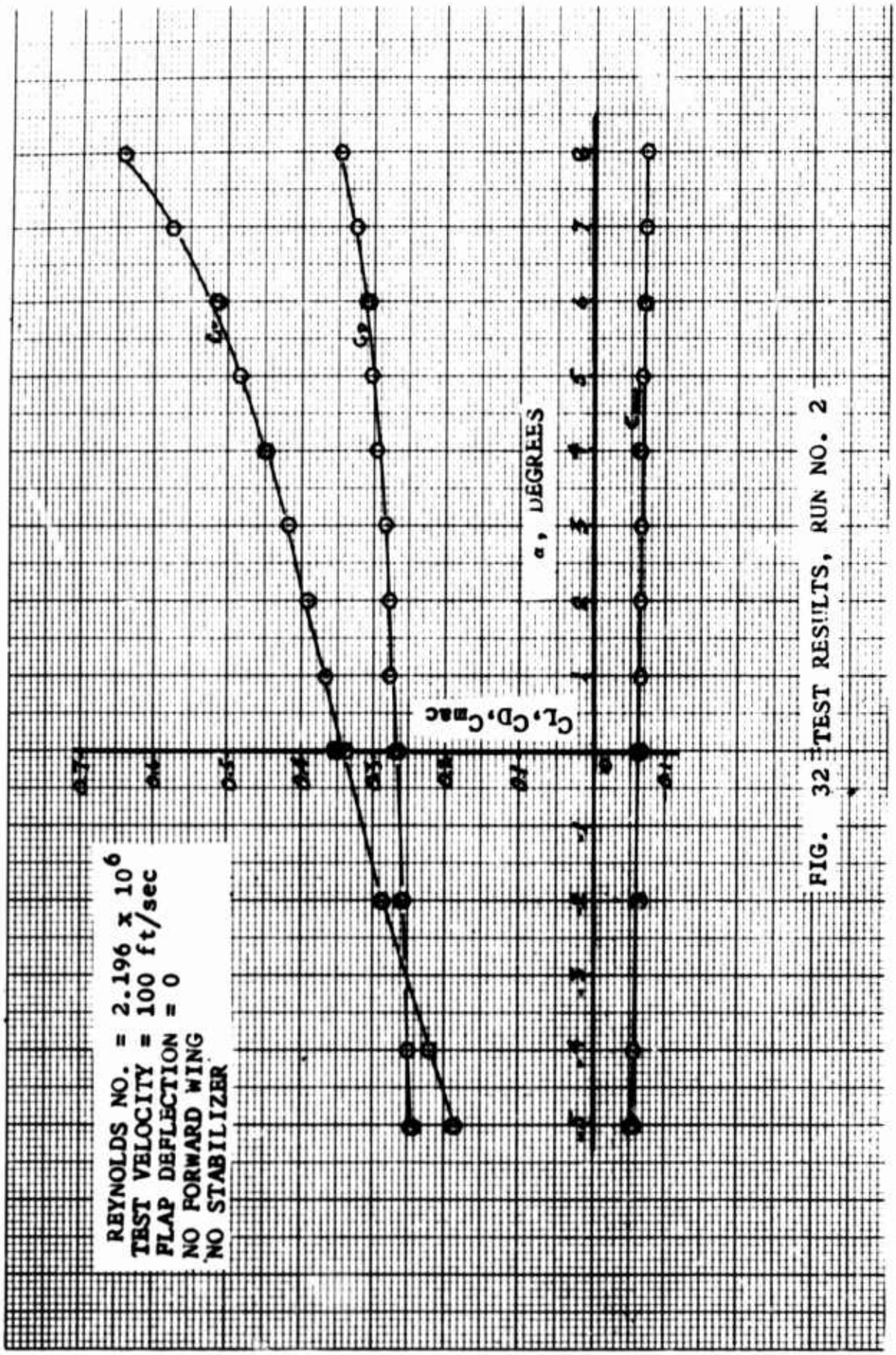

FIG. 32 TEST RESULTS, RUN NO. 2

Table I
Wind Tunnel Test Plan

Test No.	First Model	Sec. Model	Flap Pos.	Forward Wing Position				Stabilizer Pos.	Suction	Prop. Duct Open	Fan Ducts Open	Rear Slot Open	Objective
				1	2	3	4						
1	x		0°										Low Speed "Shake Down"
2	x		0°										
3	x		15°										C_D, C_L, Cmac
4	x		30°										
5	x		45°										C_{O_F} C_{L_F} C_{macF}
6	x		60°										
7	x		0	+0									"
8	x		0	+5									"
9	x		0	-5									"
10	x		0		0								C_{Lf}, C_{D_f}, Cmacf
11	x		0		+5								
12	x		0		-5								&
13	x		0			0							Optimum
14	x		0			+5							Position
15	x		0			-5							of
16	x		0				0						Forward
17	x		0				+5						Wing
18	x		0				-5						
19	x		0	Best Pos.				0					$Cmac_5$ V_s s
20	x					"		+5					
21	x					"		-5					Effect of Suction
22	x		0			"		0	x				Optimum C_Q
23	x		60			"		0	x				
24		x	0			"		0	x				C_D between Models
25		x	0			"		0	x	x			1 & 2
26		x	0			"		0	x	x	x		
27		x	0			"		0	x	x	x	x	
28		x	60			"		0	x	x	x	x	
29		x	60			"		0	x	x	x	x	
30		x	60			"		0	x	x	x	x	Final repeat run

The results of the test, while not inspiring were promising. It appears that slight separation occurred on run number one, but not on run number two, at the higher Reynolds number. The C_L was low, but not too low to preclude flight. The C_D was high, but still low enough to establish the feasibility of the vehicle. In summary the data was very promising, but left something to be desired.

The C_L reached a value of 0.640 at a vehicle angle of attack of 8 degrees. The increasing slope of the lift curve is typical of very low aspect ratio wings and indicates that no separation is present. Lampros gives the relationship between C_L and α as

$$C_L = a\alpha + C_1\alpha^2 \qquad (21)$$

where a is the slope of the lift curve as predicted by linear theory and C_1 is a function of aspect ratio (Ref 11).

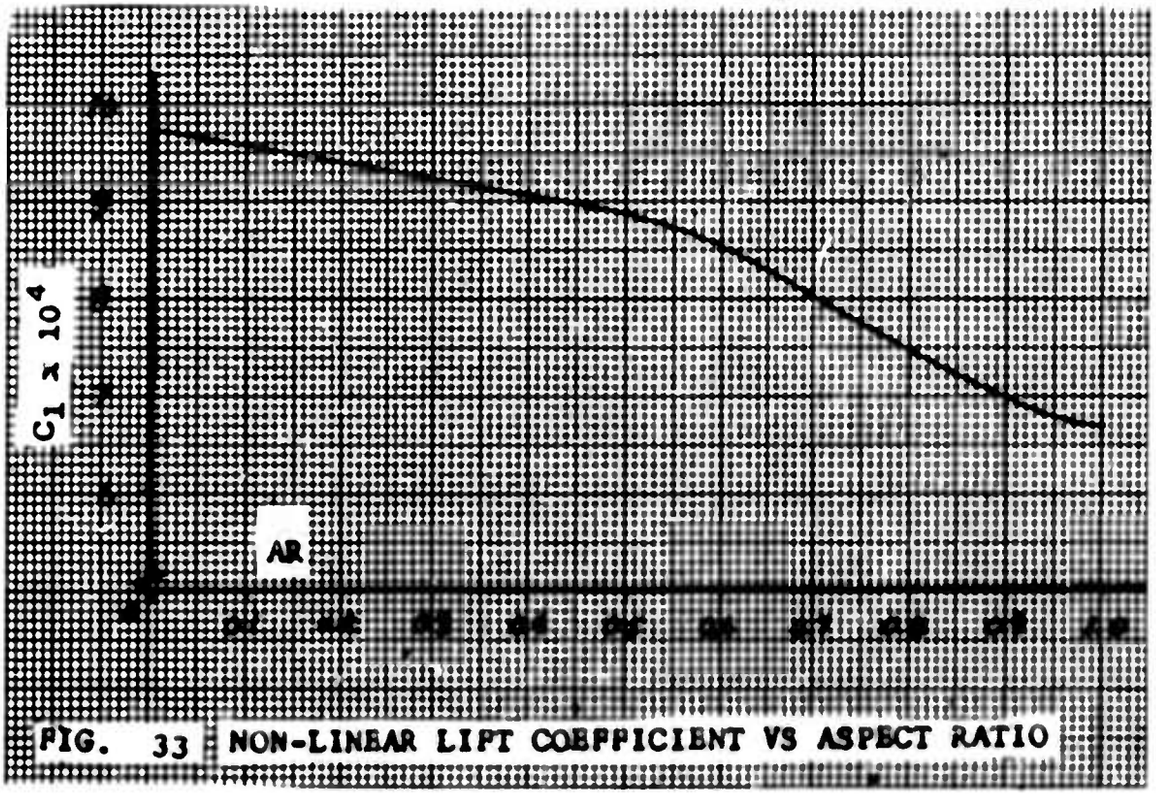

FIG. 33 NON-LINEAR LIFT COEFFICIENT VS ASPECT RATIO

That is,

$$a = \frac{a_o}{1 + \frac{a_o}{\pi e AR}} \tag{22}$$

where a_o is slope of the lift curve for infinite aspect ratio, and e is a wing efficiency factor, which equals 1.17 for rectangular wings (Ref 5). The theoretical lift curves for various aspect ratio are plotted in Fig. 34, with the test points from run number two shown. The points very closely agree with the AR = 0.6 curve, with the end plates tested.

To increase the basic lift of the wing, the aspect ratio must be increased; therefore, larger end plates were required. The problem was to determine how much larger the plates should be.

Sub-Scale Testing

A search of the literature revealed no direct reliable method for designing the new end plates. More testing in the wind tunnel was the obvious solution, but the tunnel was not operative. A fourteen-inch-diameter wind tunnel was the only one available locally with a balance system installed and operating. Several attempts were made to find other wind tunnels where the work could be continued, but in every case, the schedule would not allow time for completion, or the cost would have been as great as the repair cost to the five-foot tunnel.

It was therefore decided to use the 14-inch tunnel on a limited scale. The difference in Reynolds number was

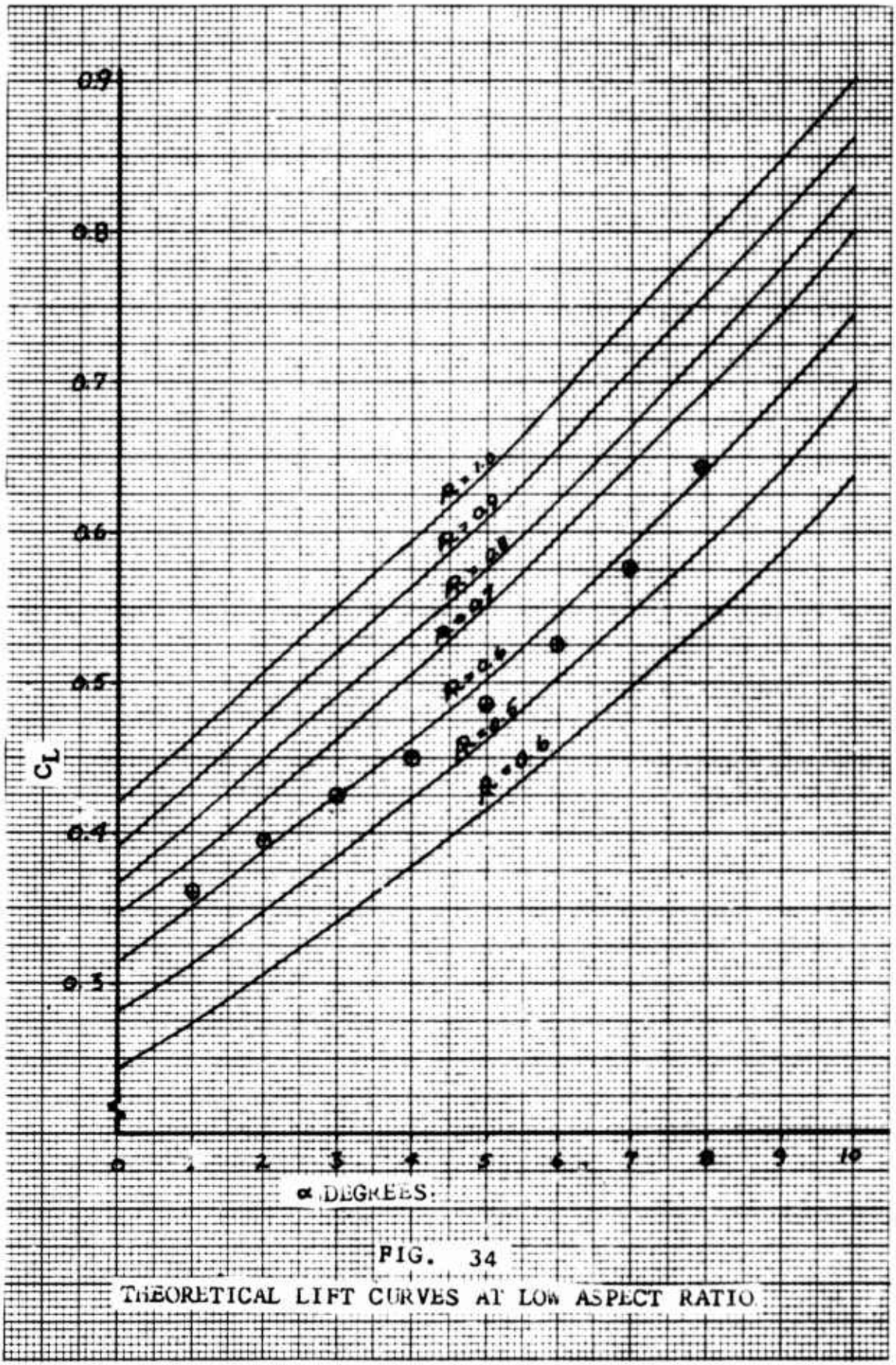

FIG. 34

THEORETICAL LIFT CURVES AT LOW ASPECT RATIO

so great, that no meaningful data could not be obtained with respect to flap performance, or the boundary layer control system. The small scale would put serious reservations on any duct evaluation. The determination of the end plates, however, did present a possible use for the smaller tunnel. While it was felt that there would be little or no correlation between the data from the smaller tunnel to the larger tunnel, the difference in performance between the various end plates should be the same in either tunnel.

Therefore a small model, as shown in Fig. 35, was constructed. The chord of the model was 6.0 inches. The size was picked because it was the largest chord that could be installed without redesigning the mounting system. The body was simulated with a block rounded at both ends, rather than building a detailed scale body. Five different size end plates were cut from 0.050-inch-thick aluminum to the outlines shown in Fig. 36. End plates number three and five extend forward in front of the leading edge. In the event that the extension might block the pilots field of view, the forward extension could be made of plexiglas.

The data from these series of tests are plotted in Figures 37 and 38. The best end plate was number five. The small extension in front of the wing proved to be very valuable and well worth the small expense in weight, particularly at the lower angles of attack. Some pre-

NOTE: THE MODEL IS BALSA, THE END PLATES ARE ALUMINUM. END PLATES NUMBER 1 ARE SHOWN

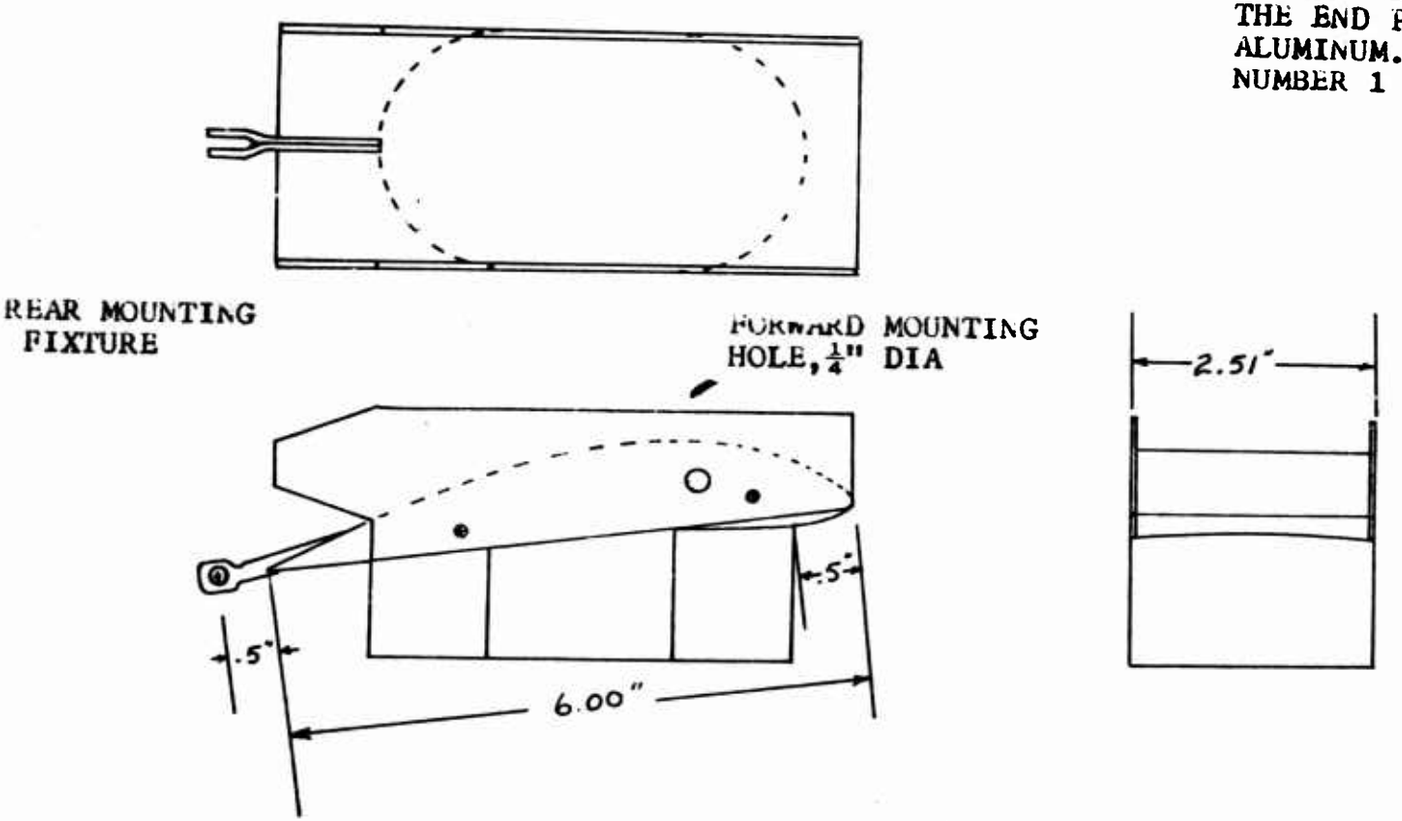

FIG. 35

SUB-SCALE TEST MODEL

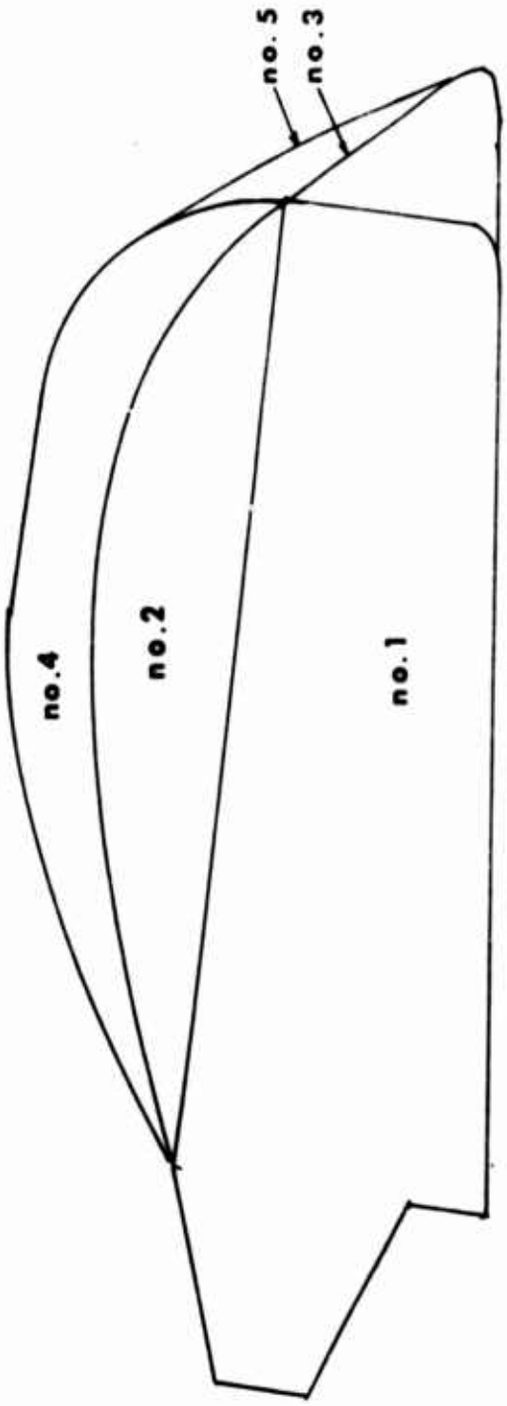

FIG. 36 END PLATE OUTLINES [FULL SIZE]

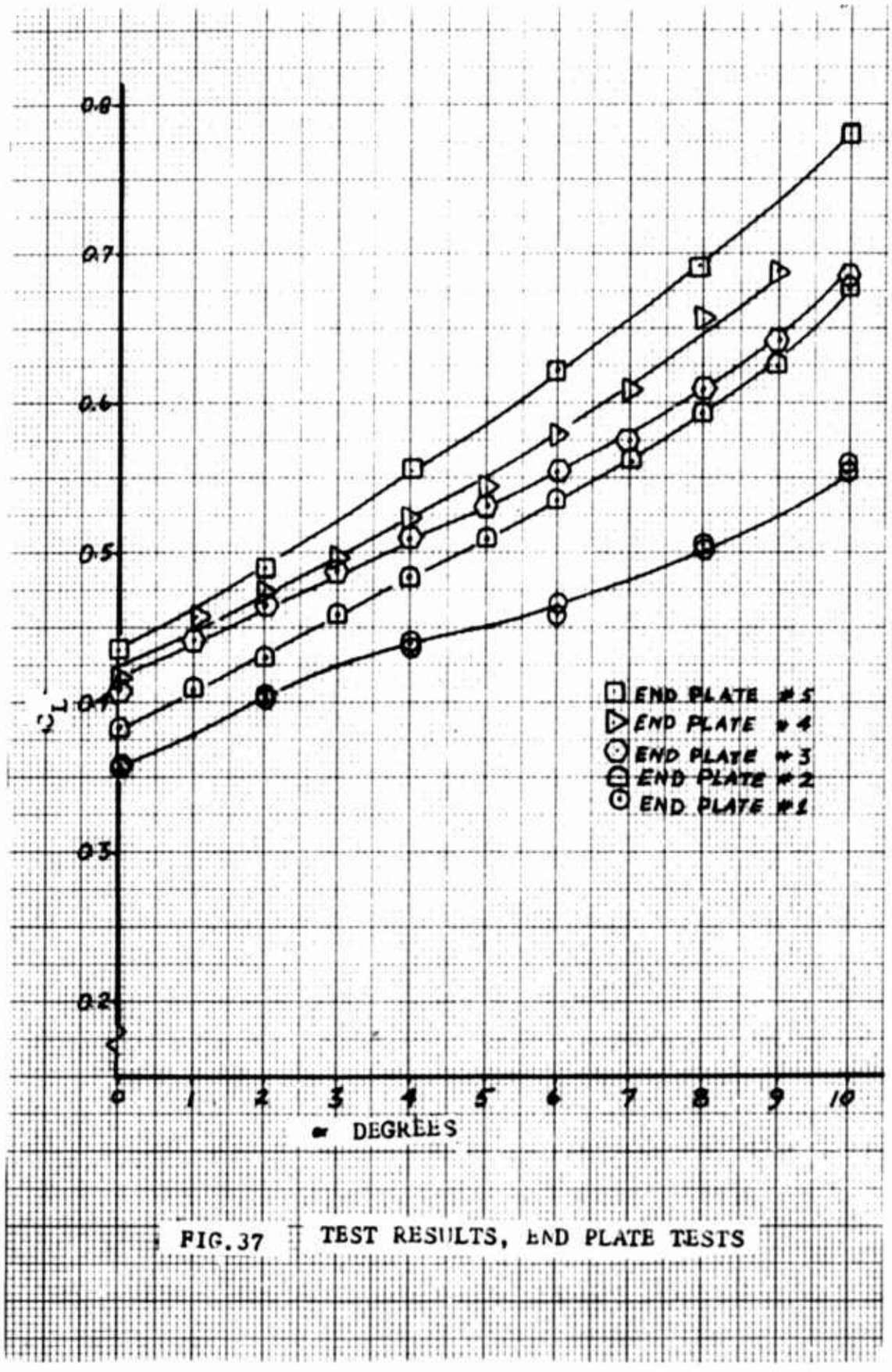

FIG. 37 TEST RESULTS, END PLATE TESTS

mature separation was evident on end plate number one, so a C_L above six degrees is not a valid point to apply. Below six degrees, however

$$C_{L_T} + \Delta C_{L_{EP_5}} = C_L \qquad (23)$$

was assumed valid. The points thus obtained coincide very

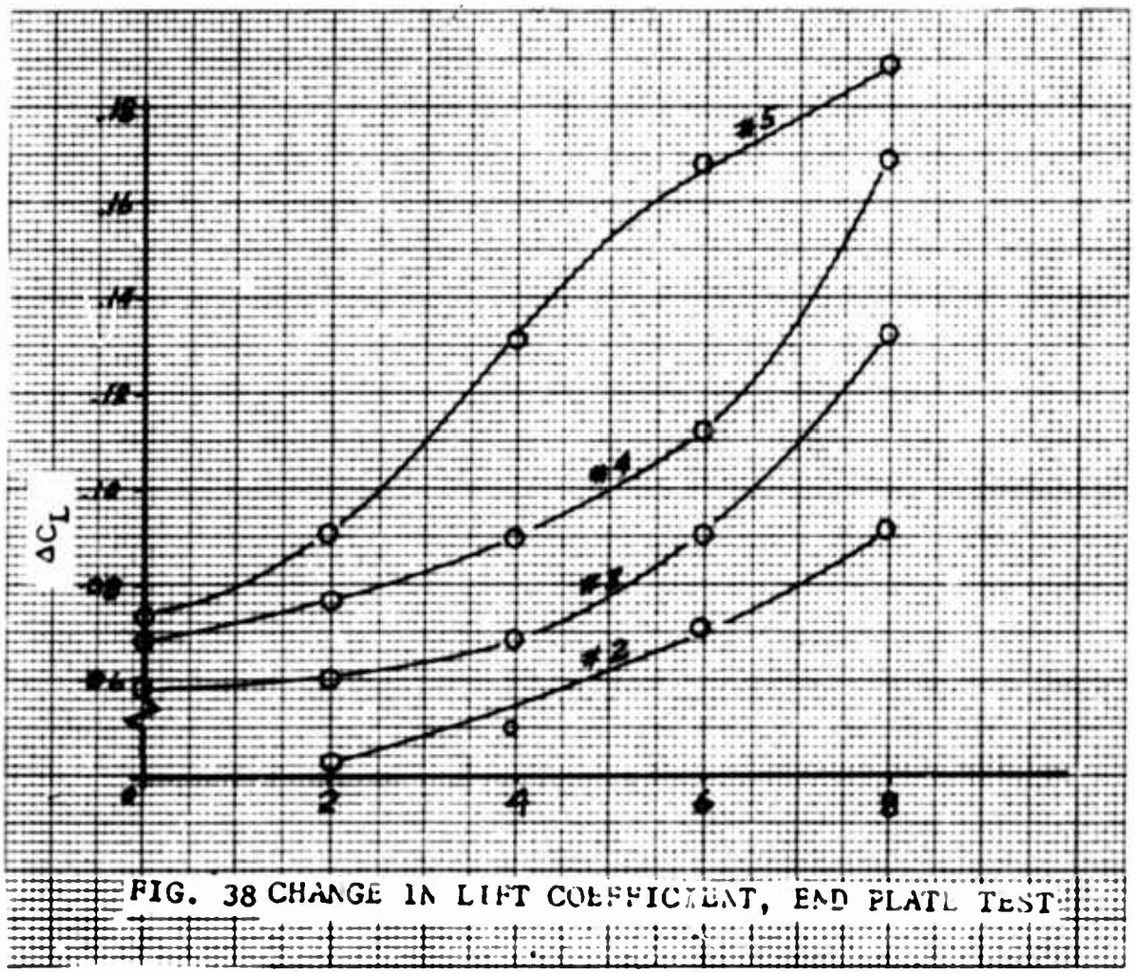

FIG. 38 CHANGE IN LIFT COEFFICIENT, END PLATE TEST

nearly with the theoretical AR = 1 curve in Fig. 34. Since the airfoil showed no signs of separation even at the low Reynolds number, it was assumed that if the vehicle were equipped with end plates number five, the performance

FIG. 39. SIDE-SLIDE MODEL IN 14 INCH WIND TUNNEL

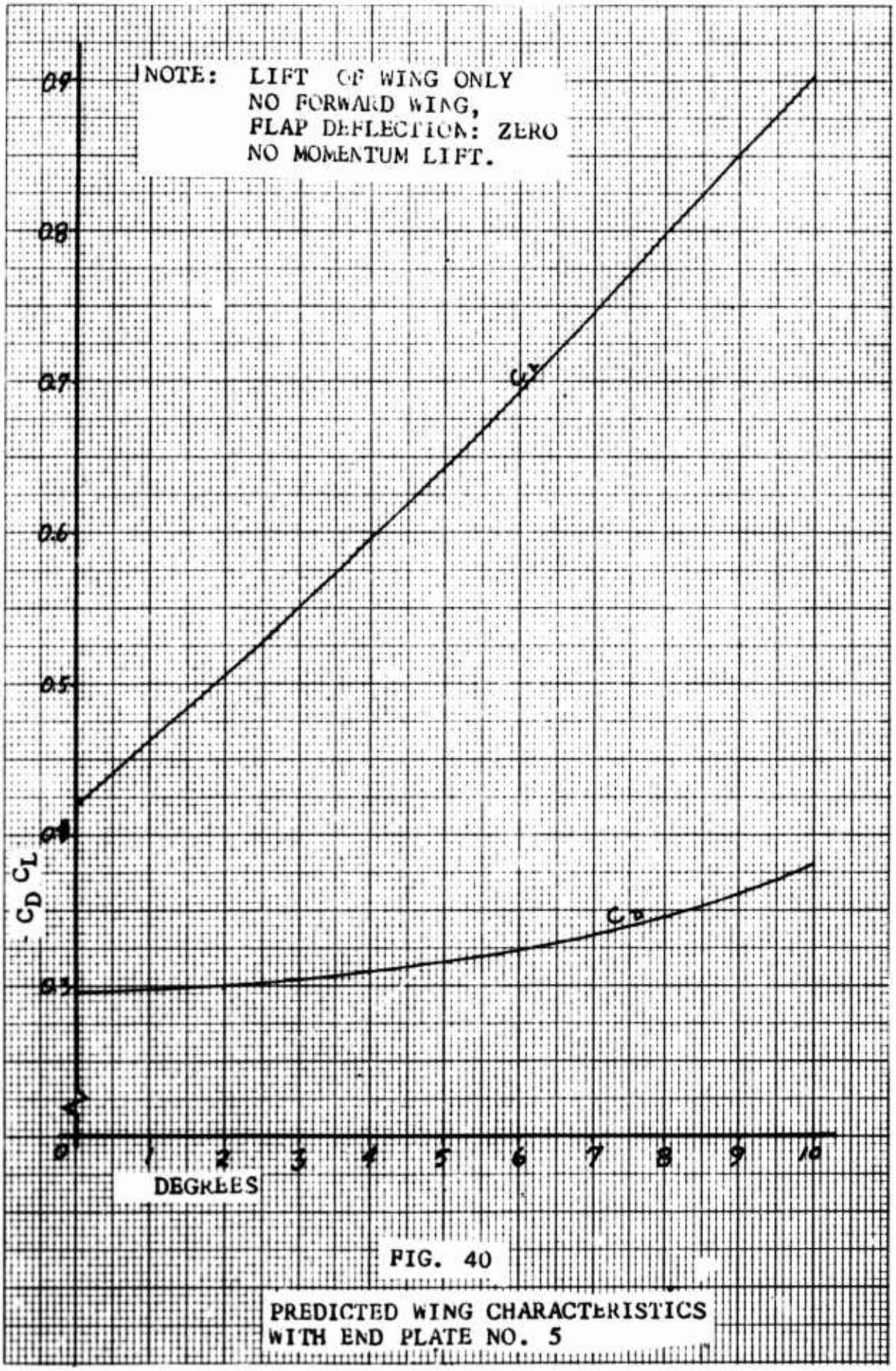

FIG. 40

PREDICTED WING CHARACTERISTICS
WITH END PLATE NO. 5

would be as shown in Fig. 40.

The same technique was used to predict drag coefficients, and the results are also shown on Fig. 40.

As a result of the successful end plate tests, a series of test were conducted with the forward wing positioned between the number five end plates, as shown in Fig. 41. The angle of attack of the forward wing (as defined in Fig. 41) was set at -15,-10,-5, and 0. The results are plotted in Figs. 42, 43, and 44.

The forward wing proved to be an efficient means of increasing the lift of the vehicle so long as the gap

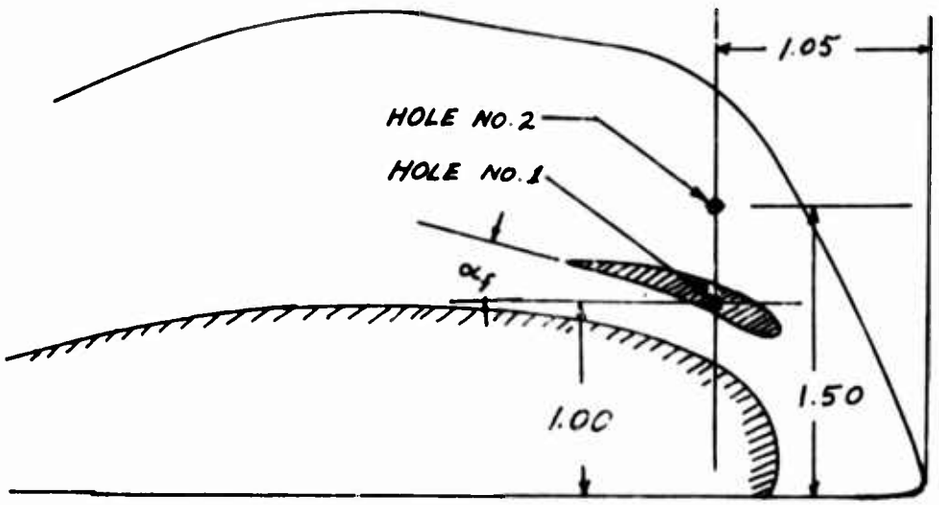

FIG. 41 LOCATION OF FORWARD WING, SUB-SCALE TESTS

between the trailing edge of the forward wing and the surface of the main wing is not too small, as in the test

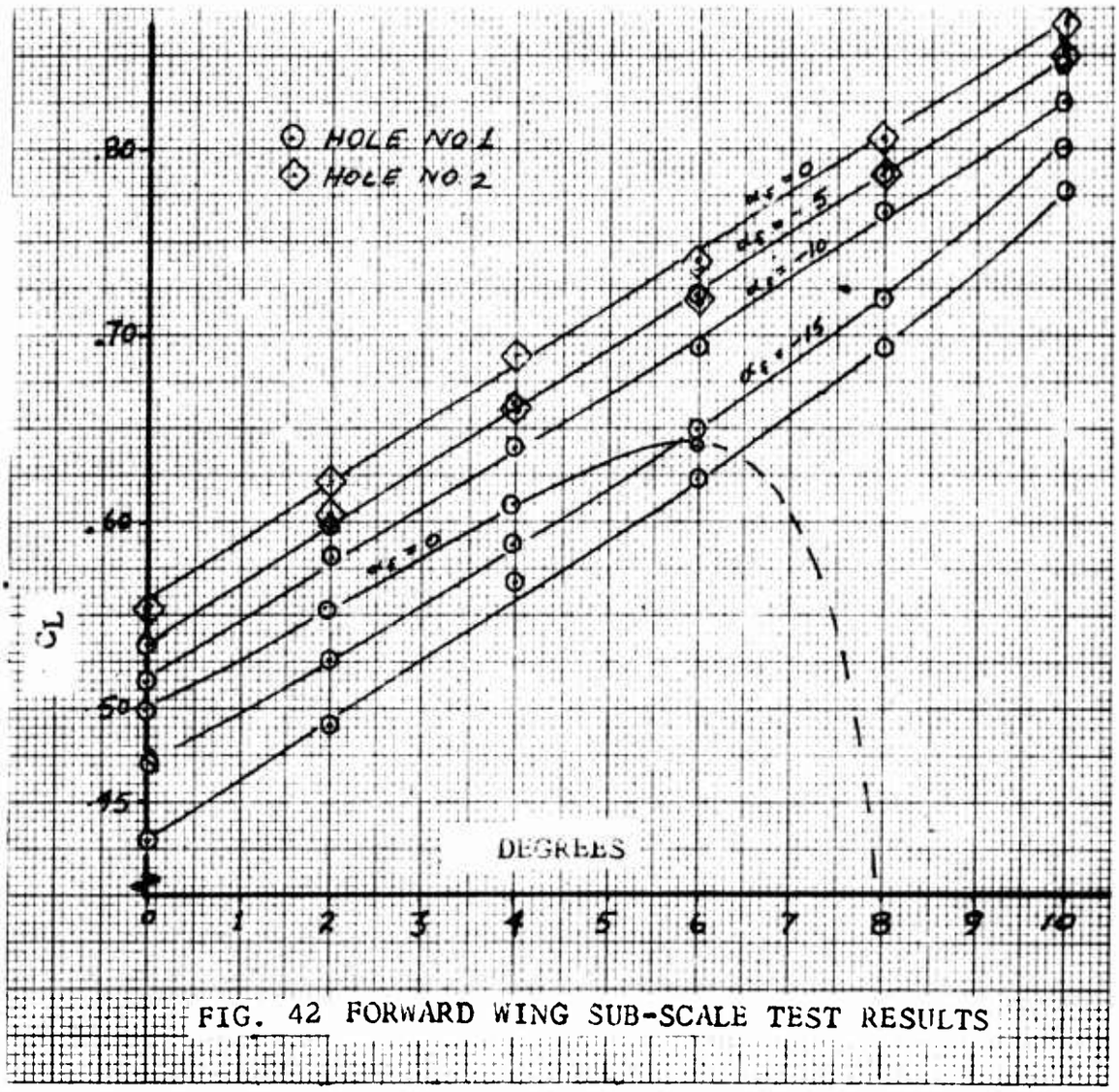

FIG. 42 FORWARD WING SUB-SCALE TEST RESULTS

of $\alpha_{f=0}$. At this angle, the small wing stalled at a vehicle angle of attack of 6.5 degrees, and the resulting disturbance also caused a stall of the main wing.

At lower values of α_f, the ΔC_L was essentially constant for any α_v, and ΔC_L versus α_f was linear. Pitching moment data was somewhat erratic but definitely showed that the forward wing can be used effectively as a control surface to counteract the nose-down moment of the flap.

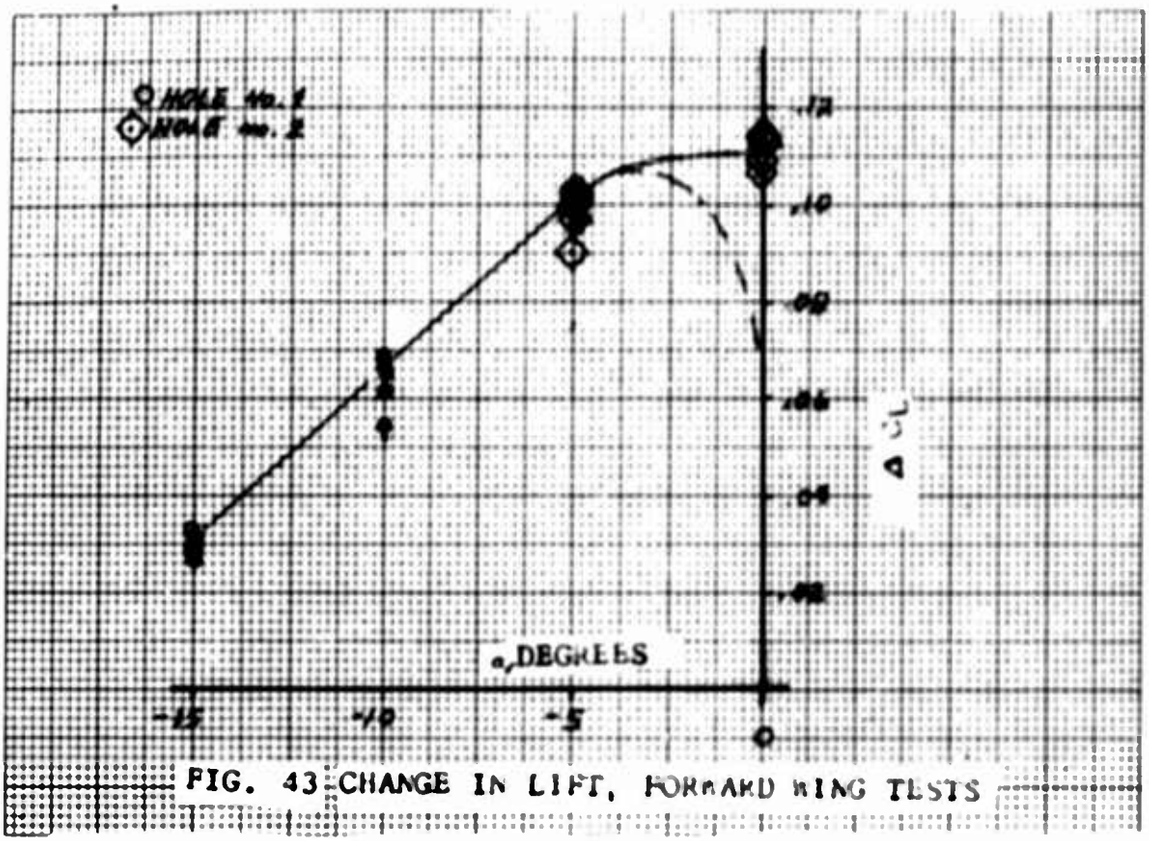

FIG. 43 CHANGE IN LIFT, FORWARD WING TESTS

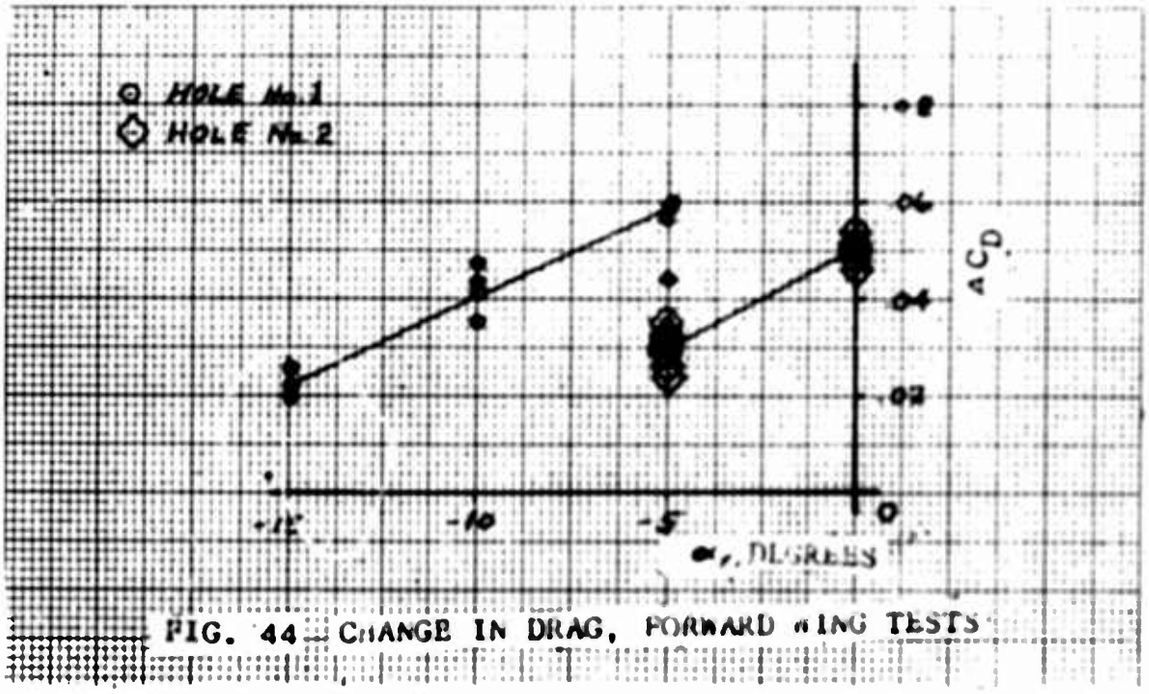

FIG. 44 CHANGE IN DRAG, FORWARD WING TESTS

Despite the loss of the large tunnel, the test program determined, the basic characteristics of main wing, the effect of the forward wing and the effect of end plate shape and size. Although this data is far from optimum, and the full test program (as shown in Table I) is still needed, the data is of sufficient accuracy to proceed with a preliminary design of the full scale vehicle.

VI. Full Scale Vehicle Design

Engine Description

The Wankel engine, licensed in the United States to Curtiss-Wright, is a rotating cylinder internal combustion engine. The "piston" is a eccentric cam with three curved sides which rotates in a trochoirdal chamber which resembles a "fat" figure eight (Ref 13). The volume between the rotor (the cam) and the walls of the chamber changes during the rotation of the rotor in a manner analogous to the familiar intake-compression-power-exhaust cycle of a convention piston engine.

When the volume is the least (compression) the fuel-air mixture is ignited by a spark plug. The mixture expands, giving an impulse to the rotor, which causes the rotor to continue rotating (power). This process is repeated so that there are three "power strokes" per revolution of the rotor, as compared with one power stroke per two revolutions in a conventional engine.

The higher ratio of power strokes to revolution is the major factor contributing to the high power to weight ratio of the Wankel engine. The engine selected for this vehicle, the RC-2-90-Y consists of two chambers, each with 90 cubic inches of volume between the rotor and the chamber. The maximum power of the engine is 330 horsepower, but the dry weight of the engine is only 317 pounds.

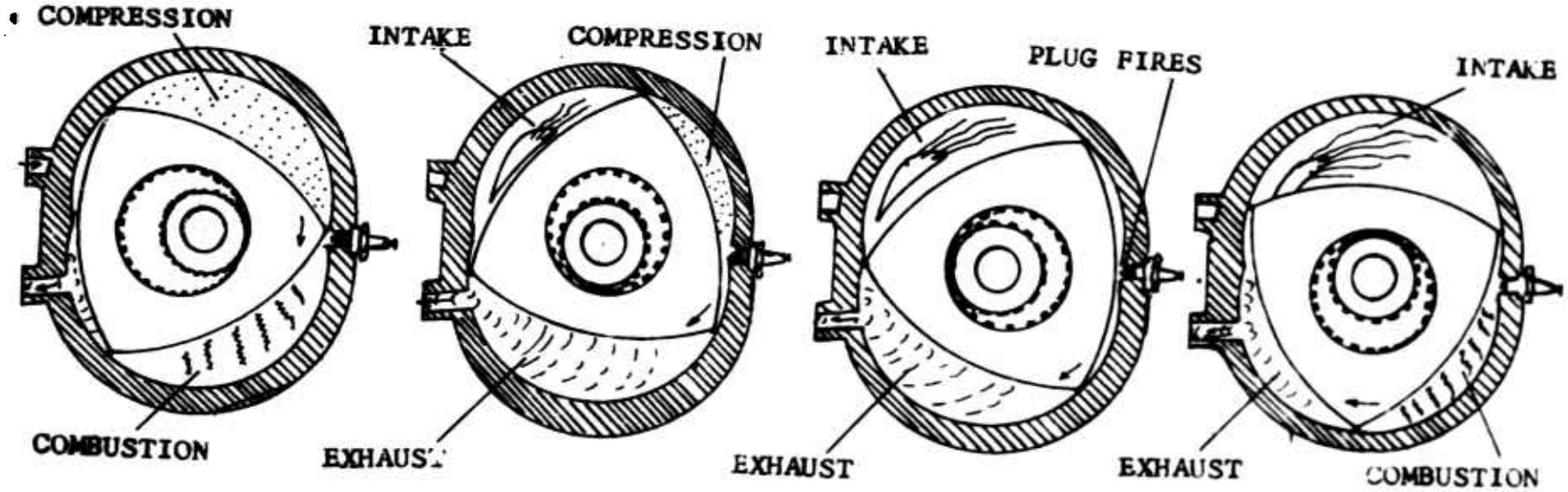

FROM LEFT TO RIGHT: (1) The compression phase is beginning. The intake port is closed, the exhaust phase and the combustion phase are ending. As the rotor advances.(2) The intake port is exposed while compression continues and the exhaust phase begins. The plug fires (3) against one face of the rotor while exhaustand intake continue on the other two sides. The combustion (4) gives an impulse to the rotor and the cycle begins again.

FIG. 45 WANKEL ENGINE

Construction

For resistance to small arms fire, the primary material was chosen to be an aluminum and foam sandwich as shown in Fig. 46. The basic structure of the vehicle is a

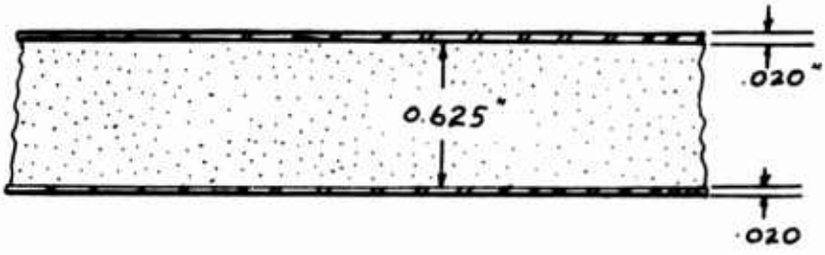

FIG. 46 FOAM/ ALUMINUM SANDWICH

momocoque shell of this material. The engine mount was assumed to be two aluminum half-rings, one at the front and one at the rear of the engine. The rings are supported by a welded aluminum tubular truss attached to the sandwich floor.

The ducting, nacelles and straighteners are made of fiberglas. This choice was determined from the requirement for ease of maintenance. The compound curves of the propeller duct also make the choice of fiberglas attractive from the fabrication viewpoint. The fuel tanks and flexible skirt would be made of synthetic rubber.

The pilot would sit between the fan ducts and above the propeller duct. The flat top of the fan ducts are large enough to accommodate two passengers in a prone position, or wounded in stretchers. The flap, rudders, forward wing and stabilizer would be of standard aluminum

skin and rib construction. Four aluminum wheels are included for ground handling.

Weight and Balance

The weight of each component was estimated and its position of its center of mass in the vehicle was estimated. Some of the component weights were known, such as the machine guns, the engine, and the radio. Most were estimated by knowing the volume required and the density of the material. Others, such as the pilot, transmission and controls, were simply estimated from experience. The center of mass of each component was estimated by dividing complex sections into simple sections, such as rectangles, circles, cones, frustrum of cones, etc.

The center of gravity of the vehicle was determined by the formula

$$X_{C.G.} = \frac{\sum m_i X_i}{\sum m_i} \qquad (24)$$

The control system was omitted from the center of gravity determination because the system was assumed to distributed throughout the vehicle.

The weight and balance summary is shown in Table III.

The flight weight of the vehicle is defined as the minimum weight of the vehicle in a flying configuration. That is, no machine guns or passengers. The armed weight is the flight weight plus the weight of the machine guns and ammunition. The emergency weight is the armed weight

plus the weight of two passengers. In each case, there is a range of weight depending on the weight of the people, who can vary from 130 to 250 pounds, and the fuel load.

The distance to the center of gravity is shown in Table II. The $X_{C.G.}$ max represents the location of the center of gravity when maximum fuel and the lightest crew are aboard. The $X_{C.G.}$ min represents the location of the center of gravity when the heaviest crew and no fuel are combined.

Table II
Location of Center of Gravity

Weight	$X_{C.G.MIN}$	$X_{C.G.MAX}$
Flight	9.15	9.39
Armed	8.64	8.91
Emergency	7.99	8.50

Table III
Weight and Balance Estimate

	Item	Material(s)	Density lb_f/ft^3	Volume ft^3	Weight lb_f	X, ft	WX $lb_f ft$	Remarks
Structure	Vehicle Floor	Aluminum/Foam Sandwich	19.7	4.98	98	7.35	721	"Density" in lb_f per lineal foot
	Stiffeners	4"Aluminum Channels	2.5	24	60	8.48	509	
	Windshield	5/8" Plexiglass	72	1.12	83	1.40	116	
	Wing Surface	Aluminum/Foam Sandwich	19.7	8.39	166	9.10	1509	
	Body & Plates	Aluminum/Foam Sandwich	19.7	131	236	7.20	1699	Includes Rudders
	Fw'd Wing	Built-up Aluminum	169	.083	14	1.00	14	
	Stabilizer	Built-up Aluminum	169	.083	14	15.00	210	
	Front Wheels	Rubber, "Alum. Hubs" and Attachments	-	-	26	4.00	104	Electric Brakes Installed
	Rear Wheels		-	-	26	12.00	312	

Table III (cont'd)
Weight and Balance Estimate

	Item	Material(s)	Density $lb_f/f+^3$	Volume $f+^3$	Weight lb_f	X, ft	WX $lb_f ft$	Remarks
Ducting	Fan Ducts	1/8" Fiber-glas	108	1.33	143	5.10	729	2 Req'd
	Turning Vanes	1/8" Fibre-glas	108	.108	12	7.70	925	2 sets of 3 req'd
	Lift Fans	Built-up Aluminum	169	.079	27	7.70	2079	2 req'd
	Fan Housings	1/8" Fiber-glas	108	.090	9	7.70	69	2 req'd
	Straigh-eners	1/8" Fiber-glas	108	.131	114	7.70	108	10 req'd
	Propeller Duct	1/8" Fiber-glas	108	1.396	151	6.60	997	Includes rear control
	Suction Duct	1/8" Fiber-glas	108	.429	27	8.48	239	
	Blowing Duct	1/8" Fiber-glas	108	.201	22	10.52	232	
	Engine	1/8" Fiber-glas	-	-	337	10.76	3625	With oil, etc.

Table III (cont'd)

Weight and Balance Estimate

	Item	Material(s)	Density $lb_f/_{f+}{}^3$	Volume $f+^3$	Weight lb_f	X, ft	WX lb_f ft	Remarks
Propulsion	Mounting Ring	1/2" Aluminum Plate	169	.035	6	10.76	65	2 half-rings
	Bracing	1/2" Aluminum Rods	169	.014	14	10.76	151	
	Nacelle	1/8" Fiber-glas	108	.405	44	10.20	449	
	Straight-eners	1/8" Fiber-glas	108	.064	7	10.76	75	5 req'd
	Propeller	Aluminum	169	.173	29	8.53	247	
	Shaft & Gears	Steel, 1" Diam.	488	.022	11	7.98	88	
	Trans-mission	Unknown	-	-	50	8.12	406	
	Fuel Tanks	Buna Rubber	72	.333	24	9.65	232	Includes fuel lines
	Instru-ment panel	Fiberglas + instruments	-	-	20	3.00	60	

Table III (cont'd)
Weight and Balance Estimate

Item	Material(s)	Density $lb_f/_{f+}{}^3$	Volume $f+^3$	Weight lb_f	X, ft	WX lb_f ft	Remarks
Controls	Handles, cables, etc.	-	-	43	-	-	Not included in C.G.
Pilot's seat	Foam and Fiberglas	-	-	5	6.10	31	
Fastener & Brackets	Foam and Fiberglas	-	-	20	-	-	Not included in C.G.
Basic, dry vehicle				1727		16001	
Pilot				130-250	6.10	794-1524	
Fuel				100-300	9.65	965-2895	
Flight Weight:				1957-2277			
Machine Guns	Fairchild AR-10, Alum. Mounts			25	3.0	75	7.62 mm machine guns.
Ammu-nition	7.26 mm NATO round			150	3.0	450	2800 rounds @375 grains
Wounded				2132-2452 260- 450			
Emergency weight:				2392-2902			

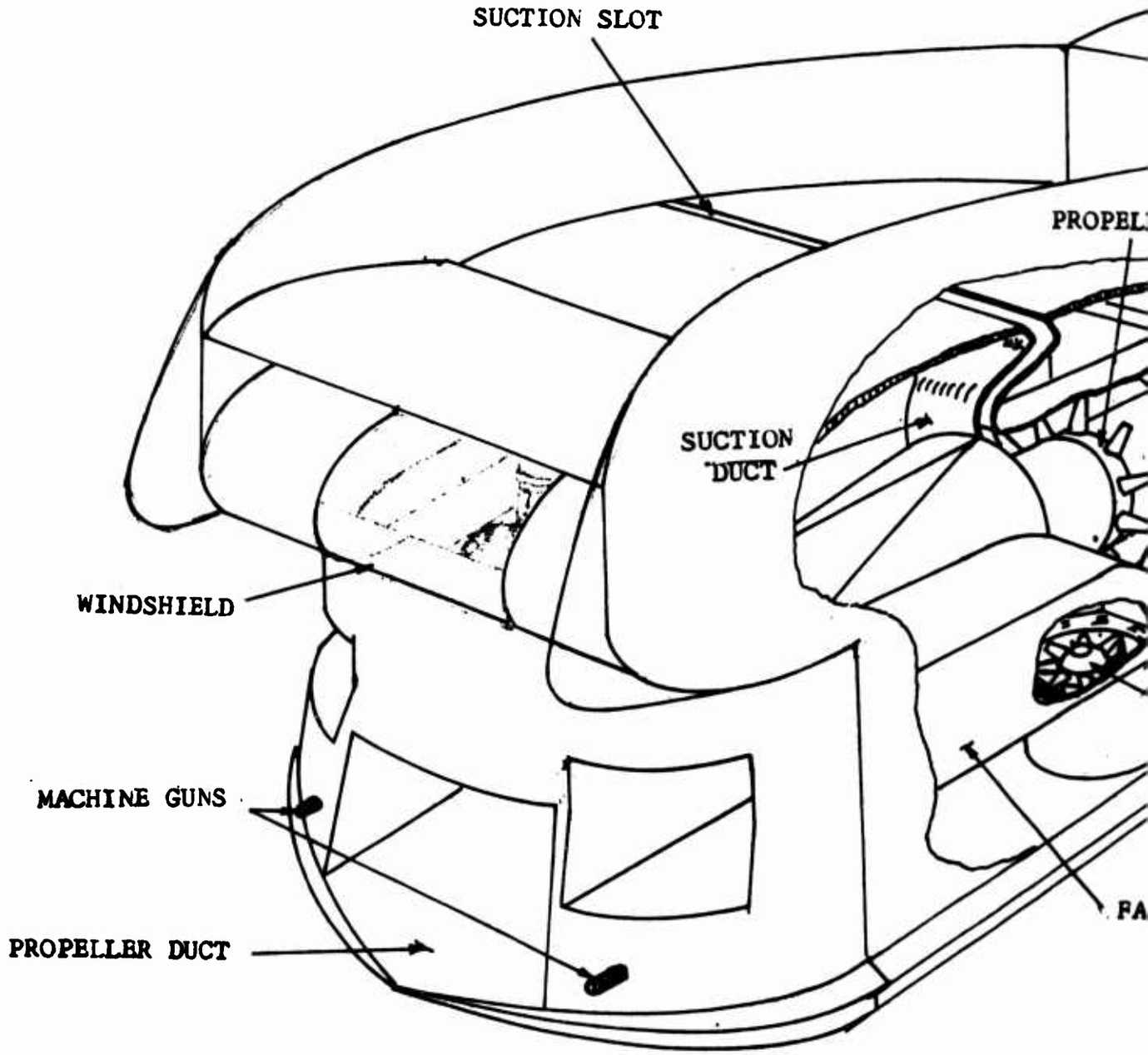

FIG. 47 SKETCH OF VEHICLE SHOWING

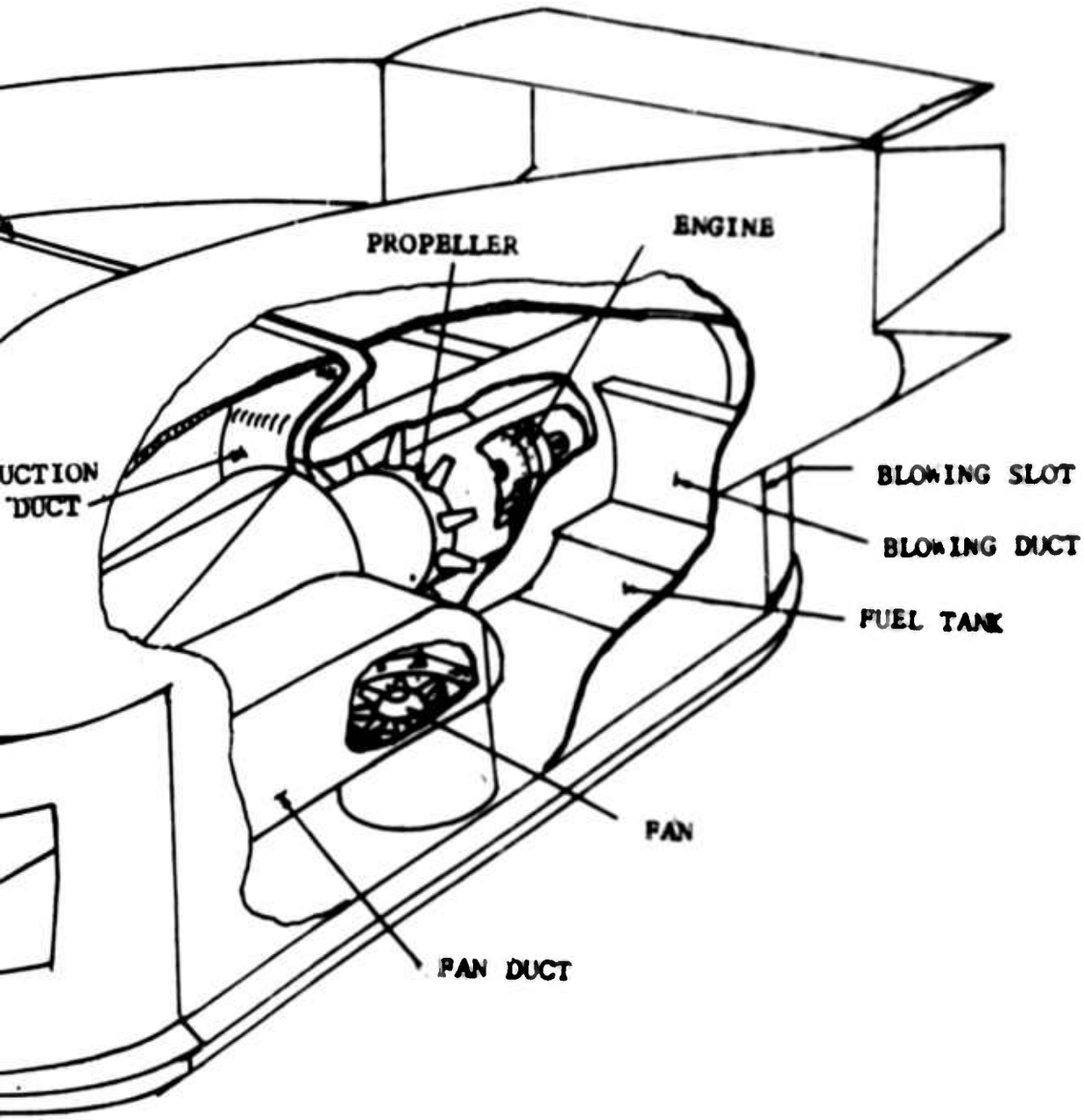

' SKETCH OF VEHICLE SHOWING LOCATION OF MAJOR COMPONENTS

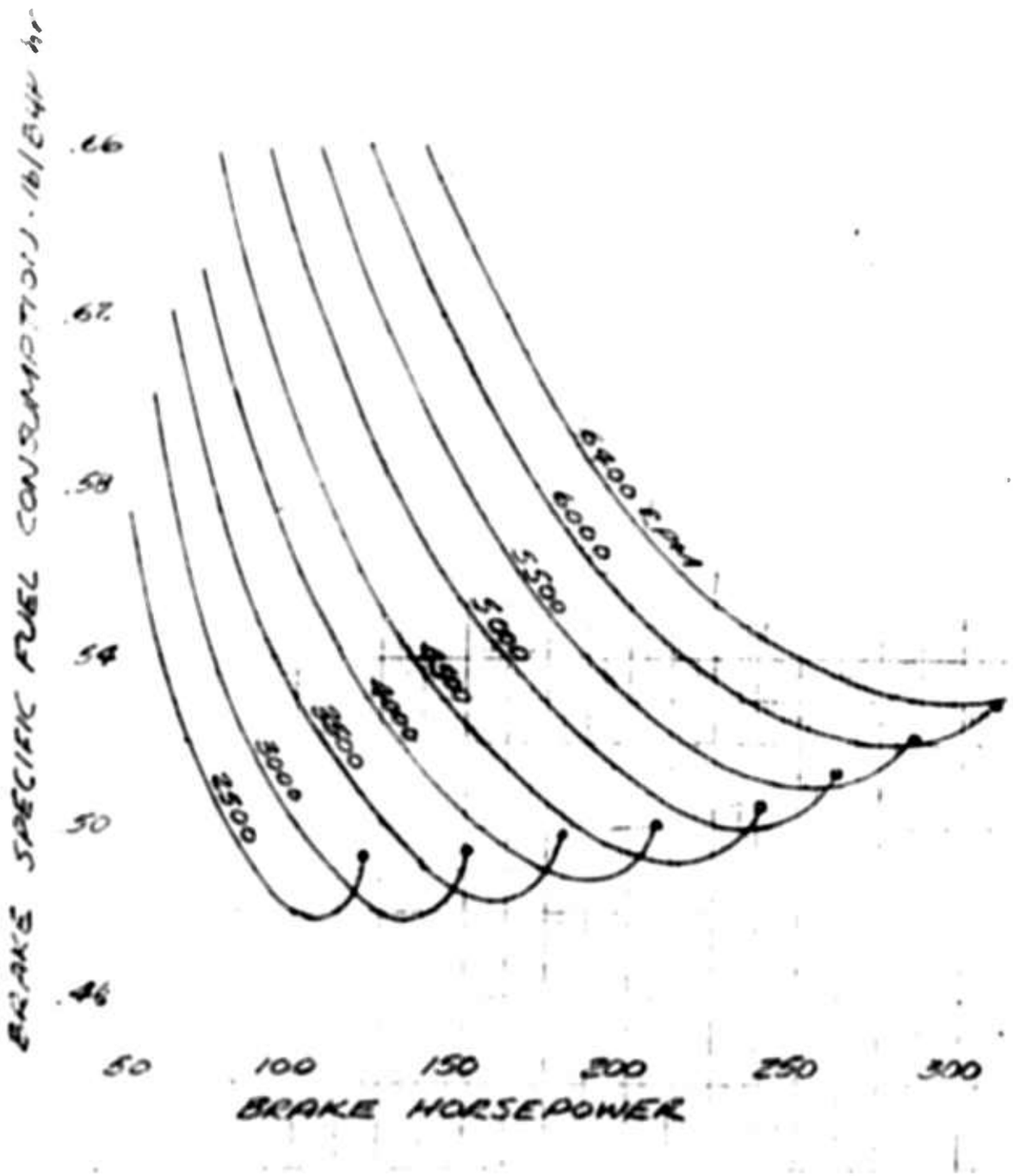

FIG. 48 ENGINE PERFORMANCE

VII. Full Scale Vehicle Performance

The size and weight of the vehicle have now been determined. The basic aerodynamic characteristics have been determined. The final step in the design is to determine the vehicle performance.

Duct Performance

There are two parameters of duct performance of interest to the performance of the vehicle, namely, internal drag and loss in total pressure. The internal drag is important for estimation of vehicle total drag, and loss in total pressure is important to the performance of the propulsion system.

A ducted propeller can be considered as a mechanism to raise the pressure in the duct. The method to raise the pressure is to induce a rotational velocity to the air flow, then to cancel the rotational velocity with straighteners. The resultant change in pressure is equal to the dynamic pressure of the rotational velocity (Ref 14). The longitudinal velocity remains constant through the propeller. To change the velocity would violate the law of continuity or the assumption of constant density. Therefore, thrust is generated by the pressure increase of the propeller, rather than a momentum change in the duct. Loss of pressure due to friction is therefore very important to propulsion.

The change in total pressure in a duct is given by

Shapiro as:

$$-\frac{dp_o}{p_o} = \frac{\gamma M^2}{2} \; 4C_f \frac{dx}{D} \tag{25}$$

under the assumptions of adiabatic flow, ideal gas and constant mass flow rate (Ref 18). In this equation M is the Mach number, D is the hydraulic diameter, is the ratio of specific heats, and f is the friction coefficient.

In this application, from the definition of hydraulic diameter and Mach number;

$$-\frac{dp_o}{p_o} = \frac{\gamma v^2}{a^2} \frac{2C}{A} \; C_f dx \tag{26}$$

where a is the speed of sound, A is the cross sectional area of the duct and C is the total circumference of the duct.

Under standard conditions, this becomes

$$\frac{dp_o}{p_o} = \left[-2.29\text{x}10^{-6}\right] \frac{v^2 C}{A} \; C_f dx \tag{27}$$

which can be approximated by

$$\frac{\Delta p_o}{p_o} = -2.29\text{x}10^{-6} \; \frac{v^2 \; C}{A} \; C_f \Delta x \tag{28}$$

or

$$\left.-\frac{\Delta p_o}{p_o}\right|_{\text{total}} = 2.29\text{x}10^{-6} \sum_{x=0}^{x=13.29} \frac{v^2 \; C}{A} \; C_f \; \Delta x \tag{29}$$

The internal drag of the duct is made up of skin friction drag throughout the duct and pressure drag on the nacelle. The pressure drag on the straighteners is assumed negligible. The estimation of the skin friction drag was accomplished by applying the equation

$$D = C_f \tfrac{1}{2} \rho V^2 \quad A_w \cos \gamma \tag{30}$$

where A_w is the "wetted area", C_f is the local coefficient of the skin friction drag and γ is the angle of the duct wall with the longitudinal axis of the vehicle. The only problem is the determination of C_f. Here, the assumption was made that each elemental area of the duct wall would have the same C_f as if it were a flat plate exposed to the same Reynold's number as exists in the duct. Then by Schoenherr's equation for turbulent flow,

$$C_f^{-\frac{1}{2}} = 4.13 \log_{10} (R_{ex} C_f) \tag{31}$$

which is solved graphically in Reference 10. The turbulent case was assumed because most of the duct is considerably above the critical Reynolds number, and the drag for a turbulent boundary layer is higher, which makes the estimate conservative.

The total internal skin friction drag was assumed to be

$$D = \int_A C_f \tfrac{1}{2} \rho U^2 \cdot \cos \gamma \; dA \tag{32}$$

To evaluate this integral, the duct was divided into 32 sections. The C_f for each section was calculated from the Reynolds number, assuming a V of 100 ps. The wetted area was known and was known. The drag was then estimated as

$$D \cong \sum_{i=1}^{32} \left[C_f \tfrac{1}{2}\rho u^2 \cos\gamma A_w \right]_i \qquad (33)$$

The drag coefficient, then is

$$C_D \cong \sum_{i=1}^{32} \left[C_f \frac{U^2}{V^2} \cos\gamma \frac{A_w}{S} \right]_i \qquad (34)$$

The nacelle pressure drag was evaluated as a "blunt" body of revolution with a rounded nose. Hoernerr gives the pressure drag coefficient for a body with dimensions similiar to this nacelle as $C_D = 0.4$, based on the cross sectional area of the body (Ref 7). The pressure drag coefficient of the nacelle is then

$$C_{D_n} = 0.4 \left(\frac{U}{V}\right)^2 \left(\frac{A_n}{S}\right) \qquad (35)$$

The duct through the nacelle was ignored, because, in the real vehicle, this duct will be full of engine, propeller hub, transmission and other equipment whose pressure drag would be approximately the same as if the duct were closed.

The same method of calculation was employed in the fan ducts. The duct was divided into 17 sections along

Table IV
Duct Characteristics

Propeller Duct								
Distance Along Duct	Cross Section Area, ft^2	C_p	$Re_x \times 10^{-6}$ @ V =100	$C_f \times 10^3$	Circumference C, ft	cos γ	$C_D \times 125{,}000$	$-\Delta P_o \times 10^{-6}$
3.00	6.00	+0.000	1.92	4.30	10.0	1.000	129.0	493
3.66	6.00	0.000	2.34	4.26	11.00	0.985	29.0	118
4.20	7.50	0.085	2.56	4.15	11.01	0.985	21.3	69
4.51	7.84	0.162	2.64	4.15	11.00	0.985	11.8	35
4.82	7.99	0.190	6.75	4.14	10.90	0.985	11.3	32
5.14	8.13	0.219	2.90	4.13	10.90	0.985	10.8	31
5.45	8.14	0.221	3.08	4.12	10.82	0.985	10.6	31
5.76	8.05	0.205	3.28	4.10	10.80	0.985	10.7	31
6.08	8.03	0.200	3.46	4.09	10.71	0.985	10.6	31
6.40	7.95	0.180	3.71	4.08	10.60	0.985	10.6	31
6.71	5.54	-.482	5.21	3.94	13.08	0.985	19.0	99
7.02	4.96	-.871	6.14	3.80	16.50	0.980	30.8	169
7.34	4.51	-1.221	6.96	3.71	17.42	0.970	42.5	228
7.65	4.31	-1.440	7.62	3.62	17.74	0.965	46.9	261
7.96	4.62	-1.240	7.43	3.62	17.76	1.000	44.9	223
8.28	4.62	-1.240	7.70	3.63	17.76	1.000	45.1	221
8.59	4.62	1.240	7.98	3.56	17.76	1.000	44.3	219
8.90	4.62	-1.240	8.26	3.46	29.38	1.000	43.0	212
9.22	4.62	-1.240	8.57	3.40	28.78	1.000	56.0	348
9.53	4.62	-1.240	8.85	3.36	28.78	1.000	68.4	337
9.84	3.53	-1.240	9.15	3.30	28.78	1.000	66.5	433
10.16	3.53	-1.240	9.44	3.24	28.78	1.000	65.2	425
10.47	3.53	-1.240	9.74	3.16	28.78	1.000	63.6	411
10.78	3.53	-1.240	10.02	3.08	28.78	1.000	62.0	404
11.10	4.21	+0.492	8.68	3.38	28.78	1.000	45.0	248
11.41	4.99	+0.063	7.54	3.61	16.15	1.000	27.0	90
11.72	5.86	-0.230	6.64	3.74	16.10	1.000	14.6	57

Table IV (cont'd)
Duct Characteristics

Distance Along Duct	Cross Section Area, $f+^2$	C_p	$Re_x \times 10^{-6}$ @ V =100	$C_f \times 10^3$	Circumference C, f+	cos γ	$C_D \times 125{,}000$	$-\Delta Po \times 10^{-6}$
Propeller Duct								
12.04	6.40	-0.351	6.21	3.79	15.61	0.999	12.2	43
12.35	6.86	-0.436	5.94	3.82	12.88	0.999	9.6	29
12.66	7.30	-0.412	6.22	3.79	9.62	0.998	7.9	22
12.98	7.04	-0.368	6.62	3.76	9.50	0.997	7.1	23
13.29	7.01	-0.364	6.81	3.73	9.42	0.995	7.0	23
C_D = .0087 (friction drag only) ΔPo = - .0055 Po								
Fan Duct								
1	4.00	0.000	.64	5.75	4.16	1.000	23.90	128
2	4.00	0.000	1.28	4.20	8.00	1.000	33.60	193
3	4.00	0.000	1.92	4.18	8.00	1.000	33.40	192
4	4.00	0.000	2.56	4.17	8.00	1.000	33.35	191
4.25	4.00	0.000	2.72	4.16	8.00	1.000	8.32	48
4.50	4.00	0.000	2.88	4.14	18.00	.965	18.01	105
4.75	3.99	0.005	2.98	4.12	20.00	.866	17.90	113
5.00	3.98	0.011	3.22	4.10	20.00	.707	14.67	113
5.25	3.98	0.011	3.37	4.09	20.00	.500	10.32	113
5.50	3.98	0.011	3.53	4.08	20.00	.258	5.34	113
5.75	3.98	0.011	3.69	4.07	20.00	.139	2.08	112
6.17	3.98	0.011	3.95	4.06	7.06	.139	2.02	64
6.67	3.64	0.210	4.66	3.98	10.94	1139	3.68	166
7.67	3.98	0.210	5.37	3.92	13.56	.139	8.95	362
8.09	3.98	0.011	5.17	3.96	10.94	.139	2.55	106
8.43	3.98	0.011	5.40	3.92	7.06	.139	2.05	55
8.68	3.98	0.011	5.56	3.90	7.06	.139	.75	40
C_D = 0.00177 (friction drag only) ΔPo = -.0022 Po								

the center line of the duct and the fan housing was treated like the engine nacelle.

The results are presented in Table IV.

Determination of Lift

Lift, in this vehicle, comes from several sources: the main wing, the forward wing, the momentum change in the fan ducts, and the flap. The lift of the wing and the forwerd wing were determined by test. The momentum change and the flap contribution were calculated analytically.

The momentum change at zero power to the fans is

$$L = \rho A_D V_\infty^{\ 2} \cos^2\alpha \cos(\alpha - 8) \qquad (36)$$

or in terms of coefficients,

$$C_{L_{MOM}} = \frac{2A_D}{S} \cos^2(\alpha - 8^o) = 0.128(\cos\alpha - 8^o) \qquad ((37)$$

The flap increment was determined from the method of Lowry and Polhamus (Ref 12). They predict the increase in lift as

$$C_L = a_o (\alpha S) C_L \delta_f K_b \qquad (38)$$

where the term $(\alpha S) C_L$ is three-dimensional flap effectiveness factor dependent on aspect ratio and the relative chord of the flap, a_o is as defined in equation (22), δ_f is the flap deflection in degrees, and K_b is a factor dependent upon the flap span to wing span ratio. For this vehicle, the theoretical lift increment.

$$C_{LF} = 0.0117 S_F \qquad (39)$$

because the flap is essential to the feasibility of this vehicle it would be unwise to accept this theoretical value as accurate. A more conservative approach would be to apply a "confidence factor" to this value, which in this case was arbitrarily taken as 0.7, giving

$$\Delta C_{L_F} = 8.20 \times 10^{-3} \, \delta_F \tag{40}$$

The total lift coefficient is then

$$C_L = C_{L_w} + \Delta C_{L_f} + \Delta C_{L_{MOM}} + \Delta C_{LF} \tag{41}$$

The C_L for the vehicle with $\alpha = 10^o$, $\delta_F = 60^o$ and $\alpha_f = 0$, is $C_L = 0.903 + 0.110 + .126 + .496 = 1.635$

Determination of Drag

Drag also originates in this vehicle from several sources: all the lift sources and the ducting. The drag of the wing and the forward wing are known. The drag of the ducts has been calculated. The flap is assumed to increase drag through the mechanism of induced drag. In linear theory

$$C_D = C_{D_o} + \frac{C_L^2}{\pi e AR} \tag{42}$$

where C_{D_o} is the drag at no lift, and e is a wing efficiency factor. The drag curve for this vehicle resembles a parabola, but text book values of e do not produce results consistent with the test data. The equation was assumed to be of the form

$$C_D = C_{D_o} + K C_L^2 \tag{43}$$

The test data were then used to determine the factors C_{D_o} and K, by the method of least squares. This analysis yielded $C_D = .264 + 0.132\ C_L^2$ (44) which was used as the basis for extrapolation of the C_L versus $C_{D_{w,F}}$ curve, which is plotted in Fig. 49. The drag coefficient can then be determined by

$$C_{Dtotal} = C_{D_{w,F}} + \Delta C_{D_{duct}} + \Delta C_{D\ BLOW} + \Delta C_{D_s} + \Delta C_{D_f} + \Delta C_{DMOM} \quad (45)$$

The $C_{Dw,F}$ is the drag coefficient of the wing, flap, and fuselage with the ducts closed. The change in drag with the ducting open was approximated by

$$C_{D_{duct}} = -C_{D_o} \left[\frac{\text{A ducting}}{\text{A frontal}}\right] + C_{D\ \text{internal}} \quad (46)$$

The frontal area of the vehicle is 65 square feet. The internal drag is taken from Table IV. These values give:

$$\Delta C_{D_{duct}} = -.0249 \quad (47)$$

The drag on the stabilizer was taken from the literature of the NACA 0012 airfoil and then referenced to the vehicle wing area, which gives $C_{D_S} = .002$ at zero lift on the stabilizer. The momentum change that creates drag is

$$\rho A_D V_\infty^2 \cos^2\alpha \left[1-\sin(\alpha - 8^o)\right] \quad (48)$$

or

$$C_{D_{MOM}} = 0.128 \cos^2\alpha \left[1-\sin(\alpha-8^o)\right] \quad (49)$$

The change in C_D due to blowing was estimated from Hoernerr to be -0.10 based on cross sectional area

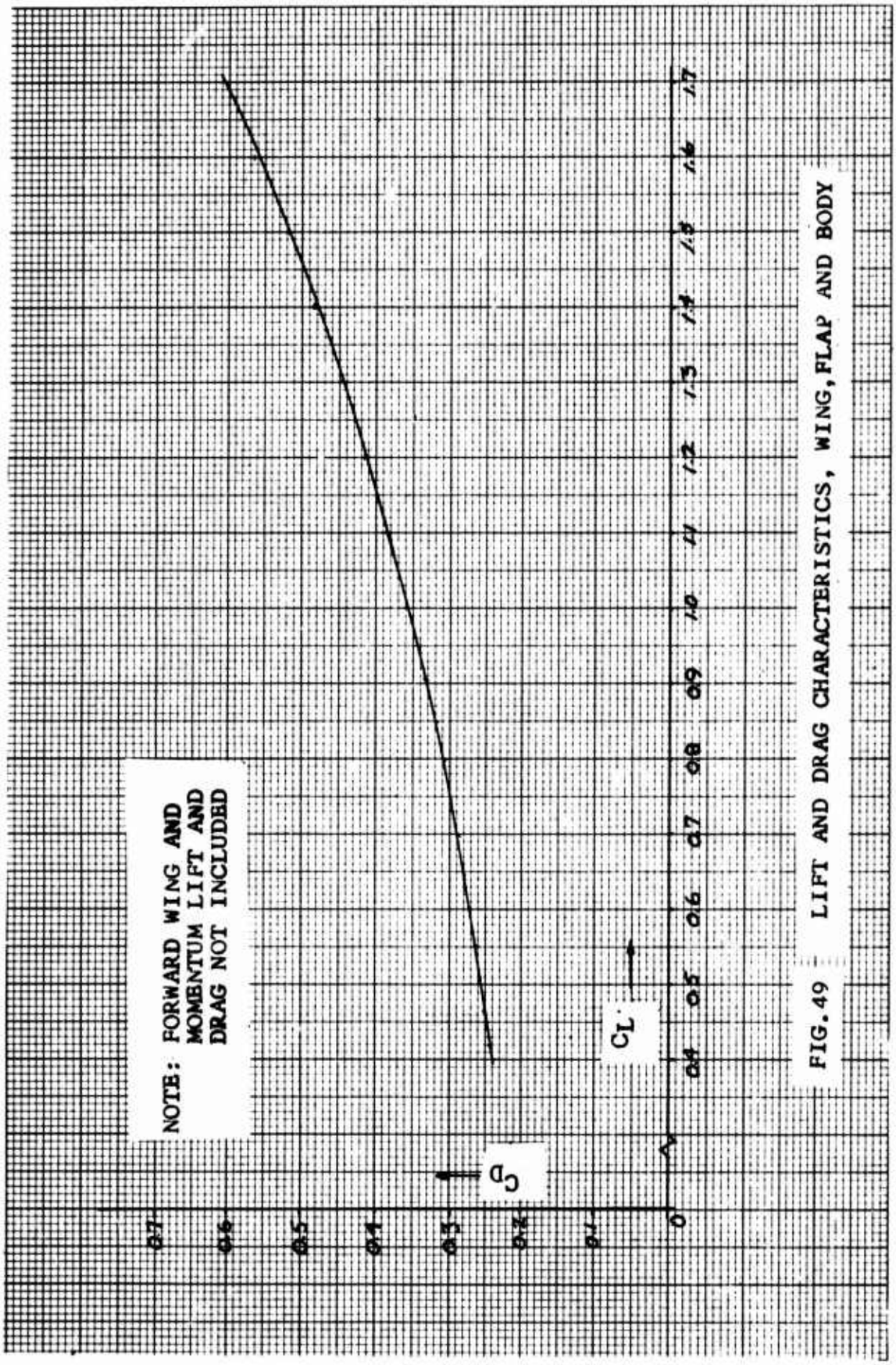

FIG. 49 LIFT AND DRAG CHARACTERISTICS, WING, FLAP AND BODY

of the rear of the fuselage. This basis is consistant with the assumption stated in the design of the blowing slot that the rear of the fuselage acts like the rear half of a cylinder. Corrected to wing area the change becomes

$$C_{D_{BLC}} = -0.10\left(\frac{22.4}{125}\right) = -0.017 \qquad (50)$$

The final drag coefficient, then is the sum of the changes of Eq (45) plus the induced drag of the wing and the flap and the forward wing.

$$C_D = 0.224+0.132C_L^2+0.128\cos^2\alpha\left[1-\sin(\alpha-8^\circ)\right]+\Delta C_{D_f} \qquad (51)$$

This equation gives the drag of the vehicle as a function of the lift coefficient, the angle of attack of the vehicle and the setting of the forward wing. It assumes continuous blowing, open ducts, and trim stabilizer.

Ground Performance

The base area of the vehicle is 90 ft^2. The pressure existing under the vehicle is $P_B = \frac{W-L}{A_B}$ (52)

The escape velocity of air leaving the underside of a ground effect machine is a function of the base pressure. In a plenum chamber vehicle (see Fig. 1) the base pressure can be considered as the total pressure, with the chamber acting as a reservoir; hence

$$V_e = \sqrt{\frac{2P_B}{\rho}} \qquad (53)$$

which for standard conditions is

$$V_e = 29\sqrt{P_B} \qquad (54)$$

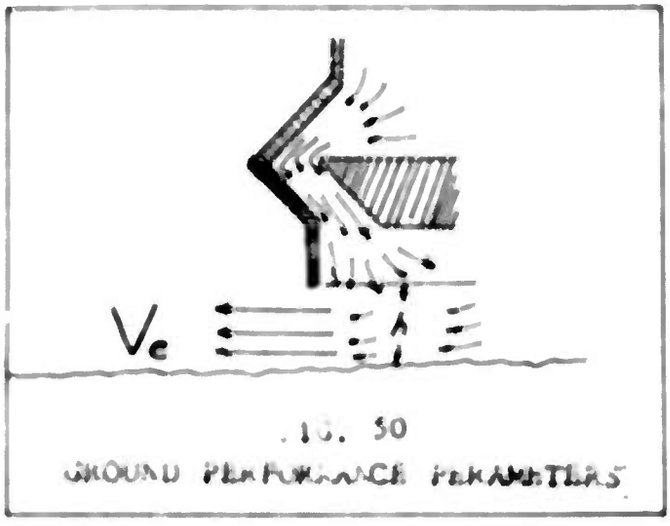

10. 50
GROUND PERFORMANCE PARAMETERS

In annular jet and peripheral jet schemes, the net result of injecting air laterally inward is to decrease the coefficient of the P_B term. It was assumed that the peripheral jet concept would reduce the coefficient to 22, or

$$V_e = 22\sqrt{P_B} \tag{55}$$

The mass flow rate required for ground cushion is then

$$\dot{m} = ChV_e \tag{56}$$

or

$$\dot{m} = 749\ h\sqrt{P_b} \tag{57}$$

This mass flow rate must be supplied by the fan ducts. Therefore, the mass flow rate in the fan ducts,

$$\dot{m} = \lambda_D \rho V_D = \delta \rho V_D$$

must equal the mass flow rate leaving the underside of the vehicle. The required duct velocity is then

$$V_D = (99.3\ \sqrt{P_J})\ h \tag{58}$$

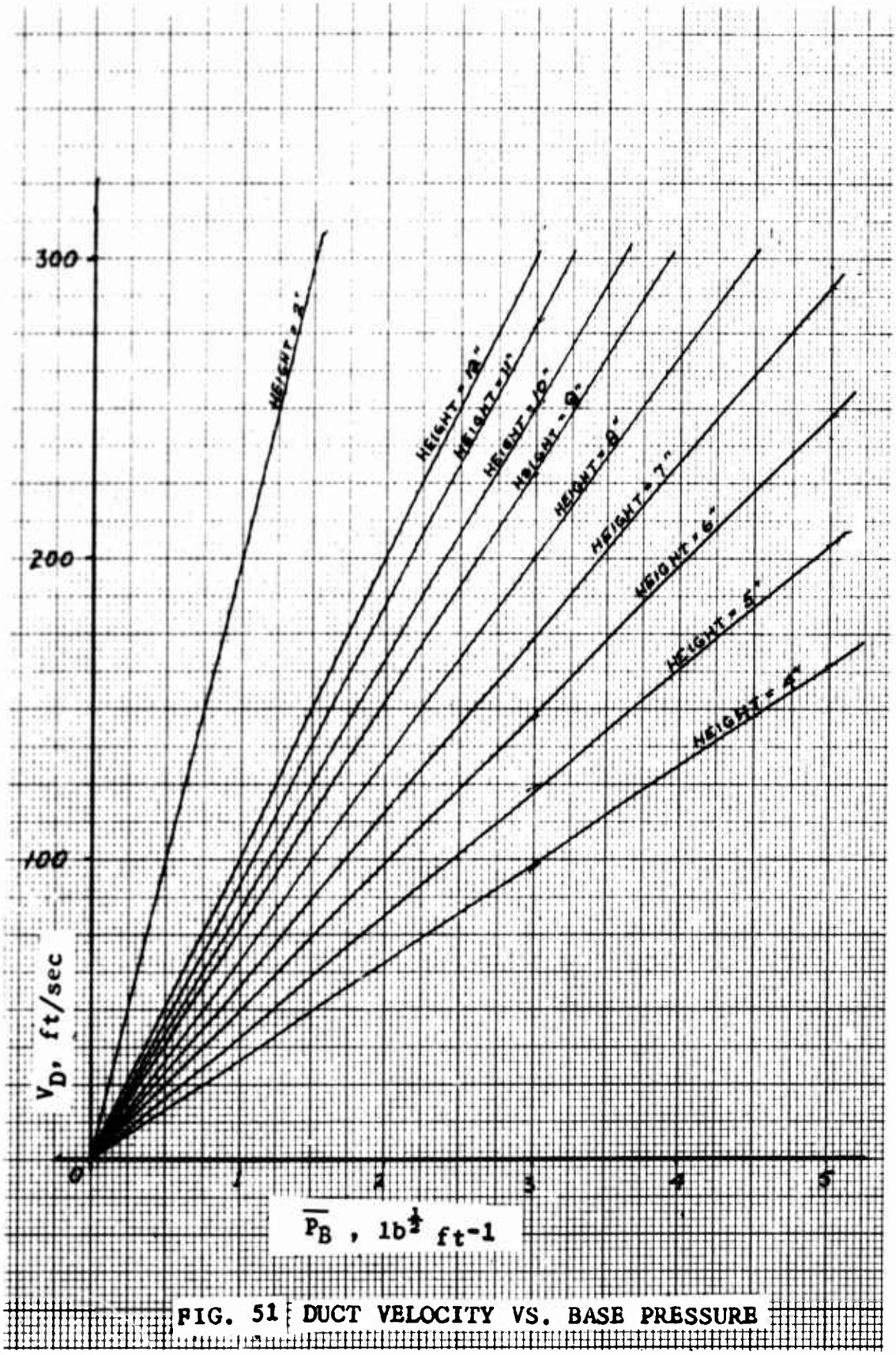

FIG. 51 DUCT VELOCITY VS. BASE PRESSURE

which gives a relation between the velocity in the fan ducts and the ground clearance height. The power required to provide the mass flow rate is

$$P_D = \frac{\frac{1}{2}\rho A_D \left(V_D^3 - V_\infty^3 \right)}{550} \tag{59}$$

The power required to travel at a known velocity is

$$P_p = \frac{DV}{550} \tag{60}$$

and the total power required is the sum of equations (60) and (59).

Most ground cruising will be accomplished at a vehicle angle of attack of zero, no flap deflection, and the forward wing at -15° angle of attack. Therefore from equation (41) C_L = .576 and C_D = .373, from equation (51). Assuming a vehicle weight of 2400 pounds, the performance was calculated and plotted on Fig. 52.

The maximum power available is assumed to be 270 horsepower. The RC-2-90-Y is rated at 330 horsepower maximum. However, 300 horsepower is a more reasonable design figure (it is not known what the basis of the 330 figure is, it may include for example the power required for the fuel pump). Assuming 300 horsepower is a good figure, then an efficiency must be applied, which was taken as 0.90. Patterson (Ref 14) indicates that this is not an unreasonable figure for fan-straightener combinations.

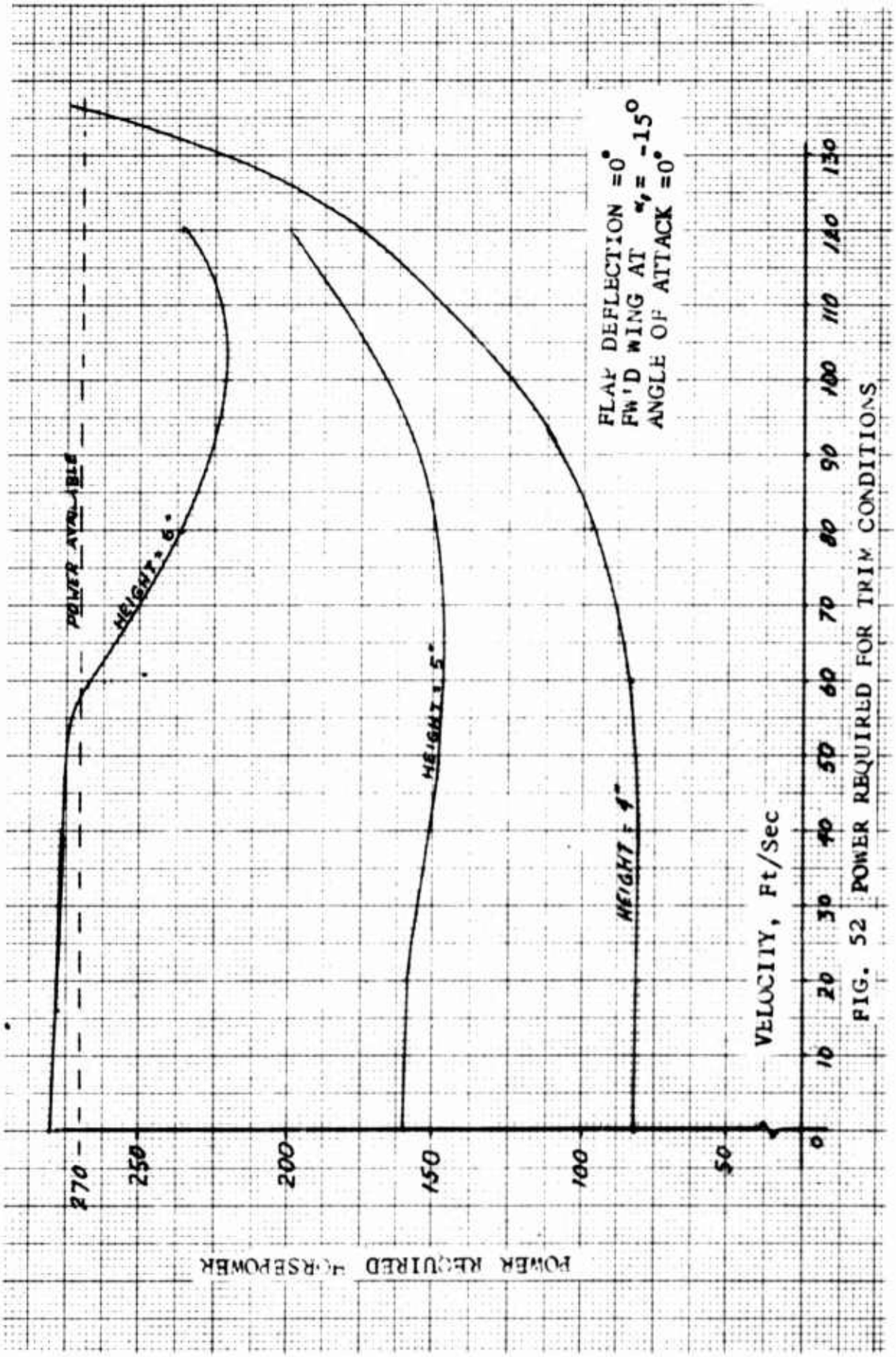

FIG. 52 POWER REQUIRED FOR TRIM CONDITIONS

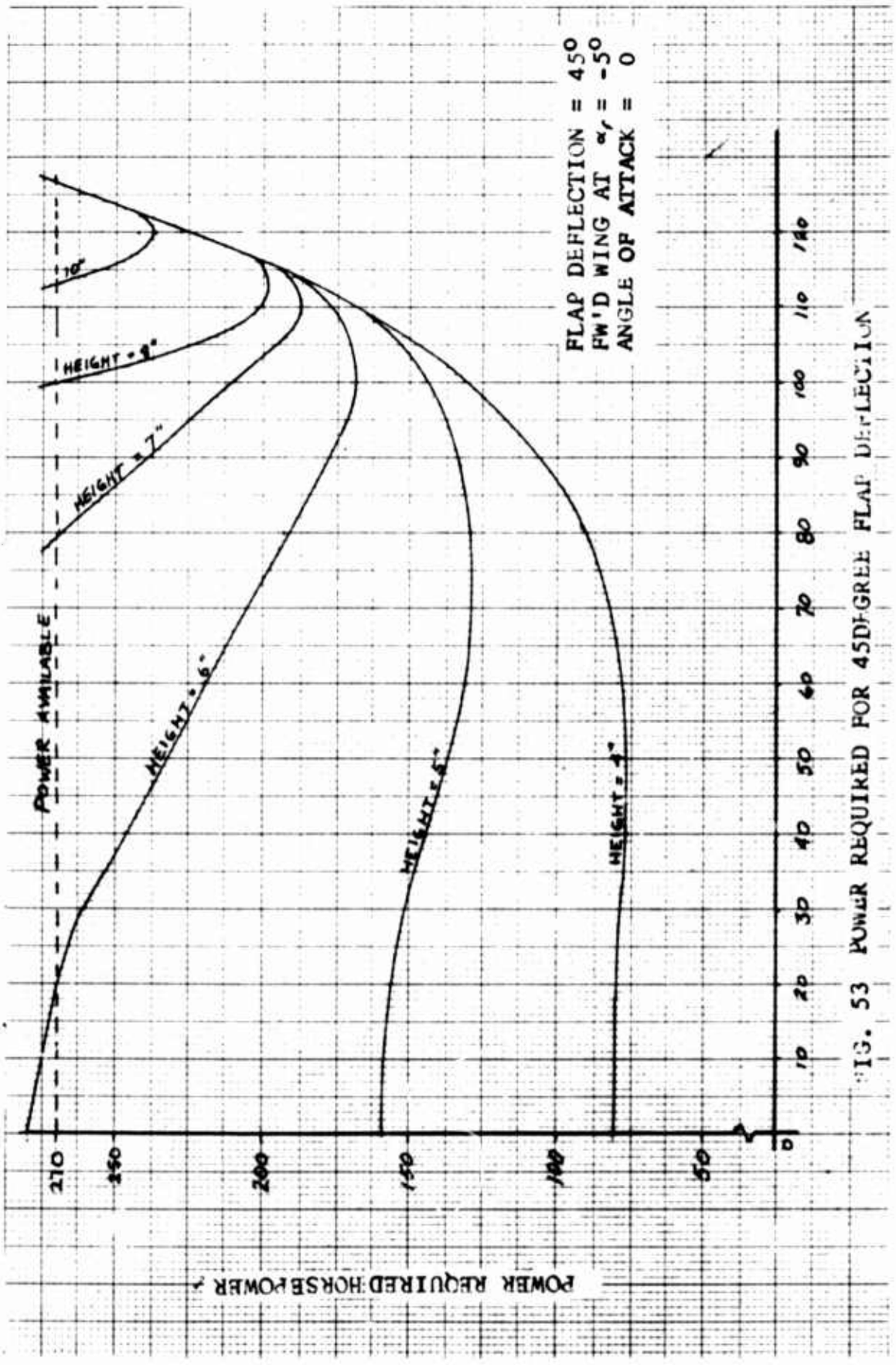

FIG. 53 POWER REQUIRED FOR 45DEGREE FLAP DEFLECTION

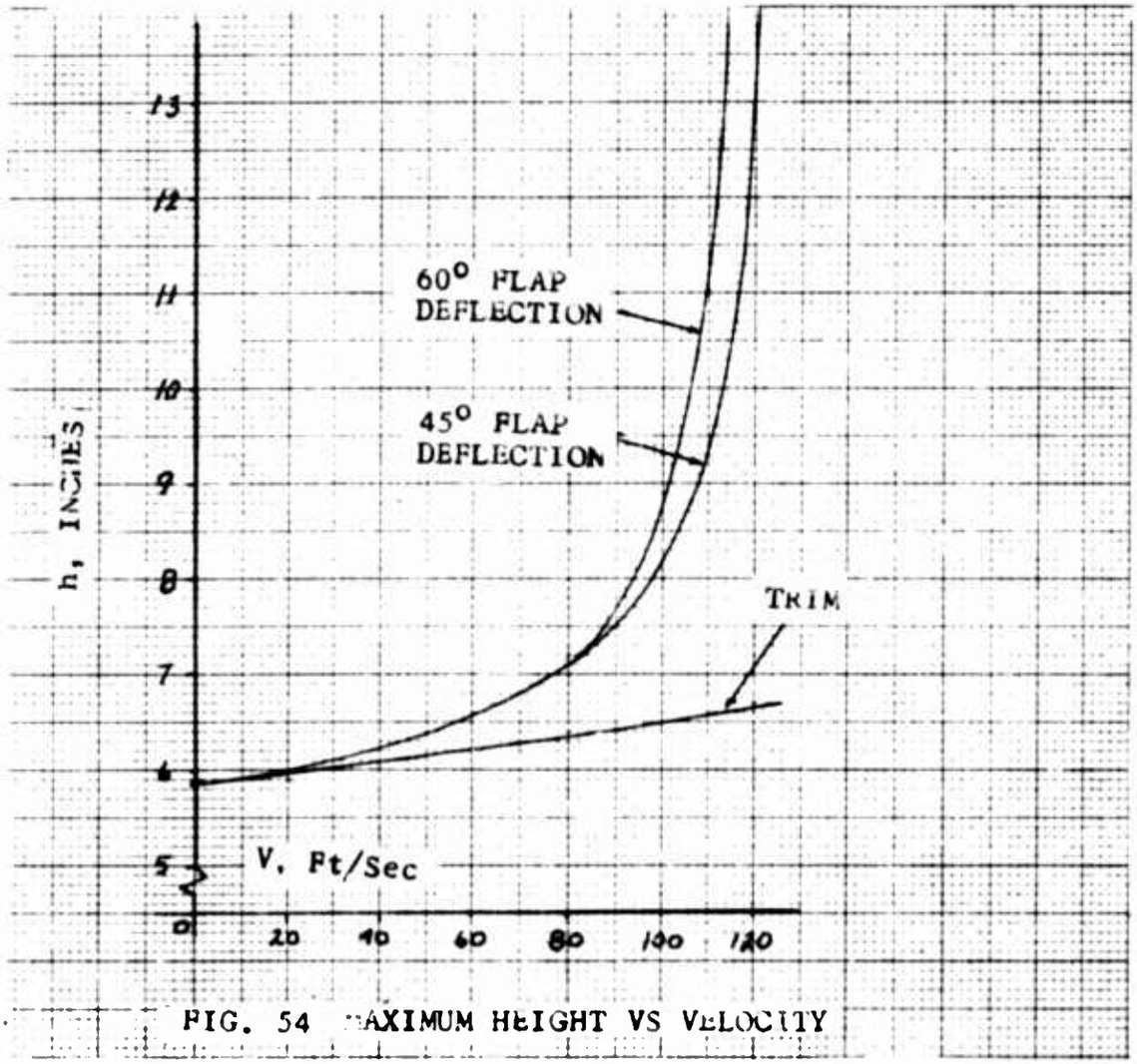

FIG. 54 MAXIMUM HEIGHT VS VELOCITY

Flight Performance

The flight performance was calculated from standard techniques, assuming a nominal vehicle weight of 2400 pounds. The minimum take off speed is taken as the speed at which lift is equal to weight. The maximum speed is given as that speed at which power available for propulsion is equal to power required.

In computing take off roll, a net thrust of 500 pounds was assumed to be available, unless the excess power available indicated that less thrust could be pro-

duced; that is

$$F_{EX} = \frac{\text{Power Excess (550)}}{V} \leq 500 \text{ lbs} \qquad (61)$$

The value, 500 pounds, was chosen arbitrarily; however it is a conservative estimate. The thrust of the propeller is simply the pressure increase across the propeller times the propeller area. In this case the propeller area is the total duct area at the propeller minus the area of the nacelle exhaust, which is 8.85 square feet. The pressure rise across the propeller is, theoretically, the dynamic pressure of the rotational velocity. To achieve 500 pounds of static thrust, a perfect propeller in this duct would have to rotate at 1440 RPM. Since the engine can operate up to 6400 RPM (see Fig. 48), the 500-pound figure is quite conservative.

The vehicle was considered to be in take-off configuration but at zero angle of attack, and continued until take-off speed was attained, when the angle of attack was increased to 10 degrees. The take-off roll is plotted in Fig. 56 as a function of initial velocity. This is necessary because the vehicle will not always be at zero velocity when it is decided that take-off is necessary. This curve does not include any allowance for pilot reaction time.

The rate of climb for this vehicle in feet per second, is given by

$$R.C. = \left(\frac{\text{Excess Power}}{W}\right) 550 \qquad (62)$$

which, at 100 feet per second take-off velocity and 2400 pounds weight, is equal to 9.16 feet per second. The distance required to clear a 50 foot obstacle is then 545 feet plus the take-off distance, which depends on initial velocity. Under a typical condition, if a vehicle were cruising along a rough jungle trail, with the flap deflected 60° (to achieve high ground clearance) at 50 feet per second, then saw a ten foot barricade across the trail, a minimum distance of 669 feet would be required to clear the obstacle. Under similar conditions, a distance of 1105 feet would be required to clear a 50-foot obstacle.

This is felt to be quite acceptable short take-off performance. The ground performance, while not spectacular, is also acceptable. The heights given in Figs. 52 through 54 are augmented by 11 inches of flexible skirt, which means that a height of six inches will allow the vehicle to go over a seventeen-inch rock, bump, or log.

The flight performance for sustained flight was not calculated because the mission of the vehicle is primarily ground reconnaissance, and flight would be used only to negotiate obstacles. However, sustained flight is possible, and could be used in emergency situations. For example, to fly at 120 feet per second, a C_L of 1.12 would be required, giving a C_D of 0.484. Power required for this condition would be 228 horsepower.

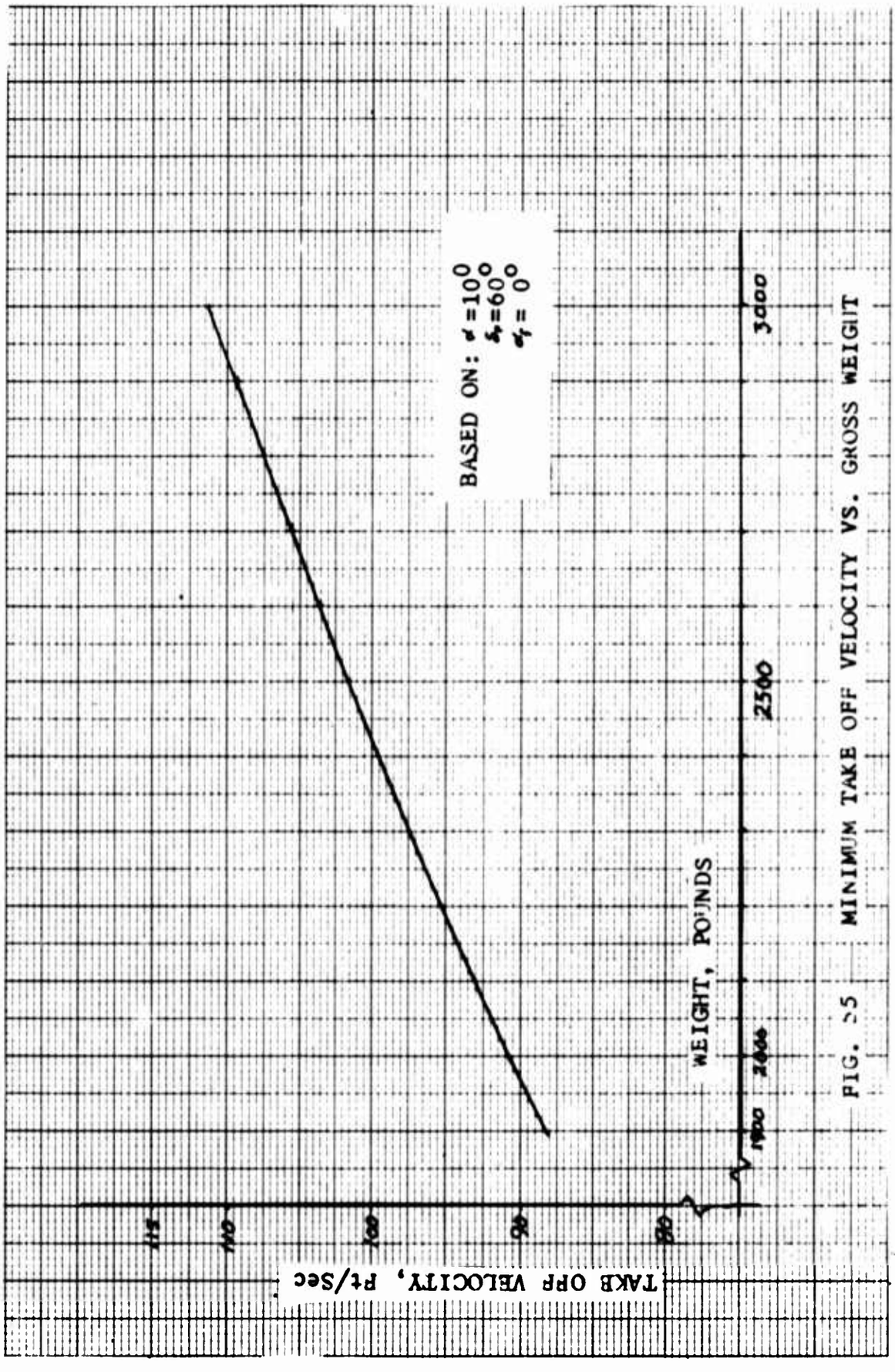

PIG. 25 MINIMUM TAKE OFF VELOCITY VS. GROSS WEIGHT

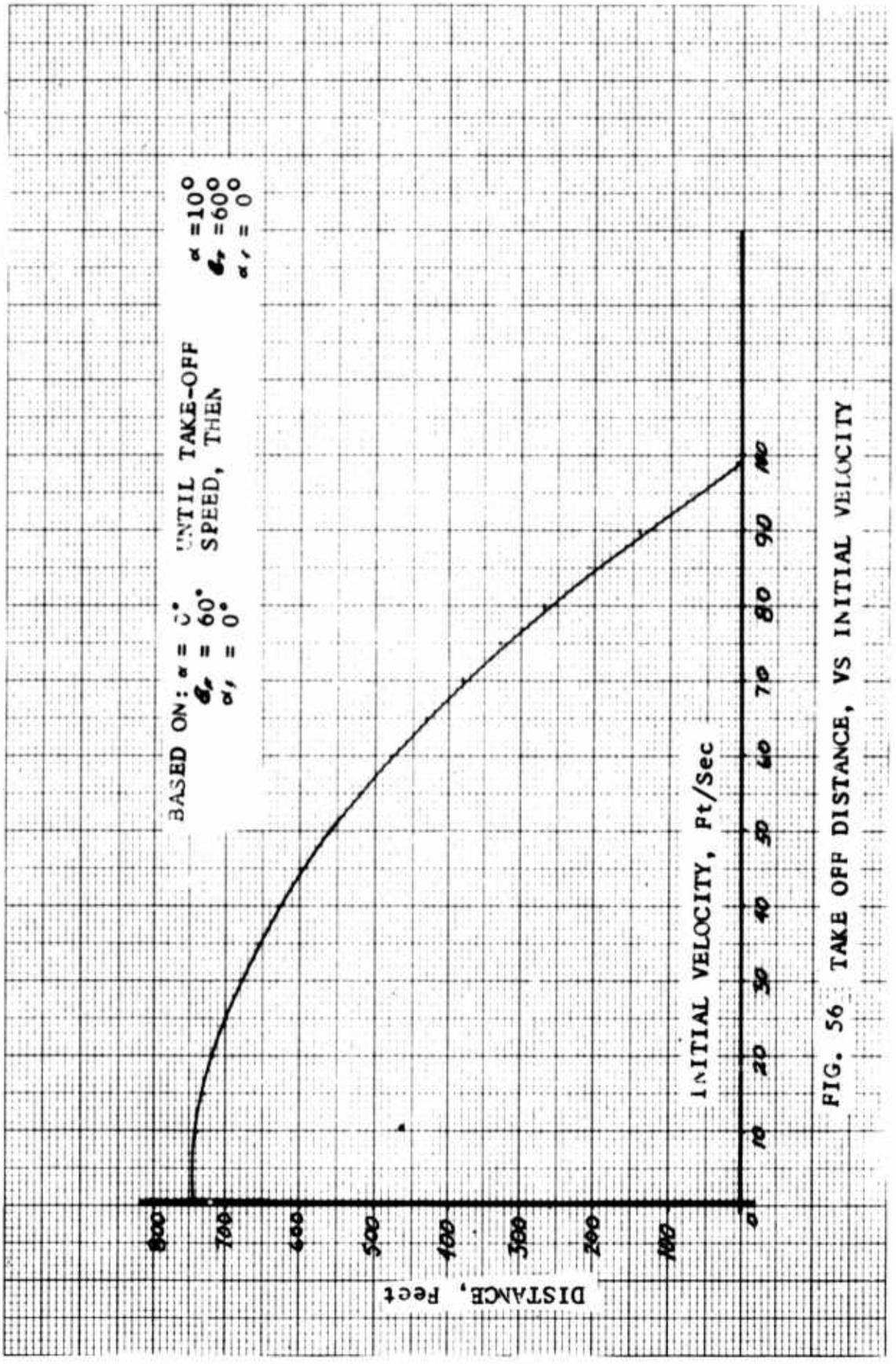

FIG. 56 TAKE OFF DISTANCE, VS INITIAL VELOCITY

VIII. Conclusions and Recommendations

Conclusions

The basic idea has been proven feasible. The vehicle proposed in this study is a practical machine, made of many plastic parts which are easily repaired. The power is a single internal combustion engine using regular gasoline. The maintenance on the vehicle should be minimal.

Take-off distances and velocities are quite reasonable. A vehicle with a full fuel load, two machine guns with 150 pounds of ammunition, and a 200- pound pilot can become airborne at highway speeds. With two heavy passengers and the same load, the take-off velocity is 109 feet per second.

On the ground, the vehicle will operate over water, land, swamp or ice. Since the vehicle is only 7.2 feet wide, most trails and all roads are negotiable, and weather, i.e. mud, is not a factor. For take-off and landing a minimum straight run is required such as a clearing, a 600-foot stretch of straight road, a river, or a small pond.

In short, the vehicle performs satisfactorily all the requirements of Section II, Mission.

Recommendations

The preliminary design of this vehicle looks very good and quite promising, enough so to warrant further work in this area.

Specifically recommended for further investigation are:

1. Completion of the test plan outlines in Table I with the large end plates. The data at the higher Reynolds number is essential to further study.

2. A detailed structural design, including exact weight estimate and stress analysis.

3. A stability and control study of the vehicle, both in flight and on the ground.

The completion of these recommendations would allow the construction and testing of a prototype vehicle, which could be the basis for production of such a flying ground effect machine.

Table V
Summary of Vehicle Characteristics

Length	17.9 feet
Height	13.0 "
Width	7.2 "
Wing Area	12.6 $feet^2$
Forward Wing Area	21.6 $feet^2$
Elevator Area	21.6 $feet^2$
Flap	30% chord, plan flap
Boundary Layer Control	suction on wing surface blowing on rear fuselage
Empty Weight	1718 pounds
Minimum Flight Weight	1948 pounds
Maximum Gross Weight	2902 pounds
Nominal Weight	2400 pounds
Take off Velocity (2400 pounds)	99 feet/sec.
Take off Velocity (2902 pounds)	109 feet/sec.
Take off Velocity (1948 pounds)	89 feet/sec.

Bibliography

1. American Society of Mechanical Engineers. Report on Fluid Flow Meters; Their Design and Use.

2. Armfield, William S. IV, et al. Air Cushion Vehicles: Transportation of the Future. New York: N.Y. Transportation Research Associates 1962.

3. Bielkowicz, Peter. Class Notes, A.E. 3.10, unpublished. 1966.

4. Cuno, Otto. Experimental Determination of the Thickness of the Boundary Layer along a Wing Section. NACA Technical Memorandum No. 679, Langley Field, Va., 1932.

5. Domasch, Daniel O. et al. Airplane Aerodynamics 2nd Edition, N.Y. Pitman Publishing Co. 1957.

6. Goldsmith, Alexander, et al. Handbook of Thermophysical Properties of Solid Materials. Revised Edition, Volume IV. N.Y. The MacMillan Co,, 1961.

7. Hoerner, Sighard F. Hoerner. Fluid-Dynamic Drag. Midland Park, Sighard F. Hoerner, 1965. N.J.

8. Jacobs, Eastman N. and Sherman, Albert. Airfoil Section Characteristics of Affected by Variations of the Reynolds Number. Langley Field, Va. NACA Report 586, 1937.

9. Jacobs, Eastman N., et al. The Characteristics of 78 Related Airfoils Section from Tests in the Variable Density Wind Tunnel. Langley Field, Va. NACA Report 460, 1933.

10. Kuethe, A.M. and Schetzer, J.D. Foundations of Aerodynamics 2nd Edition, New York. John Wiley and Sons, Inc; 1959.

11. Lampros, A.F. Estimation of the Lift Characteristics of Very Low Aspect Ratio Wings at Subsonic Speeds. U.S. Naval Missile Center, Point Mugu, California. 1963.

12. Lowry, John G. and Colhamus Edward C. A Method for Predicting Lift Increments Due to Flap Deflections at Low Angles of Attack in Incompressible Flow. NACA Technical Note 3911. Langley Field, Va., 1957.

Bibliography

13. Norbye, Jan P. Test Drive of U.S. car with Rotating Combustion Engine. Popular Science, Popular Science, April 1966.

14. Patterson, G. N. Ducted Fans: Design for High Efficiency. Reports ACA 7-10, Australian Council for Aeronautics, Melborne, 1946.

15. Pope, Alan. "Wind Tunnel Testing, 2nd E. N.Y. John Wiley and Sons Inc, 1954.

16. Proceedings of the Hydrofoils and Air Cushion Vehicles. N.Y. Institute of the Aerospace Sciences. 1962.

17. Schichting, Hermann. Boundary Layer Theory. N.Y. McGraw Hill Book Company, 1960.

18. Shapiro, Ascher J. The Dynamics and Thermodynamics of Compressible Fluid Flow. N.Y. Roland Press Co., 1953.

19. Smith, W.H.B. and Smith, Joseph E. Small Arms of the World, 7th Edition. The Stack pole Co., Harrisburg, Pa., 1962.

20. Theodorsen, Theodore and Naiman, Irven. Pressure Distributions for Representative Airfoils and Related Profiles. Langley Field, Va. NACA TN-1016. 1946.

Vita

James C. McSherry [redacted] PII Redacted

[redacted]. After schooling in Oklahoma, Austria, and the Philippines, he enrolled at the University of Oklahoma in 1954. He was graduated in June 1958 with the degree of Bachelor of Science in Aeronautical Engineering. He was employed as an engineer by McDonnell Aircraft Corporation until his entry on active duty at the Air Force Missile Development Center, in August, 1958. There he served as Project Officer on several research and test programs, including the X-7A, Pegasus, Hound Dog, Q-2C, Mace, Matador, and Athena programs. Prior to his acceptance to the Air Force Institute of Technology, he was assigned to the Development Engineering Division of the Thiokol Chemical Corporation Contract Management Office.

Permanent address: [redacted]

PII Redacted

This thesis was typed by Mrs. Edith Wik.

UNCLASSIFIED
Security Classification

DOCUMENT CONTROL DATA - R & D

(Security classification of title, body of abstract and indexing annotation must be entered when the overall report is classified)

1. ORIGINATING ACTIVITY (Corporate author)
Air Force Institute of Technology (AFIT-SE)
Wright-Patterson AFB, Ohio 45433

2a. REPORT SECURITY CLASSIFICATION
UNCLASSIFIED

2b. GROUP

3. REPORT TITLE
Optimization of a Ground Effect Machine

4. DESCRIPTIVE NOTES (Type of report and inclusive dates)
AFIT Thesis

5. AUTHOR(S) (First name, middle initial, last name)
James C. McSherry

6. REPORT DATE	7a. TOTAL NO OF PAGES	7b. NO OF REFS
June 1967	111	20

8a. CONTRACT OR GRANT NO N/A
b. PROJECT NO N/A
c.
d.

9a. ORIGINATOR'S REPORT NUMBER(S)
AFIT Thesis GAM/AE/67-1

9b. OTHER REPORT NO(S) (Any other numbers that may be assigned this report)

10. DISTRIBUTION STATEMENT This document is subject to special export controls and each transmittal to foreign governments or foreign nationals may be made only with prior approval of the Dean, School of Engineering, Air Force Institute of Technology (AFIT-SE), Wright-Patterson Air Force Base, Ohio 45433.

11. SUPPLEMENTARY NOTES

12. SPONSORING MILITARY ACTIVITY
Department of Aeronautical Engineering
Air Force Institute of Technology
(AFIT-SEA)
Wright-Patterson AFB, Ohio 45433

13. ABSTRACT Professor Peter Bielkowicz conceived the idea of a ground effect machine that could also fly. This thesis tests the concept and improves on the original design. Two wind tunnel models were built to determine the aerodynamic characteristics of the vehicle. When the wind tunnel was closed because of safety problems after the test program had just begun, a third, sub-scale, model was built and tested in a smaller tunnel to test improvements dictated by first tests.

The results from these tests were combined with some analytical techniques to predict the performance of the full scale vehicle.

The final vehicle will carry one pilot and two passengers (if necessary). When armed with two 7.62 mm machine guns, carrying a full fuel load and a 200-lb. pilot, the gross weight of the vehicle is 2400 pounds. Its dimensions are 7.2 feet wide, 17.9 feet long and 13.0 feet high, including the end plates necessary for such a low aspect ratio wing. This small size will allow the vehicle to travel over back trails or unimproved roads. Despite the severe limitations imposed by the dimensions, the vehicle will become airborne at 99 feet per second, and clear a 50-foot obstacle 545 feet from the take off point, when powered by the 300-horsepower Curtiss-Wright RC-2-90-y rotating cylinder engine.

DD FORM 1 NOV 65 1473

UNCLASSIFIED
Security Classification

14 KEY WORDS	LINK A		LINK B		LINK C	
	ROLE	WT	ROLE	WT	ROLE	WT
Ground effect machine Lifting upper surface Controls Flight over obstacles						

Vita

James C. McSherry [redacted]. After schooling in Oklahoma, Austria, and the Philippines, he enrolled at the University of Oklahoma in 1954. He was graduated in June 1958 with the degree of Bachelor of Science in Aeronautical Engineering. He was employed as an engineer by McDonnell Aircraft Corporation until his entry on active duty at the Air Force Missile Development Center, in August, 1958. There he served as Project Officer on several research and test programs, including the X-7A, Pegasus, Hound Dog, Q-2C, Mace, Matador, and Athena programs. Prior to his acceptance to the Air Force Institute of Technology, he was assigned to the Development Engineering Division of the Thiokol Chemical Corporation Contract Management Office.

Permanent address: [redacted]

This thesis was typed by Mrs. Edith Wik.